

# 8 Transients and Variable Stars

*R. Lynne Jones, Lucianne M. Walkowicz, Julius Allison, Scott F. Anderson, Andrew C. Becker, Joshua S. Bloom, John J. Bochanski, W. N. Brandt, Mark W. Claire, Kem H. Cook, Christopher S. Culliton, Rosanne Di Stefano, S.G. Djorgovski, Ciro Donalek, Derek B. Fox, Muhammad Furqan, A. Gal-Yam, Robert R. Gibson, Suzanne L. Hawley, Eric J. Hilton, Keri Hoadley, Steve B. Howell, Željko Ivezić, Stylani (Stella) Kafka, Mansi M. Kasliwal, Adam Kowalski, K. Simon Krughoff, Shrinivas Kulkarni, Knox S. Long, Julie Lutz, Ashish A. Mahabal, Peregrine M. McGehee, Dante Minniti, Anjum S. Mukadam, Ehud Nakar, Hakeem Oluseyi, Joshua Pepper, Arne Rau, James E. Rhoads, Stephen T. Ridgway, Nathan Smith, Michael A. Strauss, Paula Szkody, Virginia Trimble, Andrew A. West, Przemek Wozniak*

## 8.1 Introduction

*Rosanne Di Stefano, Knox S. Long, Virginia Trimble, Lucianne M. Walkowicz*

Transient and variable objects have played a major role in astronomy since the Chinese began to observe them more than two millennia ago. The term nova, for example, traces back to Pliny. Tycho's determination that the parallax of the supernova of 1576 was small (compared to a comet) was important in showing the Universe beyond the Solar System was not static. In 1912, Henrietta Leavitt reported that a class of pulsating stars (now known as Cepheid variables) had a regular relation of brightness to period (Leavitt & Pickering 1912). Edwin Hubble's subsequent discovery, in 1929, of Cepheids in the Andromeda nebula conclusively showed that it was a separate galaxy, and not a component of the Milky Way (Hubble 1929).

Fritz Zwicky's 18-inch Palomar Schmidt program was the first systematic study of the transient sky. He undertook a vigorous search for supernovae, and with Walter Baade promoted them as distance indicators and the source of cosmic rays (Baade & Zwicky 1934a,b). Just 10 years ago, supernovae came back into the mainstream. The first indication of a new constituent of the Universe, dark energy, was deduced from the dimming of type Ia supernovae located at cosmological distances (Perlmutter et al. 1999; Riess et al. 1998). The last decade has seen a flowering of the field of gamma ray bursts, the most relativistic explosions in nature. Meanwhile, the most accurate metrology systems ever built await the first burst of gravitational radiation to surpass their sensitivity threshold, revealing the signature of highly relativistic interactions between two massive, compact bodies.

Astronomical progress has been closely linked to technological progress. Digital sensors (CCDs and IR detectors) were invented and funded by military and commercial sectors, but their impact on

astronomy has been profound. Thanks to Moore’s law<sup>1</sup>, astronomers are assured of exponentially more powerful sensors, computing cycles, bandwidth, and storage. Over time, such evolution becomes a revolution. This windfall is the basis of the new era of wide field optical and near-infrared (NIR) imaging. Wide-field imaging has become a main stream tool as can be witnessed by the success of the Sloan Digital Sky Survey (SDSS). The renaissance of wide field telescopes, especially telescopes with very large étendue (the product of the field of view and the light collecting area of the telescope, § 1.2), opens new opportunities to explore the variable and transient sky. LSST will add to this legacy by exploring new sky and reaching greater depth.

The types of variability LSST will observe depends on both intrinsic variability and limitations of sensitivity. From an observational perspective, transients are objects that fall below our detection threshold when they are faint and for which individual events are worthy of study, whereas by variables, we generally mean objects are always detectable, but change in brightness on various timescales. From a physical perspective, transients are objects whose character is changed by the event, usually as the result of some kind of explosion or collision, whereas variables are objects whose nature is not altered significantly by the event. Furthermore, some objects vary not because they are intrinsically variable, but because some aspect of their geometry causes them to vary. Examples of this kind of variability are objects whose light is amplified by gravitational lenses, or simply binary systems containing multiple objects, including planets, which occult other system components.

In this chapter, we discuss some of the science associated with “The Transient and Variable Universe” that will be carried out with LSST: transients, or objects that explode (§ 8.2–§ 8.4); objects whose brightness changes due to gravitational lensing (§ 8.5); variable stars (§ 8.6–§ 8.10); and planetary transits (§ 8.11). In this chapter we focus on what the variability tells us about the objects themselves; using such objects to map the structure of galaxies, characterize the intracluster medium, or study cosmology is discussed elsewhere in this book.

As discussed in § 8.2, LSST has a fundamental role in extending our knowledge of transient phenomena. Its cadence is well-suited to the evolution of certain objects in particular, such as novae and supernovae. The combination of all-sky coverage, consistent long-term monitoring, and flexible criteria for event identification will allow LSST to probe a large unexplored region of parameter space and discover new types of transients. Many types of transient events are expected on theoretical grounds to inhabit this space, but have not yet been observed. For example, depending on the initial mass of a white dwarf when it begins accreting matter, it may collapse upon achieving the Chandrasekhar mass instead of exploding. This accretion-induced collapse is expected to generate an event whose characteristics are difficult to predict, and for which we have no good candidates drawn from nature. LSST should be sensitive to accretion-induced collapse – just one of a wider range of transient phenomena than we have not yet been able to observe.

As described in § 8.5, geometrical effects can cause the amount of light we receive from a star to increase dramatically, even when the star itself has a constant luminosity. Such a transient brightening occurs when starlight is focused by an intervening mass, or gravitational lens. LSST will either discover MAssive Compact Halo Objects (MACHOs) by their microlensing signatures, or preclude them. LSST will also detect tens of thousands of lensing events generated by members

---

<sup>1</sup>The number of transistors in commodity integrated circuits has been approximately doubling every two years for the past five decades.

of ordinary stellar populations, from brown dwarfs to black holes, including nearby sources that have not been revealed by other measurement techniques. Microlensing can detect exoplanets in parameter ranges that are difficult or impossible to study with other methods. LSST identification of lensing events will, therefore, allow it to probe a large range of distant stellar populations at the same time as it teaches us about the nature of dark and dim objects, including black holes, neutron stars, and planets in the solar neighborhood.

LSST will make fundamental contributions to our understanding of variability in stars of many types as is described in § 8.6. It will identify large numbers of known variable types, needed both for population studies (as in the case of cataclysmic variables) and for studies of Galactic structure (as in the case of RR Lyrae stars). Photometric light curves over the ten-year lifetime of LSST of various source populations will establish patterns of variability, such as the frequency of dwarf nova outbursts in globular clusters and the time history of accretion in magnetic cataclysmic variable and VY Sculptoris stars, differing behaviors of the various types of symbiotic stars, and activity cycles across the main sequence. Huge numbers of eclipsing systems and close binary systems will be revealed, allowing detailed studies of binary frequency in various populations. The automatic generation of light curves will effectively support all detailed studies of objects in the LSST field of view during the period of LSST operations.

Finally in § 8.11, we describe another form of geometric variability: the dimming of stars as they are occulted by transiting planets. The cadence of the survey makes LSST most sensitive to large planets with short orbital periods. Much will be known about planets and planetary transits by the time LSST is operational, both from ongoing studies from the ground and from space-based missions. However, LSST has the distinct advantages of its brightness and distance limits, which will extend the extrasolar planet census to larger distances within the Galaxy. Thousands of “hot Jupiters” will be discovered, enabling detailed studies of planet frequency as a function of, for example, stellar metallicity or parent population.

## 8.2 Explosive Transients in the Local Universe

*Mansi M. Kasliwal, Shrinivas Kulkarni*

The types of objects that dominate the Local Universe differ from those typically found at cosmological distances, and so does the corresponding science. The following discussion of explosive transient searches with LSST reflects this distinction: we first discuss transients in the Local Universe, followed by more distant, cosmological transients.

Two different reasons make the search for transients in the nearby Universe ( $d \lesssim 200$  Mpc) interesting and urgent. First, there exists a large gap in the luminosity of the brightest novae ( $M_v \sim -10$  mag) and that of sub-luminous supernovae ( $M_v \sim -16$  mag). However, theory and reasonable speculation point to several potential classes of objects in this “gap.” Such objects are best found in the Local Universe. Second, the nascent field of Gravitational Wave (GW) astronomy and the budding fields of ultra-high energy cosmic rays, TeV photons, and astrophysical neutrinos are likewise limited to the Local Universe by physical effects (Greisen-Zatsepin-Kuzmin (GZK) effect, photon pair production), or instrumental sensitivity (in the case of neutrinos and GWs). Unfortunately, the positional information provided by the telescopes dedicated to these new fields

is poor, and precludes identification of the host galaxy (with attendant loss of distance and physical diagnostics). Both goals can be met with wide field imaging telescopes acting in concert with follow-up telescopes.

### 8.2.1 Events in the Gap

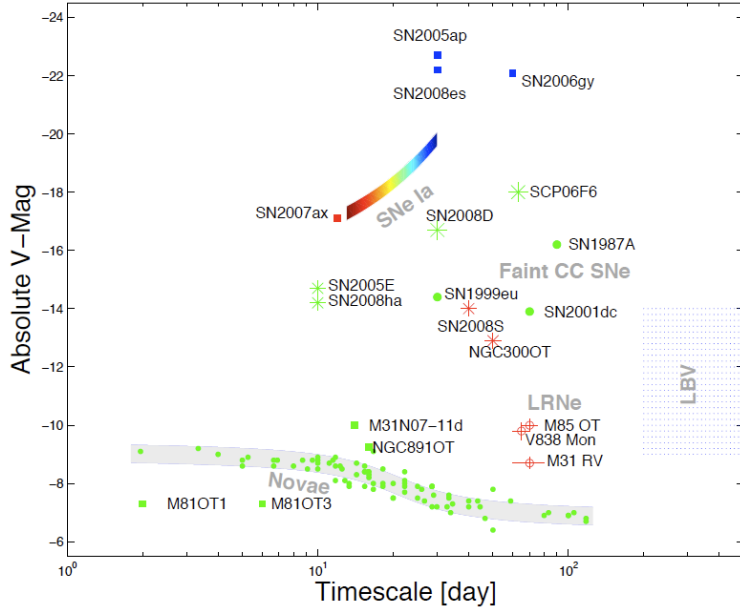


Figure 8.1: The phase space of cosmic transients : peak V-band luminosity as a function of duration, with color a measure of the true color at maximum. Shown are the known explosive (supernovae) and eruptive (novae, luminous blue variables (LBV) transients. Also shown are new types of transients (all found over the last two years): the peculiar transients M 85 OT2006-1, M31-RV, and V838 Mon, which possibly form a new class of “luminous red novae,” for which a variety of models have been suggested – core collapse, common envelope event, planet plunging into star, a peculiar nova, and a peculiar AGB phase; the baffling transient with a spectrum of a red-shifted carbon star, SCP 06F6 (see [Barbary et al. 2009](#); [Soker et al. 2008](#)); a possible accretion induced collapse event SN 2005E ([Perets et al. 2009](#)); the extremely faint, possibly fallback, SN 2008ha ([Valenti et al. 2009](#)); and peculiar eruptive events with extremely red progenitors SN 2008S and NGC300-OT ([Thompson et al. 2008](#); [Smith et al. 2008](#); [Bond et al. 2009](#)) Figure adapted from [Kulkarni et al. \(2007\)](#).

A plot of the peak luminosity versus characteristic duration (based on physics or convention) is a convenient way to summarize explosive events. We first focus on novae and supernovae of type Ia (SNe Ia). As can be seen from Figure 8.1, novae and SNe Ia form distinctly different loci. Brighter supernovae take a longer time to evolve (the Phillips relation; [Phillips 1993](#)) whereas the opposite is true of novae: the faster the nova decays the higher the luminosity (the “Maximum Magnitude Rate of Decline”, MMRD relation; see, for example, [Della Valle & Livio 1995](#); [Downes & Duerbeck 2000](#)).

The primary physical parameter determining the optical light curve in SNe Ia is the amount of nickel synthesized. There is almost a factor of 10 variation between the brightest (“1991T-like”) and the dimmest (“1991bg-like”) SNe Ia. The Phillips relation has been quantified with high precision, and the theory is well understood. In contrast, the MMRD does not enjoy the same quantity or quality

of light curves as those of type Ia supernovae. Fortunately, dedicated ongoing nova searches in M31 and the P60-FaSTING project have vastly increased the number of well-sampled light curves.

A discussion of potential new classes of events in the gap would benefit from a review of the basic physics of explosions. An important factor is the potential heat source at the center: a hot white dwarf (novae) or gradual release of radioactive energy (supernovae).

The primary physical parameters are: the mass of the ejecta ( $M_{\text{ej}}$ ), the velocity of the ejecta ( $v_s$ ), the radius of the progenitor star ( $R_0$ ), and the total energy of the explosion ( $\mathcal{E}_0$ ). Two distinct sources of energy contribute to the explosive energy: the kinetic energy of the ejecta,  $\mathcal{E}_k \equiv (1/2)M_{\text{ej}}v_s^2$ , and the energy in the photons (at the time of the explosion),  $\mathcal{E}_{\text{ph}}$ .

Assuming spherical symmetry and homogeneous density, the following equation describes the gains and losses suffered by the store of heat ( $E$ ):

$$\dot{E} = \varepsilon(t)M_{\text{ej}} - L(t) - 4\pi R(t)^2 Pv(t). \quad (8.1)$$

Here,  $L(t)$  is the luminosity radiated at the surface and  $\varepsilon(t)$  is the heating rate (energy per unit time) per gram from any source of energy (e.g., radioactivity or a long-lived central source).  $P$  is the total pressure and is given by the sum of gas and photon pressure.

Next, we resort to the so-called “diffusion” approximation (see Arnett 1996; Padmanabhan 2000),

$$L = E_{\text{ph}}/t_d, \quad (8.2)$$

where  $E_{\text{ph}} = aT^4V$  is the energy in photons ( $V$  is the volume,  $(4\pi/3)R^3$ ), and

$$t_d = B\kappa M_{\text{ej}}/cR \quad (8.3)$$

is the timescale for a photon to diffuse from the center to the surface. The pre-factor  $B$  in Equation 8.3 depends on the geometry and, following Padmanabhan, we set  $B = 0.07$ .  $\kappa$  is the mass opacity.

We will make one simplifying assumption: most of the acceleration of the ejecta takes place on the initial hydrodynamic timescale,  $\tau_h = R_0/v_s$ , and subsequently coasts at  $R(t) = R_0 + v_s t$ .

First, let us consider a “pure” explosion i.e., no subsequent heating ( $\varepsilon(t) = 0$ ). If photon pressure dominates then  $P = 1/3(E/V)$  and an analytical formula for  $L(t)$  can be obtained (Arnett 1996):

$$L(t) = L_0 \exp\left(-\frac{t\tau_h + t^2/2}{\tau_h t_d}\right); \quad (8.4)$$

here,  $\tau_d = B(\kappa M_{\text{ej}}/cR_0)$  is the initial diffusion timescale and  $L_0 = \mathcal{E}_{\text{ph}}/\tau_d$ .

From Equation 8.4 one can see that the light curve is divided into 1) a plateau phase which lasts until about  $\tau = \sqrt{\tau_d \tau_h}$  after which 2) the luminosity undergoes a (faster than) exponential decay. The duration of the plateau phase is

$$\tau = \sqrt{\frac{B\kappa M_{\text{ej}}}{cv_s}} \quad (8.5)$$

and is independent of  $R_0$ . The plateau luminosity is

$$L_p = \mathcal{E}_{\text{ph}}/\tau_d = \frac{cv_s^2 R_0}{2B\kappa} \frac{\mathcal{E}_{\text{ph}}}{\mathcal{E}_k}. \quad (8.6)$$

As can be seen from [Equation 8.6](#) the peak luminosity is independent of the mass of the ejecta but directly proportional to  $R_0$ . To the extent that there is rough equipartition<sup>2</sup> between the kinetic energy and the energy in photons, the luminosity is proportional to the square of the final coasting speed,  $v_s^2$ .

Pure explosions satisfactorily account for supernovae of type IIp. Note that since  $L_p \propto R_0$  the larger the star the higher the peak luminosity. SN 2006gy, one of the brightest supernovae, can be explained by invoking an explosion in a “star” which is much larger (160 AU) than any star (likely the material shed by a massive star prior to its death; see [Smith & McCray 2007](#)).

*Conversely*, pure explosions resulting from the deaths of compact stars (e.g., neutron stars, white dwarfs, or even stars with radius similar to that of the Sun) will be very faint. For such progenitors, visibility in the sky would require some sort of additional subsequent heat input, which is discussed next.

First we will consider “supernova”-like events, i.e., events in which the resulting debris is heated by radioactivity. One can easily imagine a continuation of the type Ia supernova sequence. We consider three possible examples for which we expect a smaller amount of radioactive yield and a rapid decay (timescales of days): coalescence of compact objects, accreting white dwarfs (O-Ne-Mg), and final He shell flash in AM CVn systems.

Following [Li & Paczyński \(1998\)](#), [Kulkarni \(2005\)](#) considers the possibility of the debris of neutron star coalescence being heated by decaying neutrons. Amazingly (despite the 10-min decay time of free neutrons) such events (dubbed as “macronovae”) are detectable in the nearby Universe over a period as long as a day, provided even a small amount ( $\gtrsim 10^{-3} M_\odot$ ) of free neutrons is released in such explosions. [Bildsten et al. \(2007\)](#) consider a helium nova (which arise in AM CVn systems). For these events (dubbed “Ia” supernovae), not only radioactive nickel but also radioactive iron is expected. Intermediate mass stars present two possible paths to sub-luminous supernovae. The O-Ne-Mg cores could either lead to a disruption (bright SN but no remnant) or a sub-luminous explosion ([Kitaura et al. 2006](#)). Separately, the issue of O-Ne-Mg white dwarfs accreting matter from a companion continues to fascinate astronomers. The likely possibility is a neutron star, but the outcome depends severely on the unknown effects of rotation and magnetic fields. One possibility is an explosion with low nickel yield (see [Metzger et al. 2008](#) for a recent discussion and review of the literature).

An entirely different class of explosive events is expected to arise in massive or large stars: birth of black holes (which can range from very silent events to gamma-ray bursts (GRBs) and everything in between), strong shocks in supergiants ([van den Heuvel 2008](#)) and common envelope mergers. Equations 8.5 and 8.6 provide guidance to the expected appearance of such objects. [Fryer et al. \(2007\)](#) developed a detailed model for faint, fast supernovae due to nickel “fallback” into the black hole. For the case of the birth of a black hole with no resulting radioactive yield (the newly synthesized material could be advected into the black hole), the star will slowly fade away on a timescale of  $\min(\tau_d, \tau)$ . Modern surveys are capable of finding such wimpy events ([Kochanek et al. 2008](#)).

---

<sup>2</sup>This is a critical assumption and must be checked for every potential scenario under consideration. In a relativistic fireball most of the energy is transferred to matter. For novae, this assumption is violated (Shara, personal communication).

In the spirit of this open-ended discussion of new transients, we also consider the case where the gas pressure could dominate over photon pressure. This is the regime of weak explosions. If so,  $P = 2/3(E/V)$  and [Equation 8.1](#) can be integrated to yield:

$$L(t) = \frac{L_0}{(t/\tau_h + 1)} \exp\left(-\frac{\tau_h t + t^2/2}{\tau_h \tau_d}\right). \quad (8.7)$$

In this case the relevant timescale is the hydrodynamic timescale. This regime is populated by luminous blue variables and hypergiants. Some of these stars are barely bound and suffer from bouts of unstable mass loss and photometric instabilities.

As can be gathered from [Figure 8.1](#) the pace of discoveries over the past two years gives great confidence to our expectation of filling in the phase space of explosions.

### 8.2.2 New Astronomy: Localizing LIGO Events

LSST's new window into the local transient Universe will complement four new fields in astronomy: the study of cosmic rays, very high energy (TeV and PeV) photons, neutrinos, and gravitational waves. Cosmic rays with energies exceeding  $10^{20}$  eV are strongly attenuated owing to the production of pions through interaction with the cosmic microwave background (CMB) photons (the famous GZK effect). Recently, the Pierre Auger Observatory ([The Pierre Auger Collaboration 2007](#)) has found evidence showing that such cosmic rays with energies above  $6 \times 10^{19}$  eV are correlated with the distribution of galaxies in the local 75-Mpc sphere. Similarly, very high energy (VHE) photons (TeV and PeV) have a highly restricted horizon. The TeV photons interact with CMB photons and produce electron-positron pairs. A number of facilities are now routinely detecting extra-galactic TeV photons from objects in the nearby Universe (VERITAS, MAGIC, HESS, CANGAROO). Neutrino astronomy is another budding field with an expected vast increase in sensitivity. The horizon here is primarily limited by sensitivity of the telescopes (ICECUBE). GW astronomy suffers from both poor localization (small interferometer baselines) and sensitivity. The horizon radius is 50 Mpc for enhanced LIGO (e-LIGO) and about 200 Mpc for advanced LIGO (a-LIGO) to observe neutron star coalescence. The greatest gains in these areas, especially GW astronomy, *require* arc-second electromagnetic localization of the event.

Table 8.1: Galaxy Characteristics in LIGO Localizations

	E-LIGO			A-LIGO		
	10%	50%	90%	10%	50%	90%
GW Localization (deg <sup>2</sup> )	3	41	713	0.2	12	319
Galaxy Area (arcmin <sup>2</sup> )	4.4	26	487	0.15	20.1	185
Galaxy Number	1	31	231	1	76	676
Log Galaxy Luminosity ( $M_\odot$ )	10.3	11.2	12.1	10.9	12.0	13.0

We simulated a hundred GW events (Kasliwal et al. 2009a, in preparation) and computed the exact localization on the sky (assuming a neutron-star neutron-star merger waveform and triple coincidence data from LIGO-Hanford, LIGO-Louisiana and Virgo). The localizations range between 3–700 deg<sup>2</sup> for e-LIGO and 0.2–300 deg<sup>2</sup> for a-LIGO (range quoted between 10th and 90th

percentile). The Universe is very dynamic and the number of false positives in a single LSST image is several tens for a median localization (see Figure 8.2). Fortunately, the sensitivity-limited,

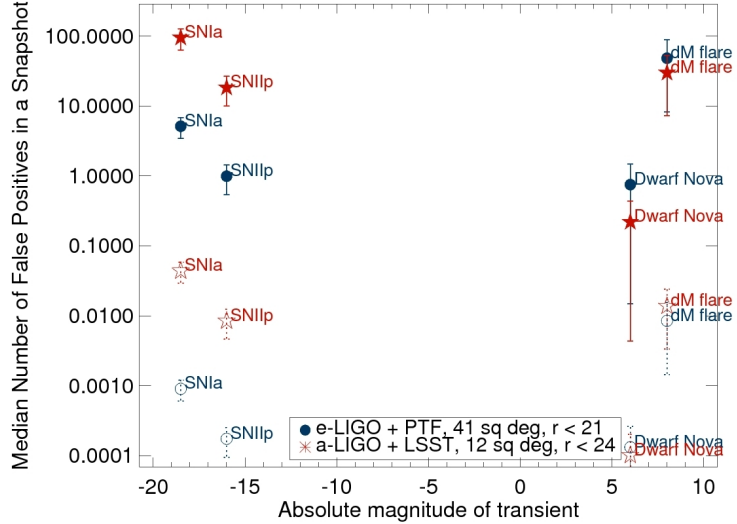


Figure 8.2: Number of false positives in a single LSST image in searching for gravitational wave events. For e-LIGO (blue circles), we assume the median localization of  $41 \text{ deg}^2$  and follow-up depth of  $r < 21$ . For a-LIGO (red stars), we use the median localization of  $12 \text{ deg}^2$  and follow-up depth of  $r < 24$ . Filled symbols denote false positives in the entire error circle and open symbols show false positives that are spatially coincident with nearby galaxies. Dwarf novae and M-dwarf (dM) flares constitute the foreground fog and the error bars on numbers represent the dependence on galactic latitude. Supernovae (Ia,IIP) constitute background haze.

$< 200 \text{ Mpc}$  horizon of GW astronomy is a blessing in disguise. The opportunity cost can be substantially reduced by restricting follow-up to those transients that are spatially coincident with galaxies within 200 Mpc. Limiting the search to the area covered by galaxies within a LIGO localization reduces a square degree problem to a square arc-minute problem — a reduction in false positives by three orders of magnitude!

Given the total galaxy light in the localization, we also find that the number of false positives due to unrelated supernovae or novae within the galaxy is negligible. To be sensitive to transients with peak absolute magnitude as faint as  $-13$  (fainter than the faintest observed short hard gamma ray burst optical afterglow), e-LIGO needs at least a 1-m class telescope for follow-up (going to  $m < 21$ , or  $50 \text{ Mpc}$ ) and a-LIGO an 8-m class ( $m < 24$ ,  $200 \text{ Mpc}$ ). Given the large numbers of galaxies within the localization (Table 8.1), a large field of view camera ( $> 5 \text{ deg}^2$ ) will help maximize depth and cadence as compared to individual pointings. Thus in the present, the Palomar Transient Factory (PTF; Law et al. 2009; § 8.2.4) is well-positioned to follow up e-LIGO events, and in the years to come, LSST to follow up a-LIGO events.

### 8.2.3 Foreground Fog and Background Haze

Unfortunately, all sorts of foreground and background transients *will* be found within the several to tens of  $\text{deg}^2$  of expected localizations. Studying each of these transients will result in significant “opportunity cost.” Ongoing projects of modest scope offer a glimpse of the pitfalls on the road

to understanding local transients. Nightly monitoring of M31 for novae (several groups) and a Palomar 60-inch program of nearby galaxies (dubbed “P60-FasTING”) designed to be sensitive to faint and fast transients already show high variance in the MMRD relation (Figure 8.3). The large scatter of the new novae suggests that in addition to the mass of the white dwarf, other physical parameters play a role (such as accretion rate, white dwarf luminosity, for example, Shara 1981).

A nightly targeted search of nearby rich clusters (Virgo, Coma, and Fornax) using the CFHT (dubbed “COVET”) and the 100-inch du Pont (Rau et al. 2008) telescopes has revealed the extensive foreground fog (asteroids, M dwarf flares, dwarf novae) and the background haze (distant, unrelated SN). However, even faint Galactic foreground objects will likely be detected in 3-4 of LSST bands. If they masquerade as transients in one band during outburst, basic classification data may be used to identify these sources and thus remove them as a source of “true” transient pollution. The pie-chart in Figure 8.4 dramatically illustrates that *new discoveries require efficient elimination of foreground and background events*.

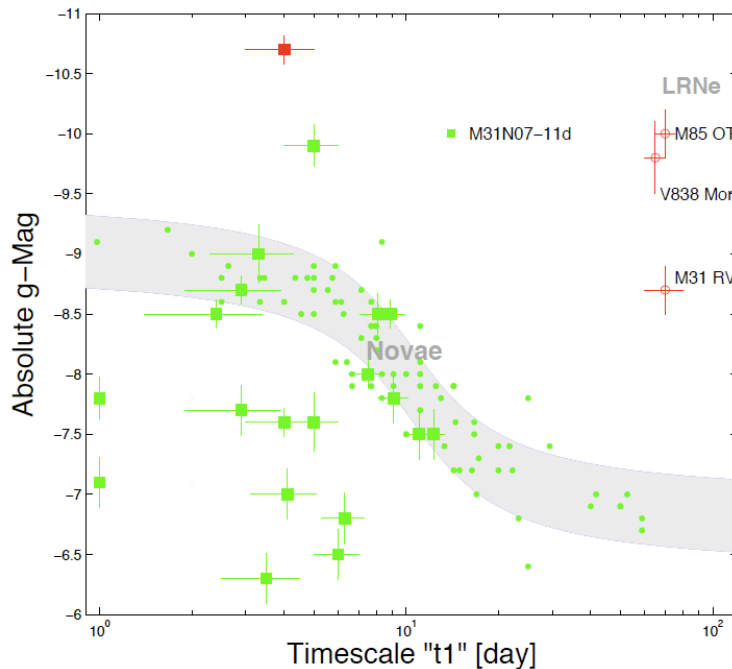


Figure 8.3: A plot of the peak absolute magnitudes versus decay timescale of novae discovered by the Palomar P60-FasTING project (low luminosity region of Figure 8.1). The shaded gray region represents the Maximum Magnitude Rate of Decline (MMRD) relationship bounded by  $\pm 3\sigma$  (Della Valle & Livio 1995). The data that defined this MMRD are shown by green circles. Squares indicate novae discovered by P60-FasTING in 2007-2008. (Preliminary results from Kasliwal et al. 2009b, in preparation.)

#### 8.2.4 The Era of Synoptic Imaging Facilities

There is widespread agreement that we are now on the threshold of the era of synoptic and wide field imaging at optical wavelengths. This is best illustrated by the profusion of operational (Palomar Transient Factory, Pan-STARRS1), imminent (SkyMapper, VST, ODI), and future facilities (LSST).

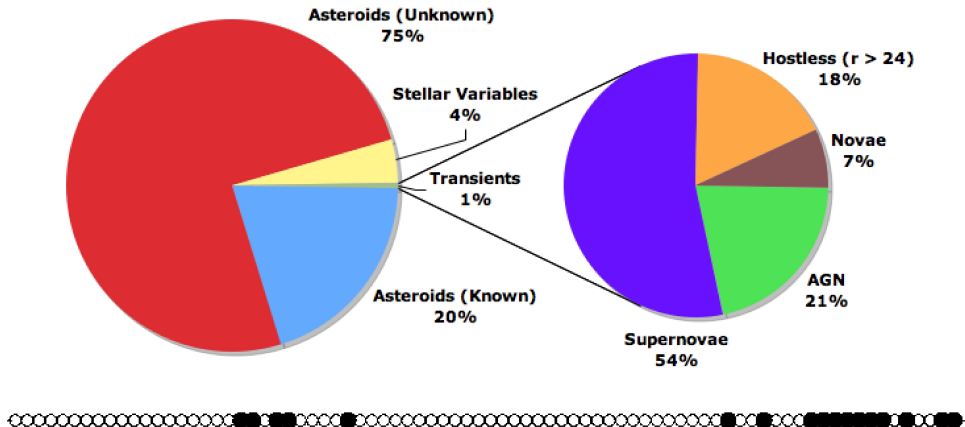


Figure 8.4: 28 COVET transients were discovered during a pilot run in 2008A (7 hours) – two novae and the remainder background supernovae and AGN. Transients with no point source or galaxy host to a limiting magnitude of  $r > 24$  are classified as hostless. Of the 2,800 candidates, the COVET pipeline automatically rejected 99% as asteroids or Galactic objects. (Preliminary version from Kasliwal et al. 2009c, in preparation.)

In Table 8.2 and Figure 8.5, we present current best estimates for the rates of various events and the “grasp” of different surveys.

Table 8.2: Properties and Rates for Optical Transients<sup>a</sup>

Class	$M_v$ [mag]	$\tau^b$ [days]	Universal Rate (UR)	PTF Rate [yr $^{-1}$ ]	LSST Rate [yr $^{-1}$ ]
Luminous red novae	-9.. - 13	20..60	$(1..10) \times 10^{-13} \text{ yr}^{-1} L_{\odot,K}^{-1}$	0.5..8	80..3400
Fallback SNe	-4.. - 21	0.5..2	$< 5 \times 10^{-6} \text{ Mpc}^{-3} \text{ yr}^{-1}$	<3	<800
Macronovae	-13.. - 15	0.3..3	$10^{-4}..-8 \text{ Mpc}^{-3} \text{ yr}^{-1}$	0.3..3	120..1200
SNe Ia	-15.. - 17	2..5	$(0.6..2) \times 10^{-6} \text{ Mpc}^{-3} \text{ yr}^{-1}$	4..25	1400..8000
SNe Ia	-17.. - 19.5	30..70	<sup>c</sup> $3 \times 10^{-5} \text{ Mpc}^{-3} \text{ yr}^{-1}$	700	200000 <sup>d</sup>
SNe II	-15.. - 20	20..300	$(3..8) \times 10^{-5} \text{ Mpc}^{-3} \text{ yr}^{-1}$	300	100000 <sup>d</sup>

<sup>a</sup>Table from Rau et al. (2009b); see references therein. <sup>b</sup>Time to decay by 2 magnitudes from peak. <sup>c</sup>Universal rate at  $z < 0.12$ . <sup>d</sup>From M. Wood-Vasey, personal communication.

The reader should be cautioned that many of these rates are very rough. Indeed, the principal goal of the Palomar Transient Factory is to accurately establish the rates of foreground and background events. Finding a handful of rare events with PTF will help LSST to define the metrics needed to identify these intriguing needles in the haystack. It is clear from Figure 8.5 that *the impressive grasp of LSST is essential to uncovering and understanding the population of these rare transient events in the Local Universe*.

### 8.3 Explosive Transients in the Distant Universe

Przemek Wozniak, Shrinivas Kulkarni, W. N. Brandt, Ehud Nakar, Arne Rau, A. Gal-Yam, Mansi

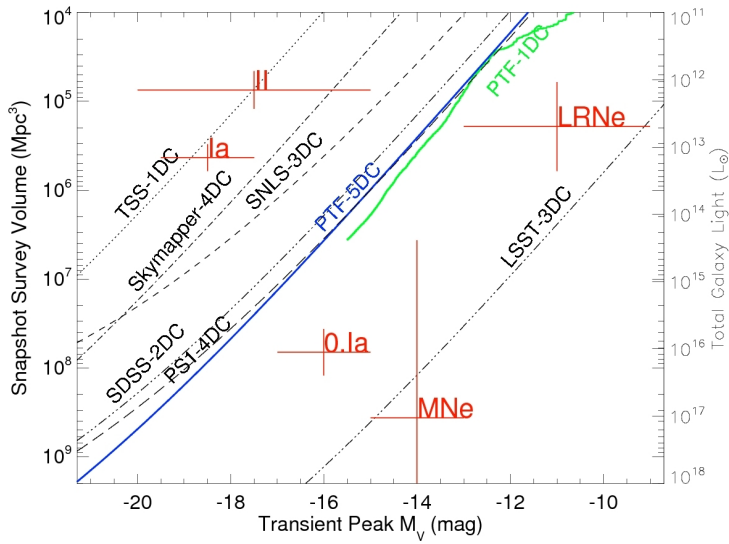


Figure 8.5: Volume probed by various surveys as a function of transient absolute magnitude. The cadence period to cover the volume is shown in days: e.g., 5DC for a five-day cadence. Red crosses represent the minimum survey volume needed to detect a single transient event (the uncertainty in the y-axis is due to uncertainty in rates). Palomar Transient Factory (PTF-5DC, blue-solid) is more sensitive than Texas Supernova Search (TSS, dotted), SkyMapper (dot-dashed), Supernova Legacy Survey (SNLS-3DC, dashed), and SDSS Supernova Search (SDSS-2DC, double-dot dashed), and is competitive with PanSTARRS-1 (PS1-4DC, long dashed). Lines for each survey represent one transient event in the specified cadence period. PTF-1D (green solid line) represents a targeted  $800 \text{ deg}^2$  survey probing luminosity concentrations in the local Universe, with a factor of three larger effective survey volume than a blind survey with same solid angle. PTF will discover hundreds of supernovae and possibly several rare events such as “0.Ia”, Luminous Red Novae (LRNe) and Macronovae (MNe) per year. The LSST (Deep Wide Fast Survey) will discover hundreds of rare events in the Local Universe. The corresponding plot for distant cosmological transients is shown in Figure 8.10. (Adapted from figure by Bildsten et al. 2009, in preparation.)

*Kasliwal, Derek B. Fox, Joshua S. Bloom, Michael A. Strauss, James E. Rhoads*

We now discuss the role of LSST in discovering and understanding cosmological transients. The phase space of transients (known and anticipated) is shown in Figure 8.6. The region marked by a big question mark is at present poorly explored and in some sense represents the greatest possible rewards from a deep wide field survey such as LSST. Here, we discuss a few example areas in which LSST will provide exciting new discoveries and insights. We leave the discussion of transient fueling events in active galactic nuclei due to tidal disruption of stars by the central black hole to § 10.6.

### 8.3.1 Orphan GRB Afterglows

Gamma-ray bursts (GRBs) are now established to be the most relativistic (known) explosions in the Universe and as such are associated with the birth of rapidly spinning stellar black holes. We believe that long duration GRBs result from the deaths of certain types of massive stars (Woosley & Bloom 2006). The explosion is deduced to be conical (“jetted”) with opening angles ranging from less than a degree to a steradian. The appearance of the explosion depends on the location of the observer (Figure 8.7). An on-axis observer sees the fastest material and thus a highly

beamed emission of gamma rays. The optical afterglow emission arises from the interaction of the relativistic debris and the circumstellar medium. Due to decreasing relativistic beaming in the decelerating flow, the light curve will show a characteristic break to a steeper decline at  $t_{\text{jet}} \sim 1\text{--}10$  days after the burst (Rhoads 1999; Sari et al. 1999). An observer outside the cone of the jet misses the burst of gamma-ray emission, but can still detect the subsequent afterglow emission (Rhoads 1997). The light curve will first rise steeply and then fade by  $\sim 1$  mag over a timescale of roughly  $\Delta t \sim 1.5t_{\text{jet}}$  (days to weeks). We will refer to these objects as “off-axis” orphan afterglows. The “beaming fraction” (the fraction of sky lit by gamma-ray bursts) is estimated to be between 0.01 and 0.001, i.e., the true rate of GRBs is 100 to 1000 times the observed rate. Since a supernova is not relativistic and is spherical, all observers can see the supernovae that accompany GRBs. Finally, there may exist entire classes of explosive events which are not as relativistic as GRBs (e.g., the so-called “X-ray Flashes” are argued to be one such category; one can imagine “UV Flashes,” and so on). Provided the events have sufficient explosive yield, their afterglows will also exhibit the behavior shown in Figure 8.7 (case B). We will call these “on-axis” afterglows with unknown parentage.

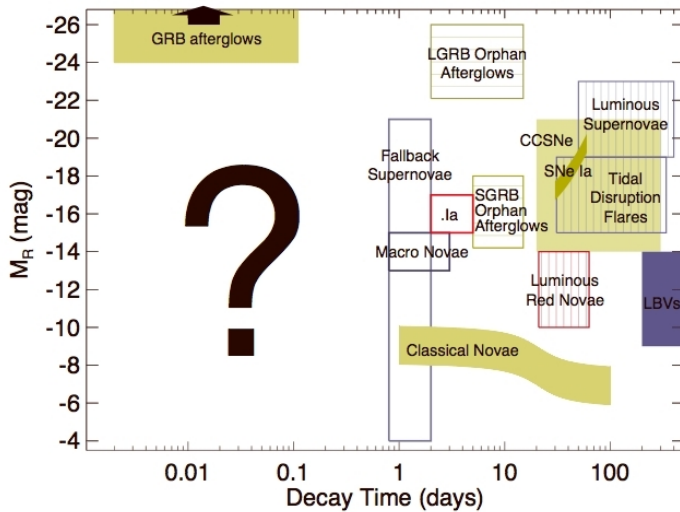


Figure 8.6: Discovery space for cosmic transients. Peak absolute  $r$ -band magnitude is plotted vs. decay timescale (typically the time to fade from peak by  $\sim 2$  mag) for luminous optical transients and variables. Filled boxes mark well-studied classes with a large number of known members (classical novae, SNe Ia, core-collapse supernovae, luminous blue variables (LBVs)). Vertically hatched boxes show classes for which only a few candidate members have been suggested so far (luminous red novae, tidal disruption flares, luminous supernovae). Horizontally hatched boxes are classes which are believed to exist, but have not yet been detected (orphan afterglows of short and long GRBs). The positions of theoretically predicted events (fall back supernovae, macronovae, 0.Ia supernovae (.Ia)) are indicated by empty boxes. The brightest transients (on-axis afterglows of GRBs) extend to  $M_R \sim -37.0$ . The color of each box corresponds to the mean  $g - r$  color at peak (blue,  $g - r < 0$  mag; green,  $0 < g - r < 1$  mag; red,  $g - r > 1$  mag). LSST will be sensitive to transients with a wide range of time scales and will open for exploration new parts of the parameter space (question mark). Figure adapted from Rau (2008).

Pending SKA<sup>3</sup>, the most efficient way to detect all three types of events discussed above is via synoptic imaging of the optical sky. Statistics of off-axis afterglows, when compared to GRBs, will

<sup>3</sup>Square Kilometer Array, planned for the next decade, is designed to cover an instantaneous field of view of 200 deg<sup>2</sup> at radio frequencies below 1 GHz.

yield the so-called “beaming fraction,” and more importantly, the true rate of GRBs. The total number of afterglows brighter than  $R \sim 24$  mag visible per sky at any given instant is predicted to be  $\sim 1,000$ , and rapidly decreases for less sensitive surveys (Totani & Panaiteescu 2002). With an average afterglow spending 1–2 months above that threshold, we find that monitoring 10,000 deg<sup>2</sup> every  $\sim 3$  days with LSST will discover 1,000 such events per year. LSST will also detect “on-axis” afterglows. The depth and cadence of LSST observations will, in many cases, allow the on- or off-axis nature of a fading afterglow to be determined by careful light curve fitting (Rhoads 2003). Continuous cross-correlation of optical light curves with detections by future all-sky high energy missions (e.g., EXIST) will help establish the broad-band properties of transients, including the orphan status of afterglows.

In Figure 8.8 we show model predictions of the forward shock emission from a GRB jet propagating into the circumstellar medium. The ability of LSST to detect GRB afterglows, and the off-axis orphan afterglows in particular, is summarized in Figure 8.9. Time dilation significantly increases the probability of detecting off-axis orphans at redshifts  $z > 1$  and catching them before or near the peak light. The peak optical flux of the afterglow rapidly decreases as the observer moves away from the jet. At  $\theta_{\text{obs}} \simeq 20^\circ$  only the closest events ( $z < 0.5$ ) are still accessible to LSST and even fewer will have well-sampled light curves. However, the true rate of GRBs and the corresponding rate of the off-axis orphans are highly uncertain. Indeed, the discovery of orphan GRB afterglows will greatly reduce that uncertainty.

It is widely agreed that the detailed study of the associated supernovae is the next critical step in GRB astrophysics, and synoptic surveys will speed up the discovery rate by at least a factor of 10 relative to GRB missions. Finally, the discovery of afterglows with unknown parentage will open up entirely new vistas in studies of stellar deaths, as we now discuss.

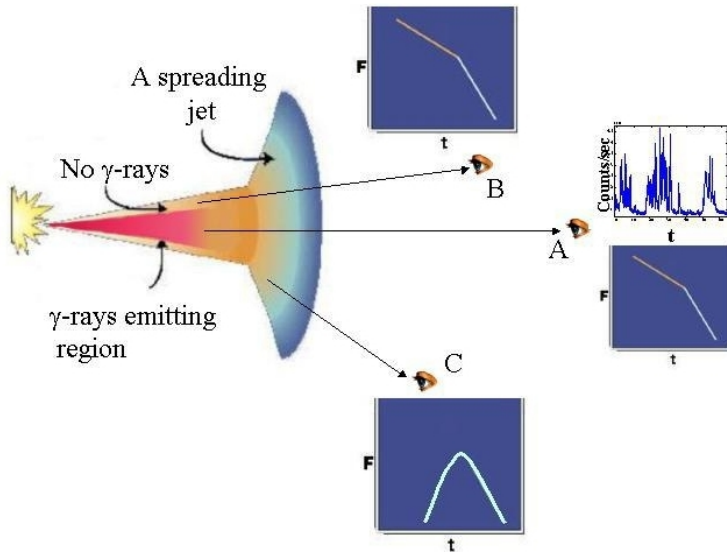


Figure 8.7: Geometry of orphan GRB afterglows. Observer A detects both the GRB and an afterglow. Observer B does not detect the GRB due to a low Lorentz factor of material in the line of sight, but detects an on-axis orphan afterglow that is similar to the one observed by A. Observer C detects an off-axis orphan afterglow with the flux rise and fall that differs from the afterglow detected by observers A and B (from Nakar & Piran 2003).

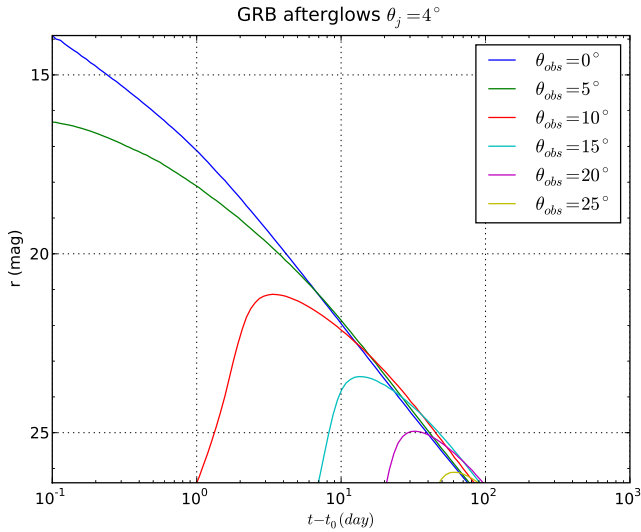


Figure 8.8: Predicted light curves of GRB afterglows. The model of the forward shock emission is from Totani & Panaiteescu 2002 (code courtesy of Alin Panaiteescu). The adopted global and microphysical parameters reproduce the properties of well observed GRBs: jet half opening angle  $\theta_j = 4^\circ$ , the isotropic equivalent energy of  $E_{\text{iso}} = 5 \times 10^{53}$  erg, ambient medium density  $n = 1 \text{ g cm}^{-3}$ , and the slope of the electron energy distribution  $p = 2.1$ . The apparent  $r$ -band magnitudes are on the AB scale assuming a source redshift  $z = 1$  and a number of observer locations with respect to the jet axis  $\theta_{\text{obs}}$ .

### 8.3.2 Hybrid Gamma-Ray Bursts

The most popular explanation for the bimodal distribution of GRB durations invokes the existence of two distinct physical classes. Long GRBs typically last 2–100 seconds and tend to have softer  $\gamma$ -ray spectra, while short GRBs are typically harder and have durations below  $\sim 2$  seconds, sometimes in the millisecond range (see review in Nakar & Piran 2003). Short GRBs are expected to result from compact binary mergers (NS-NS or NS-BH), and the available limits rule out any significant supernova component in optical emission (Bloom et al. 2006; Fox et al. 2005).

Recent developments suggest a richer picture. Deep imaging of GRB 060614 (Gal-Yam et al. 2006; Della Valle et al. 2006; Fynbo et al. 2006) and GRB 060505 (Ofek et al. 2007b; Fynbo et al. 2006) exclude a supernova brighter than  $M_V \sim -11$ . The data for GRB 060614 rule out the presence of a supernova bump in the afterglow light curve up to a few hundred times fainter than bumps seen in other bursts. The host galaxy of this burst shows a smooth morphology and a low star formation rate that are atypical for long GRB hosts (Gal-Yam et al. 2006). A very faint (undetected) event could have been powered with a small amount of  $^{56}\text{Ni}$  (e.g., Fynbo et al. 2006), as in the original collapsar model with a relativistic jet, but without a non-relativistic explosion of the star (Woosley 1993). Such events would fall in the luminosity gap between novae and supernovae discussed in § 8.2. Alternatively, a new explosion mechanism could be at play.

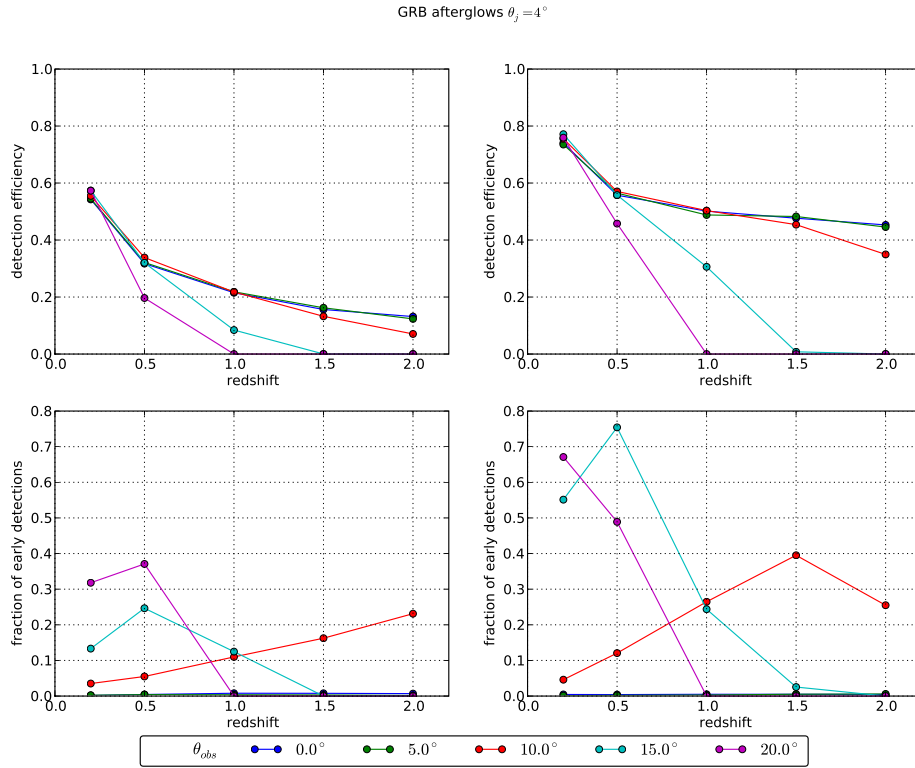


Figure 8.9: Predicted efficiency of detecting GRB afterglows in LSST (upper) and the fraction of early detections (lower) using models from Figure 8.8. The main survey area (left) is compared to the seven deep drilling fields (right). The efficiency calculation assumes that a transient is detected as soon as variability by 0.1 mag with  $S/N > 10$  from at least two  $5\sigma$  detections can be established. The early detections are those that occur before the maximum light or within 1 mag of the peak on the fading branch.

### 8.3.3 Pair-Instability and Anomalous Supernovae

The first stars to have formed in the Universe were likely very massive ( $M > 100M_{\odot}$ ) and died as a result of thermonuclear runaway explosions triggered by  $e^+e^-$  pair production instability and the resulting initial collapse. The predicted light curve of a pair-instability supernova is quite sensitive to the initial mass and radius of the progenitor with the brightest events exceeding  $M_V \sim -22$  at maximum, lasting hundreds of days and sometimes showing more than one peak (Kasen et al. 2008). The pair instability should not take place in metal-enriched stars, so the best place to look for the first stellar explosions is the distant Universe at  $z \geq 5$ , where events would appear most luminous in the  $K$  band and take up to 1,000 days to fade away due to cosmological time dilation. Short of having an all-sky survey sensitive down to  $K_{AB} = 25$ , the best search strategy is a deep survey in red filters on a cadence of a few days and using monthly co-added images to boost the sensitivity.

Recently, there have been random discoveries of anomalously bright (e.g., SN 2005ap; Quimby et al. 2007) and in one case also long-lived (SN 2006gy; Ofek et al. 2007a) supernovae in the Local Universe. While there is no compelling evidence that these objects are related to explosive pair instability, there is also no conclusive case that they are not. In fact, star formation and metal

enrichment are very localized processes and proceed throughout the history of the Universe in a very non-uniform fashion. Pockets of very low metallicity material are likely to exist at moderate redshifts ( $z \sim 1 - 2$ ), and some of those are expected to survive to present times (Scannapieco et al. 2005). The anticipated discoveries of pair-instability SN and the characterization of their environments can potentially transform our understanding of the interplay between the chemical evolution and structure formation in the Universe.

### 8.3.4 The Mysterious Transient SCP 06F6

The serendipitous discovery of the peculiar transient SCP 06F6 (Barbary et al. 2009) has baffled astronomers, and its unique characteristics have inspired many wild explanations. It had a nearly symmetric light curve with an amplitude  $>6.5$  mag over a lifetime of about 200 days with no evidence of a quiescent host galaxy or star at that position down to  $i > 27.5$  mag. Its spectrum was dissimilar to any transient or star ever seen before, and its broad absorption features have been identified tentatively as redshifted Swan bands of molecular carbon. One of the suggested explanations (Gaensicke et al. 2008) postulates an entirely new class of supernovae – a core collapse of a carbon star at redshift  $z = 0.143$ . However, the X-ray flux being a factor of ten more than the optical flux and the very faint host ( $M > -13.2$ ) appear inconsistent with this idea. Soker et al. (2008) proposed that the emission comes from a CO white dwarf being tidally ripped by an intermediate mass black hole in the presence of a strong disk wind. Another extragalactic hypothesis is that the transient originated in a thermonuclear supernova explosion with an AGB carbon star companion in a dense medium. A Galactic scenario involves an asteroid at a distance of 1.5 kpc ( $\sim 300$  km across; mass  $\sim 10^{19}$  kg) colliding with a white dwarf in the presence of very strong magnetic fields. The nature of this transient remains unknown.

### 8.3.5 Very Fast Transients and Unknown Unknowns

As can be seen from Figure 8.6 the discovery space of fast transients lasting from seconds to minutes is quite empty.

On general grounds there are two distinct families of fast transients: incoherent radiators (e.g.,  $\gamma$ -ray bursts and afterglows) and coherent radiators (e.g., pulsars, magnetar flares). It is a well-known result that incoherent synchrotron radiation is limited to a brightness temperature of  $T_b \sim 10^{12}$  K. For such radiators to be detectable from any reasonable distance (kpc to Gpc) there must be a relativistic expansion toward the observer, so that the source appears brighter due to the Lorentz boost. Coherent radiators do not have any such limitation and can achieve very high brightness temperature (e.g.,  $T_b \sim 10^{37}$  K in pulsars).

Scanning a large fraction of the full sky on a time scale of  $\sim 1$  minute is still outside the reach of large optical telescopes. However, large telescopes with high étendue operating on a fast cadence will be the first to probe a large volume of space for low luminosity transients on very short time-scales. One of the LSST mini-surveys, for example, will cover a small number of  $10 \text{ deg}^2$  fields every  $\sim 15$  seconds for about an hour out of every night (Ivezić et al. 2008). Fast transients can also be detected by differencing the standard pair of 15-second exposures taken at each LSST visit. Given the exceptional instantaneous sensitivity of LSST and a scanning rate of  $3,300 \text{ deg}^2$  per night, we

can expect to find contemporaneous optical counterparts to GRBs, early afterglows, giant pulses from pulsars, and flares from anomalous X-ray pulsars. But perhaps the most exciting findings will be those that cannot be named before we look. The vast unexplored space in Figure 8.6 suggests new discoveries lie in wait.

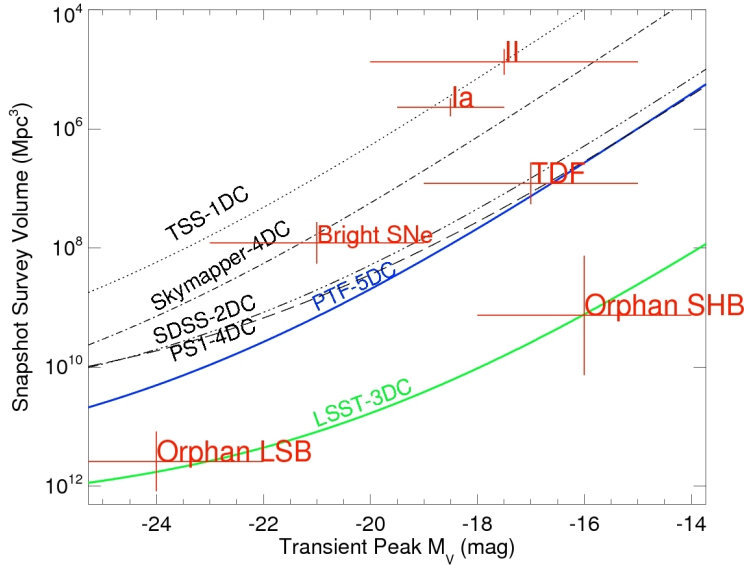


Figure 8.10: Volume probed by various surveys as a function of transient absolute magnitude. The cadence period to cover the volume is shown in days: e.g., 5DC for a five-day cadence. Red crosses represent the minimum survey volume needed to detect a single transient event. The uncertainties in the rates and luminosities translate to the displayed “error.” LSST will cover  $10,000 \text{ deg}^2$  every three days down to the limiting magnitude  $r = 24.7$ , and will have the grasp to detect rare and faint events such as orphan afterglows of Long Soft Bursts (LSB) and Short Hard Bursts (SHB) out to large distances in a single snapshot. The main LSST survey will also discover a large number of Tidal Disruption Flares (TDF). Palomar Transient Factory (PTF-5DC, blue-solid) is more sensitive than Texas Supernova Search (TSS, dotted), SkyMapper (dot-dashed), Supernova Legacy Survey (SNLS-3DC, dashed), and SDSS Supernova Search (SDSS-2DC, double-dot dashed) and competitive with PanSTARRS-1 (PS1-4DC, long dashed). Lines for each survey represent one transient event in specified cadence period. For example, TSS discovers one type Ia supernova every day – however, since type Ia supernovae have a lifetime of one month, TSS discovers the same type Ia supernova for a month. The corresponding plot for transients in the Local Universe is shown in Figure 8.5. (Original figure provided by L. Bildsten, UCSB.)

## 8.4 Transients and Variable Stars in the Era of Synoptic Imaging

*Ashish A. Mahabal, Przemek Wozniak, Ciro Donalek, S.G. Djorgovski*

The way we learn about the world was revolutionized when computers—a technology which had been around for more than 40 years—were linked together into a global network called the World Wide Web and real-time search engines such as Google, were first deployed. Similarly, the next generation of wide field surveys is positioned to revolutionize the study of astrophysical transients by linking heterogeneous surveys with a wide array of follow-up instruments as well as rapid dissemination of the transient events using various mechanisms on the Internet.

Table 8.3: Properties and Rates for Optical Cosmological Transients<sup>a</sup>

Class	$M_v$	$\tau^b$	Universal Rate (UR)	LSST Rate
	[mag]	[days]		[yr <sup>-1</sup> ]
Tidal disruption flares (TDF)	−15.. −19	30..350	$10^{-6}$ Mpc <sup>−3</sup> yr <sup>−1</sup>	6,000
Luminous SNe	−19.. −23	50..400	$10^{-7}$ Mpc <sup>−3</sup> yr <sup>−1</sup>	20,000
Orphan afterglows (SHB)	−14.. −18	5..15	$3 \times 10^{-7..-9}$ Mpc <sup>−3</sup> yr <sup>−1</sup>	~10–100
Orphan afterglows (LSB)	−22.. −26	2..15	$3 \times 10^{-10..-11}$ Mpc <sup>−3</sup> yr <sup>−1</sup>	1,000
On-axis GRB afterglows	.. − 37	1..15	$10^{-11}$ Mpc <sup>−3</sup> yr <sup>−1</sup>	~50

<sup>a</sup>Universal rates from Rau et al. (2009a); see references therein.

<sup>b</sup>Time to decay by 2 magnitudes from peak.

In Figure 8.10 we compare the ability of various surveys to detect cosmological transients. LSST will be the instrument of choice for finding very rare and faint transients, as well as probing the distant Universe ( $z \sim 2 – 3$ ) for the most luminous events. It will have data collecting power more than 10 times greater than any existing facility, and will extend the time-volume space available for systematic exploration by three orders of magnitude. In Table 8.3 we summarize the expected event rates of cosmological transients that LSST will find.

The main challenges ahead of massive time-domain surveys are timely recognition of interesting transients in the torrent of imaging data, and maximizing the utility of the follow-up observations (Tyson 2006). For every orphan afterglow present in the sky there are about 1,000 SNe Ia (Totani & Panaiteescu 2002) and millions of other variable objects (quasars, flaring stars, microlensing events). LSST alone is expected to deliver tens of thousands of astrophysical transients every night. Accurate event classification can be achieved by assimilating on the fly the required context information: multi-color time-resolved photometry, galactic latitude, and possible host galaxy information from the survey itself, combined with broad-band spectral properties from external catalogs and alert feeds from other instruments—including gravitational wave and neutrino detectors. While the combined yield of transient searches in the next decade is likely to saturate the resources available for a detailed follow-up, it will also create an unprecedented opportunity for discovery. Much of what we know about rare and ephemeral objects comes from very detailed studies of the best prototype cases, the “Rosetta Stone” events. In addition to the traditional target of opportunity programs that will continue to play a vital role, over the next few years we will witness a global proliferation of dedicated rapid follow-up networks of 2-m class imagers and low resolution spectrographs (Tsapras et al. 2009; Hidas et al. 2008). But in order to apply this approach to extremely data intensive sky monitoring surveys of the next decade, a fundamental change is required in the way astronomy interacts with information technology (Borne et al. 2008).

Filtering time-critical actionable information out of  $\sim 30$  Terabytes of survey data per night (Ivezic et al. 2008) is a challenging task (Borne 2008). In this regime, the system must be capable of automatically optimizing the science potential of the reported alerts and allocating powerful but scarce follow-up instruments. In order to realize the science goals outlined in previous sections, the future sky monitoring projects must integrate state of the art information technology such as computer vision, machine learning, and networking of the autonomous hardware and software components. A major investment is required in the development of hierarchical, distributed decision engines

capable of “understanding” and refining information such as partially degenerate event classifications and time-variable constraints on follow-up assets. A particularly strong emphasis should be placed on: 1) new classification and anomaly detection algorithms for time-variable astronomical objects, 2) standards for real-time communication between heterogeneous hardware and software agents, 3) new ways of evaluating and reporting the most important science alerts to humans, and 4) fault-tolerant network topologies and system architectures that maximize the usability. The need to delegate increasingly complex tasks to machines is the main driver behind the emerging standards for remote telescope operation and event messaging such as RTML (Remote Telescope Markup Language), VOEvent and SkyAlert ([Williams et al. 2009](#)). These innovations are gradually integrated into working systems, including the GRB Coordinates Network (GCN), a pioneering effort in rapid alert dissemination in astronomy. The current trend will continue to accelerate over the next decade.

By the time LSST starts getting data, the field of time domain astronomy will be much richer in terms of availability of light curves and colors for different types of objects. Priors, in general, will be available for a good variety of objects. LSST will add to this on a completely different scale in terms of cadence, filters, number of epochs, and so on. Virtual Observatory (VO) tools that link new optical transient data with survey and archival data at other wavelengths are already proving useful. Newer features being incorporated include semantic linking as well as follow-up information in the form of a portfolio based on expert inputs, active automated follow-up in the form of new data from follow-up telescopes as well as passive automated follow-up in terms of context-based annotators such as galaxy proximity, apparent motion, and so on, which help in the classification process.

Since a transient is an object that has not been seen before (by definition), we are still in the data paucity regime, except for the possibility that similar objects are known. The approach to reliable classification involves the following steps: 1) quick initial classification, involving rejection of several classes and shortlisting a few likely classes, 2) deciding which possible follow-up resources are likely to disambiguate the possible classes best, 3) obtaining the follow-up, 4) reclassification by folding in the additional data. This schema can then be repeated if necessary. All these steps can be carried out using Bayesian formalism.

1) Quick initial classification can be done using a) a Bayesian Network, and/or b) Gaussian Process Regression. The advantage of the Bayesian Network over some other Machine Learning applications is that it can operate better when some or most of the input data are missing. The best approach is to use both the Bayesian and Machine Learning approaches playing those to their strengths. The inputs from the priors of different classes are colors, contextual information, light curves, and spectra. With a subset of these available for the transient, one can get probabilities of that object belonging to the different classes. [Figure 8.11](#) represents such a schematic including both Bayesian and Machine Learning. There is a lot of work that still needs to be done on this topic. Currently the priors for different classes are very non-uniform in terms of number of examples in different magnitude ranges, sampling rates, length of time, and so on. Moreover, to understand transients, we will have to understand variables better. A resource such as Gaia will be exceptional in this regard.

Gaussian Process Regression, illustrated in [Figure 8.12](#), is a technique can be used to build template average light curves if they are reasonably smooth. One can use the initial LSST epochs

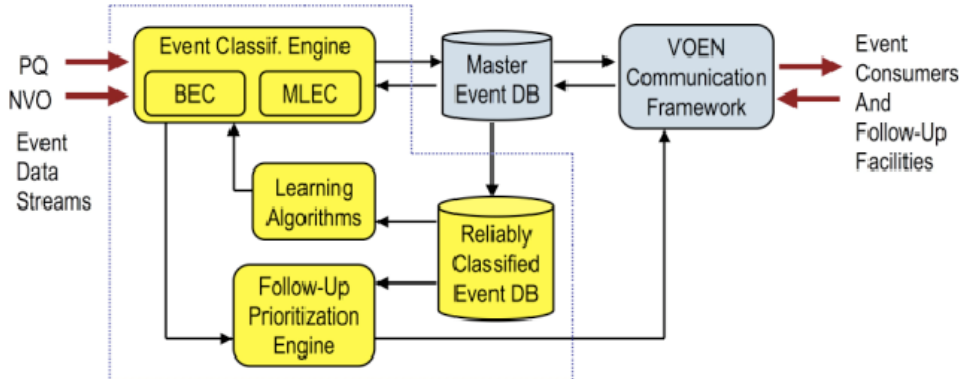


Figure 8.11: A schematic illustration of the desired functionality of the Bayesian Event Classification (BEC) engine for classifying variables and transients. The input is generally sparse discovery data, including brightness in various filters, possibly the rate of change, position, possible motion, etc., and measurements from available multi-wavelength archives; and a library of priors giving probabilities for observing these particular parameters if the event belongs to a class X. The output is an evolving set of probabilities of belonging to various classes of interest. Figure reproduced with permission from [Mahabal et al. \(2008a\)](#).

to determine if the transient is likely to belong to such a class and if so, at what stage of evolution/periodicity it lies.

2) Spectroscopic follow-up for all transients is not possible. Different research groups are inherently interested in different types of objects as well as different kinds of science. Some observatories are already beginning the process of evaluating optimal modes and spectroscopic instruments for maximal use of LSST transient data. A well-designed follow-up strategy must include end-to-end planning and must be in place before first light.

The very first observations of a transient may not reveal its class right away, and follow-up photometric observations will be required for a very large number of objects. Here too there will be a choice between different bands, available apertures, and sites. For example, follow-up with a specific cadence may be necessary for a suspected eclipsing binary, but with a very different cadence for a suspected nova. Follow-up resource prioritization can be done by choosing a set-up that reduces the classification uncertainty most. One way of accomplishing this is to use an information/theoretic approach ([Loredo & Chernoff 2003](#)) by quantifying the classification uncertainty using the conditional entropy of the posterior for  $y$ , given all the available data – in other words, by quantifying the remaining uncertainty in  $y$  given a set of “knowns” (the data). When an additional observation,  $x_+$ , is taken, the entropy (denoted here as  $H$ ) decreases from  $H(y|x_0)$  to  $H(y|x_0, x_+)$ . This is illustrated in [Figure 8.13](#), where the original classification,  $p(y|x_0)$ , is ambiguous and may be refined in one of two ways. The refinement for particular observations,  $x_A$  versus  $x_B$ , is shown.

3) For fast or repeating transients, the LSST deep drilling sub-survey ([§ 2.1](#)) will yield the highest quality data with excellent sampling. Much of the transient science enabled by LSST will rely on additional observations of selected transient objects on other facilities based on early classification using the LSST data. Some of the additional observations will be in follow-up mode, while others will be in a co-observing mode in which other multi-wavelength facilities monitor the same sky during LSST operations. For relatively bright transients, smaller robotic telescopes around the

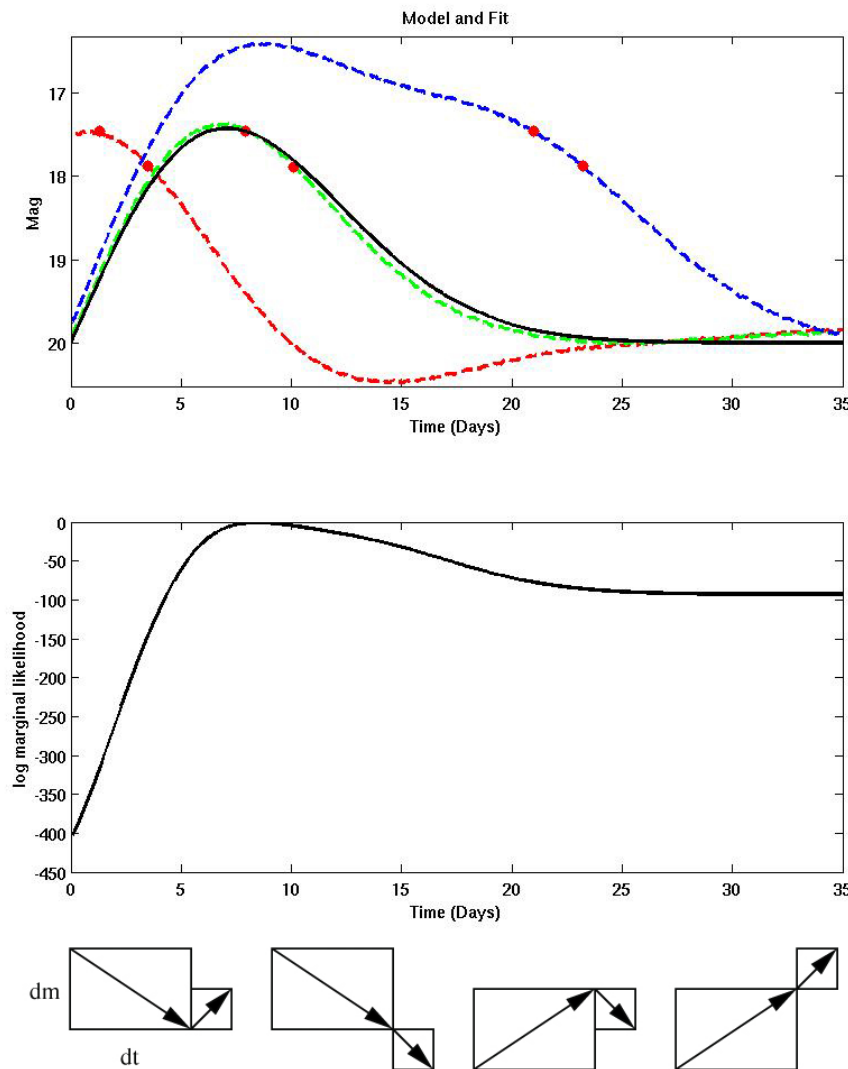


Figure 8.12: Illustrated here is the use of the Gaussian Process Regression (GPR) technique to determine the likelihood that a newly detected transient is a supernova. The solid line in the first panel is a model obtained using GPR. The two observed points with given change in magnitude,  $dm$ , over the corresponding time interval,  $dt$ , allow one to estimate which phase of the model they are likely to fit best. Three specific epochs are shown as dotted lines. The second panel shows the log marginal likelihood that the pair of observed points correspond to the entire model light curve. In order to make the best estimate for the class of a given transient, a similar likelihood curve has to be obtained for models of different variable types. These model curves are obtained using covariance functions, where different types of variability require the use of different covariance functions. As more observed points become available for comparison, a progressively larger number of previously competing hypotheses can be eliminated, thus strengthening the classification. The boxes below the second panel show the distinct possibilities when three observations are present: in each case, the larger box represents the two previously known data points, which are decreasing in  $dm/dt$ , while the smaller box indicates the direction of the light curve based on the new data point. For example, the first of the possibilities begins to brighten after initially decreasing in brightness, which is inconsistent with the behavior of a supernova light curve. The three other possibilities, where the object continues to dim, dims after an initial brightening, or continues to brighten, would all be consistent with different phases in a SN light curve. Figure reproduced with permission from Mahabal et al. (2008b, Figure 2).

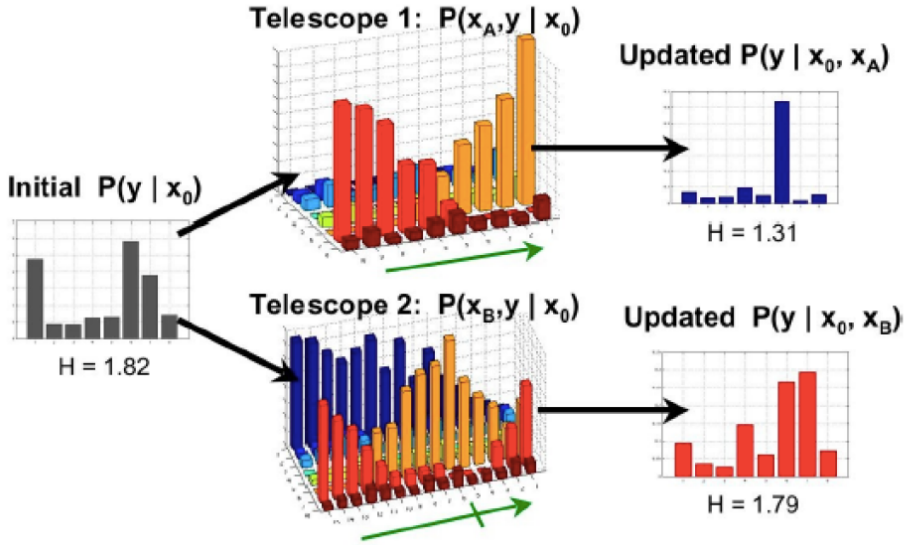


Figure 8.13: A schematic illustration of follow-up observation recommendations: At left, the initial estimated per-class probabilities for eight object classes, showing high entropy resulting from ambiguity between the object classes numbered 1, 6, and 7. Follow-up observations from two telescopes are possible (center). Their resolving capacity is shown as a function of class  $y$  (left axis) and observed value (right axis parallel to green arrows). In the diagram, for telescope 1, as observed value,  $x_A$ , moves up the green arrow, class 6 becomes increasingly preferred. For telescope 2, moderate values (near the crossbar in the arrow) indicate class 6, and other values indicate class 7. Finally, at right, are typical updated classifications. The lower-entropy classification at the top is preferred. Since the particular values used for refinement ( $x_A, x_B$ ) are unknown at decision time, appropriate averages of entropy must be used, as described in the text. Figure reproduced with permission from Mahabal et al. (2008a, Figure 3).

world can be deployed for follow-up. An example is the Las Cumbres Observatory Global Telescope Network of 2-m telescopes and photometric + IFU instruments dedicated to follow-up.

The information from these follow-up observations needs to be fed back to the LSST classification. VO tools and transient portfolios will allow LSST and non-LSST observations of the same object to be properly grouped for the next iteration of classification.

4) Together with any such new data the classification steps are repeated until a set threshold is reached (secure classification, or  $\Delta t$  exceeded for best classification, or classification entropy cannot be decreased further with available follow-up resources, etc.) In addition to semantic linking mentioned earlier, iterated and interleaved citizen science and expert plus machine learning classification will be heavily used.

#### 8.4.1 Prospects for Follow-up and Co-observing

LSST will probe 100 times more volume than current generation transient searches such as Pan-STARRS1 and PTF. It will also have somewhat faster cadence and superb color information in six photometric bands. Much of the science on repeating transients as well as on explosive one-time events will be accomplished largely from the LSST database, combined with other multi-wavelength

data sets. The logarithmic cadence of the primary survey and the deep drilling sub-survey are designed to optimize the time sampling for a wide range of variability patterns, both known and predicted from theory. As the number of multi-wavelength facilities continuously observing various areas of the sky continues to grow, “co-observing” is becoming an increasingly important avenue to discovery. However, in order to maximize the science return of LSST, a well designed program of detailed follow-up observations for a smaller sample of carefully selected transients will be required.

LSST is expected to deliver data on tens of thousands of transients every night. By the time of the initial alert, the survey will have collected detailed information on the presence, morphology, and photometric properties of the host galaxy, including a photometric redshift. For a majority of transients, existing catalogs will provide useful limits on the progenitor across the electromagnetic spectrum, and for some sources a positive identification can be made. A small fraction of the best candidates for follow-up will have a high energy identification and possibly a simultaneous detection by one of the next-generation all-sky monitors such as EXIST to follow the Swift and Fermi missions. With the help of expert systems based on Bayesian belief and decision networks, the long list of ongoing transients will be prioritized on science potential. Transients will naturally fall into two categories: 1) rare bright events and/or well covered transients with the most complete data and frequently found well before the peak light and 2) numerous fainter (22-24th mag) objects with less coverage, but suitable for statistical studies.

Transients in the first category will be relatively rare, and efficient follow-up would focus on one object at a time. New classes of exotic transients can usually be established based on a few exceptionally well-observed events. LSST will enable early detection of prototype cases for a number of theoretically predicted explosive transients which we’ve already discussed, including orphan GRB afterglows, accretion induced collapse events, fall-back and pair-instability supernovae, and the so called SN 0.Ia. Several groups are developing systems for multi-band simultaneous photometry and Integrated Field Unit (IFU) spectroscopy on rapidly deployed telescopes around the world that can continuously follow transients brighter than  $\sim 22$ nd mag. An example is the Las Cumbres Observatory Global Telescope Network of 2-m telescopes and photometric/IFU instruments dedicated to follow-up.

Historically, cutting-edge instruments have not been focussed on science that can be done with bright objects. It will be important that 1–4-m telescopes be instrumented to follow brief transients to their peak brightnesses, which can get to naked-eye level (Racusin et al. 2008). The leaders in this type of follow-up are observatories that respond to new discoveries of gravitational microlensing events (e.g., Microlensing Follow-Up Network ( $\mu$ -FUN) and Robonet-II). Target-of-opportunity programs on specialized X-ray, infrared and radio observatories such as today’s Chandra, XMM/Newton, Spitzer, and VLA will continue to provide broad-band spectra and imaging across the electromagnetic spectrum. With ALMA and projects such as Constellation-X, IXO, and JWST in the queue, we may expect higher resolution and more sensitive multi-wavelength follow-up resources to be available by the time LSST starts operating.

Somewhat less detailed follow-up will be obtained for significant numbers of fainter transients. For photometry, LSST itself provides sparsely time-sampled follow-up on timescales of hours to days. Spectroscopic and multi-wavelength follow-up is the key to breaking degeneracies in the classifications and unraveling the physics, and will necessarily be a world effort. The amount of large telescope time required to determine the redshift of optical afterglows accompanying GRBs localized by Swift is 0.5–2.5 hours, with a mean response time of 10 hours. The list of world’s large

optical telescopes includes about half dozen instruments in each of the classes: 9–10 m, 8–9 m, and 5–8 m. As of 2009, there are  $\sim 20$  optical telescopes with diameter of 3 meters or larger which can access the Southern Hemisphere at least in part; these are the facilities which will be well-placed to follow up fainter LSST transients.

Several design studies for extremely large optical telescopes are in progress (Euro50, E-ELT, MaxAT, LAMA, GMT, TMT). They will further reduce the integration time required for spectroscopic follow-up of faint sources. Major observatories around the world such as ESO and NOAO, and the astrophysics community at large are developing optimized observing modes and evaluating spectroscopic instruments that will better utilize LSST transient data. Because we expect many transients per LSST field of view, efficient spectroscopic follow-up would best be carried out with multi-slit or multi-IFU systems. BigBOSS is a newly proposed instrument for the Mayall or Blanco 4-m telescopes, capable of simultaneously measuring 4,000 redshifts over a  $3^\circ$  diameter field of view. Wide field follow-up would be possible with AAT/AAOmega and Magellan/IMACS instruments. Some northern facilities will partially overlap with the LSST survey: BigBOSS at the Mayall, GTC, Keck MOSFIRE and DEIMOS, MMT/Hectospec, and LAMOST. Smaller field of view spectroscopic follow-up in the south can be accomplished with Gemini/GMOS, the VLTs/FORS1, and SALT/RSS. It is reasonable to expect that new instruments will be built for these and other spectroscopic facilities by the time LSST sees first light.

## 8.5 Gravitational Lensing Events

*Rosanne Di Stefano, Kem H. Cook, Przemek Wozniak, Andrew C. Becker*

Gravitational lensing is simply the deflection of light from a distant source by an intervening mass. There are several regimes of lensing. In strong lensing ([Chapter 12](#)), the source is typically a quasar or very distant galaxy, and the lens is a galaxy or galaxy cluster at an intermediate distance. Lensed quasars typically have multiple images, each a distorted and magnified view of the unlensed quasar. Lensed galaxies may appear as elongated arcs or rings. *Weak lensing* is discussed in [Chapter 14](#). Weak lensing is also a geometrical effect. While no single distant source may exhibit wildly distorted images, the lensing effect can be measured through subtle distortions of many distant sources spread out over a field behind the lens. In these cases, the main effects of lensing are detected in the spatial domain. In this chapter we focus on those cases in which the primary signature of lensing is in the time domain. That is, we discuss lensing *events*, in which the time variability arises because of the relative motion of source, lens, and observer. This is generally referred to as *microlensing*. When the lens is nearby, however, the Einstein ring becomes large enough that spatial effects can also be detected. Because of this and other observing opportunities made possible by the proximity of the lens, nearby lensing is referred to as *mesolensing* ([Di Stefano 2008a,b](#)). LSST will play a significant role in the discovery and study of both microlensing and mesolensing events.

A lensing event occurs when light from a background source is deflected by an intervening mass. [Einstein \(1936\)](#) published the formula for the brightening expected when the source and lens are point-like. The magnification is 34% when the angular separation between source and lens is equal

to  $\theta_E$ , an angle now referred to as the Einstein angle.

$$\theta_E = \left[ \frac{4GM(1-x)}{c^2 D_L} \right]^{\frac{1}{2}} = 0.01'' \left[ (1-x) \left( \frac{M}{1.4 M_\odot} \right) \left( \frac{100 \text{ pc}}{D_L} \right) \right]^{\frac{1}{2}}. \quad (8.8)$$

In this equation,  $M$  is the lens mass,  $D_L$  is the distance to the lens,  $D_S$  is the distance to the source, and  $x = D_L/D_S$ . The time required for the source-lens separation to change by an Einstein diameter is

$$\tau_E = \frac{2\theta_E}{\omega} = 70 \text{ days} \left[ \frac{50 \text{ km s}^{-1}}{v_T} \right] \left[ \frac{M}{1.4 M_\odot} \frac{D_L}{100 \text{ pc}} (1-x) \right]^{\frac{1}{2}}. \quad (8.9)$$

Einstein did not consider the effect to be observable because of the low probability of such close passages and also because the observer would be too “dazzled” by the nearby star to detect changes in the background star. [Paczynski \(1986\)](#) answered both of these objections by noting that low-probability events could be detected because monitoring of large numbers of stars in dense source fields had become possible, and by suggesting lensing as a way to test for the presence of compact *dark* objects. The linking of the important dark matter problem to lensing, at just the time when nightly monitoring of millions of stars had become possible, sparked ambitious new observing programs designed to discover lensing events. Given the fact that episodic stellar variability of many types is 100 – 1,000 times more common than microlensing, success was not assured. To be certain that events they discovered had actually been caused by lensing, the monitoring teams adopted strict selection criteria.

In fact, these early teams and their descendants have been wildly successful. They have convincingly demonstrated that they can identify lensing events. More than 4,000 candidate events are now known,<sup>4</sup>, among them several “gold standard” events which exhibit effects such as parallax and lens binarity.

Perhaps the greatest influence these programs have had is in demonstrating the power afforded by frequent monitoring of large fields. In addition to discovering rare events, the “needles-in a-haystack” of other variability, they have also yielded high returns for a number of other astrophysical investigations, including stellar structure, variability, and supernova searches. One may argue that the feasibility and scientific return of wide field programs such as LSST was established by the lensing monitoring programs. Every year LSST data will contain the signature of tens of thousands of lensing events ([§ 8.5.2](#)). Many will remain above baseline for several months. This means that, with a sampling frequency of once every few nights, LSST will obtain dozens of measurements of the magnification as the event progresses. Meaningful fits to a point-lens/point-source light curve can be obtained with fewer than a dozen points above baseline. LSST will therefore be able to test the hypothesis that an ongoing event is caused by lensing.

In fact, LSST will also be able to discover if lensing events display deviations from the point-lens/point-source form. Such deviations will be common, because they are caused by ubiquitous astrophysical phenomena, such as source binarity, lens binarity, and parallax. The black light curve

<sup>4</sup>Most of the events discovered so far were generated by low-flux stellar masses along the direction to the bulge (see, e.g., [Udalski 2003](#)).

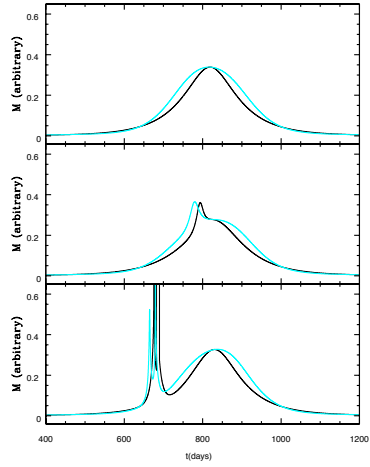


Figure 8.14: Sample lensing light curves. These particular light curves were generated by high-mass lenses (black holes with  $M = 14 M_{\odot}$ , and  $D_L = 200$  pc) and the deviations from baseline last long enough and evolve slowly enough that LSST can track the event and provide good model fits. Cyan curves include parallax effects due to the motion of the Earth around the Sun; black curves do not. *Top:* The lens is an isolated black hole. *Middle and Bottom:* The lens has a white dwarf companion with orbital period appropriate for the end of mass transfer. The orbital phase at the time of peak is the distinguishing feature between the middle and bottom panels. In these cases, data collected by LSST alone could identify the correct models. For short duration events or for some planet lenses, LSST could discover events and spark alerts to allow more frequent monitoring.

in the top panel of Figure 8.14 shows a point-lens/point-source light curve, and the blue light curve in the same panel shows the parallax effects expected if the lens is 200 pc away. In this case, the deviation introduced by parallax is several percent and lasts for a significant fraction of the event. The middle and bottom panels of Figure 8.14 illustrate that deviations caused by lens binarity similarly influence the magnification over extended times in ways that can be well-modeled (see Di Stefano & Perna 1997, for a mathematical treatment).

The good photometric sensitivity of LSST will allow it to detect these deviations. By pinning down the value of the magnification every few days, LSST will provide enough information to allow detailed model fits. We have demonstrated that the fits can be derived and refined, even as the event progresses (Di Stefano 2007). This allows sharp features (such as those in the bottom panel of Figure 8.14) to be predicted, so that intensive worldwide monitoring can be triggered. The LSST transient team will develop software to classify events in real time to allow it to call reliable alerts (§ 8.4). While there are some examples of light curves on which we will want to call alerts (some planet-lens light curves for example), many special effects will be adequately fit through LSST monitoring alone.

Figure 8.14 illustrates another point as well: many lenses discovered through LSST’s wide area coverage will be nearby. That is, they will be mesolenses. The black hole in this example would create a detectable astrometric shift. The size of its Einstein angle could thereby be measured, while the distance to the lens could be determined through the parallax effects in the light curve. Equation 8.8 then allows the lens mass to be determined. Similarly, when nearby low-mass stars

serve as lenses, radiation from the lens provides information that can also break the degeneracy and measure the lens mass.

### 8.5.1 What Can Lensing Events Teach Us?

- 1) *Dark Matter:* It is still controversial whether or not the existing lensing programs have successfully established the presence or absence of MACHOs in the Galactic halo. The upper limit on the fractional component of MACHOs was found to be approximately 20% by Alcock et al. (2000). However, if the experiments on which these estimates are based are overestimating their detection efficiencies (perhaps by missing some lens events that deviate from the point-lens/point-source form, as suggested by the under-representation of binary lenses and binary source events in the data; Night et al. 2008), the true rate and perhaps the number of MACHOs, would be larger than presently thought. Additional monitoring can definitively answer the questions of whether MACHOs exist and, if they do, whether they comprise a significant component of Galactic dark matter. To achieve this, we need to develop improved event identification techniques and reliable calculations of the detection efficiencies for events of different types.
- 2) *Planets:* The search for planets is an important ongoing enterprise (§ 8.11). Lensing can contribute to this search in several important ways. For example, in contrast to transit and radial velocity methods, lensing is sensitive to planets in face-on orbits. In addition, lensing is effective at discovering both low-mass planets and planets in wide orbits. Finally, it is ideally suited to discovering planets at large distances and, therefore, over vast volumes. In addition, we have recently begun to explore the opportunities of using lensing to study planets orbiting nearby (< 1 kpc) stars (Di Stefano 2007; Di Stefano & Night 2008). Fortunately, the Einstein ring associated with a nearby M dwarf is comparable in size to the semi-major axes of orbits in the M dwarf's zone of habitability (Figure 8.15). Events caused by nearby planets can be discovered by monitoring surveys or through targeted follow-up lensing observation.
- 3) *Distant stellar populations:* Lensing can teach us about both the star serving as the lens and the source star that was lensed. Both source and lens can be members of a distant dense source field, and binary-lens effects and/or binary-source effects should be detectable for a significant fraction of events. When the selection effects are well-understood, the fraction and characteristics of binaries in external galaxies can be derived. It is noteworthy that, unlike eclipse studies, lensing is sensitive to binaries with orbits of all orientations. In addition, finite-source effects provide information about surface features of the source star.
- 4) *The solar neighborhood:* A significant fraction of all lensing events are generated by nearby masses, most M dwarfs. As noted, lensing is particularly sensitive to planets in the habitable zones of nearby M dwarfs. LSST will also discover lensing by white dwarfs, neutron stars, and black holes (see § 8.5.2). Particularly because few nearby neutron stars and no nearby black holes are known, all-sky monitoring has the potential to make important contributions.

### 8.5.2 What Does LSST Bring to These Studies?

LSST will sample most parts of the sky every few days. Although the telescopes will return to some regions more frequently, the cadence is not well suited to study the rapid changes that can

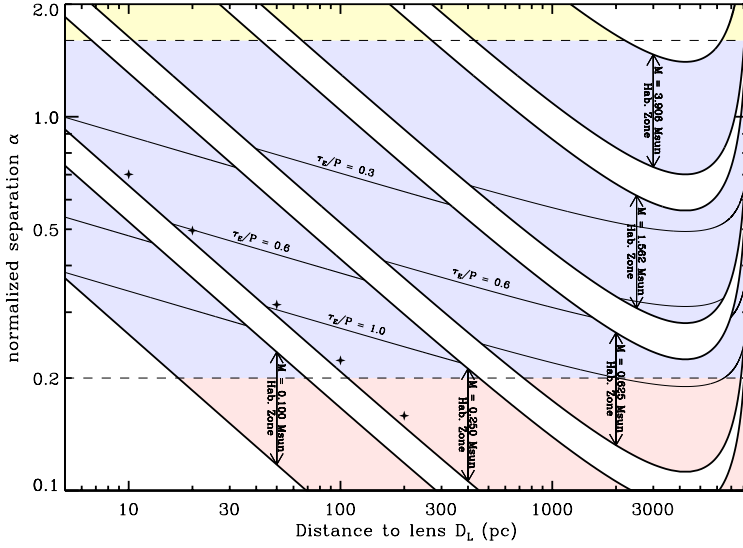


Figure 8.15: Separation between  $\alpha$  vs.  $D_L$  for the habitable zones (HZs) of low-mass stars. Each colored bar represents a star with a given mass:  $M = 0.1 M_\odot$  on the lower left, increasing by a factor of 2.5 for each subsequent bar. The lower (upper) part of each bar corresponds to the inner (outer) edge of the HZ for a star of that mass. The upper horizontal dashed line at  $\alpha = 1.6$  marks the approximate boundary between “wide” systems, in which the planet and star act as independent lenses (Di Stefano & Scalzo 1999a,b), and “close” systems in which distinctive non-linear effects, such as caustic crossings provide evidence of the planet (Mao & Paczynski 1991; Gould & Loeb 1992). All of the planets detected so far have model fits with  $\alpha$  lying between 0.7 and 1.6. In this range, the effects of caustics are the most pronounced. As  $\alpha$  decreases, the effect of the planet on the lensing light curve becomes more difficult to discern; the horizontal dashed line at  $\alpha = 0.2$  is an estimate of a lower limit. Contours with constant values of the ratio  $\tau_E/P$ , where  $P$  is the orbital period, are also shown. This is because the probability of detecting the planet in close systems ( $\alpha \leq 0.5$ ) is increased by the orbital motion. For  $\alpha > 0.2$ , systems with large orbital motion are potentially detectable by current observations.

be associated with, for example, caustic crossings. Nevertheless, LSST will become a major player in the study of lensing. It has several important advantages:

- 1) *All-sky coverage:* LSST will be able to find lensing events across most of the sky. It will probe the Galactic halo in many directions, discovering MACHOs or placing tight limits on their existence, and exploring the stellar populations of the halo. Lensing of stars will be detected in a wide range of external galaxies, including Local Group dwarf galaxies and galaxies within several Mpc. In addition, lensing of stars in our own Galaxy will also be observed. To illustrate, we note that limited monitoring has already discovered the lensing of an A0 star just one kpc away by an unknown intervening mass (Fukui et al. 2007; Gaudi et al. 2008).
- 2) *Excellent photometric sensitivity:* When an event deviates from the point-source/point-lens form, the deviations are typically long-lasting, even if the most dramatic effects occur during a short time interval. Sampling the light curve with good photometric sensitivity at a modest number of points can therefore identify its unique features and help determine the physical characteristics of the lens.
- 3) *The opportunity to develop superior selection criteria:* When the lensing monitoring teams first started, they had to prove that it is possible to identify lensing events among the much larger background “noise” of intrinsic variations exhibited by stellar systems. They, therefore, used strict

Table 8.4: **Nearby Microlens Event Rates**

Lens type	<b>Past</b> per decade per deg <sup>2</sup>	<b>Present</b> per decade per deg <sup>2</sup>	<b>Future</b> per decade per deg <sup>2</sup>	<b>Future</b> per decade <b>over 150</b> deg <sup>2</sup>
M dwarfs	2.2	46	920	$1.4 \times 10^5$
L dwarfs	0.051	1.1	22	3200
T dwarfs	0.36	7.6	150	$2.3 \times 10^4$
WDs	0.4	8.6	170	$2.6 \times 10^4$
NSs	0.3	6.1	122	$1.8 \times 10^4$
BHs	0.018	0.38	7.7	1200

Each predicted rate is valid for the direction toward the Bulge (see [Di Stefano 2008a,b](#), for details). *Past*: the observing parameters apply to the first generation of monitoring programs, including MACHO. *Present*: applies to the present generation, including OGLE III and MOA. *Future*: applies to upcoming projects such as Pan-STARRS and LSST. The effective area containing high-density source fields is  $\sim 150$  deg<sup>2</sup>; this is used in the last column. In fact, near-field source stars spread across the sky will also be lensed, adding to the rate of lensing by nearby masses; the above estimates for lensing by nearby masses are fairly conservative.

criteria designed to identify the point-lens/point-source light curves first predicted by Einstein. Despite their remarkable success, with more than 4,000 lensing candidates identified, many of the events that should be associated with common astrophysical systems (binary sources, binary lenses, etc.) have been found only rarely. The detection efficiencies are not well understood, making it difficult to draw general conclusions based on the events that have been discovered. We have the opportunity to use the years before LSST data acquisition to develop procedures to identify *all* lensing events with an efficiency that can be calculated.

4) *The opportunity to predict mesolensing events:* LSST will identify and track the motions of many nearby stars, measuring parallaxes and proper motions. This detailed look at the local sky will supplement what has been learned from SDSS and other surveys (see, e.g., [Lépine 2008](#)), and will allow us to predict when nearby stars will pass close enough to distant objects to generate detectable lensing events. The ability to predict lensing events, based on LSST data, will turn lensing into a more flexible tool for astronomical studies. While the predicted events may be detected with LSST, other telescopes can learn a good deal by providing frequent multiwavelength monitoring.

5) *Studies of both the astrometric and photometric effects for mesolensing events:* LSST will make sensitive astrometric as well as sensitive photometric measurements. Because lensing creates multiple images, whose positions and intensities change as the event progresses, astrometric shifts are expected (see, e.g., [Dominik & Sahu 2000](#)). For nearby lenses, the shifts can be several milli-arcseconds, potentially measurable with LSST. Indeed, a unique combination of astrometric as well as photometric monitoring is possible with LSST and can be valuable to both discover and study lensing events.

The bottom line is that LSST can advance fundamental science through the detection, identification, and correct interpretation of lensing events. In order for this to happen, we will have to

devote significant effort to laying the necessary foundation in theory, event selection, and analysis.

## 8.6 Identifying Variables Across the H-R Diagram

*Steve B. Howell, Dante Minniti*

The LSST will address three major science objectives related to variable stars: 1) production of very large samples of already known variable types, 2) discovery of theoretically predicted populations of variables not yet discovered, and 3) discovery of new variable types. Large samples for specific types of variable star provide enormous leverage in terms of the statistical properties attributed to or deduced from them. For example, small color deviations, unnoticeable in samples of 100-500, may illustrate metallicity effects and other evolutionary properties for the class. Theoretical models often set boundaries in  $T_{\text{eff}}$  and  $\log g$  space for classes of pulsators. These can be exquisitely determined from big samples. Additionally, large samples obtained in a systematic way with uniform properties and biases enable stronger conclusions from limited samples. This type of new knowledge about old, “well studied” variable star classes was very well shown by the MACHO observations of RR Lyrae and Cepheids toward the Galactic bulge.

Several classes of variable stars are shown in [Figure 8.16](#). The figure primarily includes pulsating variables, which are likely to be the focus of many LSST research programs. Known types of periodic variables are either quite luminous,  $M_V < +2.5$ , or are pulsating variable stars. [Figure 8.16](#) also shows non-periodic type low-mass M dwarfs, intrinsically variable objects which produce large amplitude (>1 mag) transient flares, and the T Tauri stars. Additional periodic variable star types include eclipsing binaries and solar-like stars, which show a rotational modulation due to star spots.

[Figure 8.16](#) shows that all known pulsating variables (with the exception of white dwarfs), have  $M_V < +2.5$ . The major reason for this “bright limit” is observational selection effects in terms of areal coverage, limiting magnitude, observed sample size, photometric precision, and time coverage. LSST will lessen all of these biases by orders of magnitude, which will completely revolutionize the science of periodic variable stars.

A useful overview of stellar variability is presented in the recent paper by [Eyer & Mowlavi \(2008\)](#). Gathering summary information from the MACHO, OGLE-II and III, HAT, ASAS, SuperWASP, HIPPARCOS, and other surveys, Eyer and Mowlavi attempt to separate variables based on type (periodic or not) and subtype while providing summary statistics for each group. While time sampling and photometric precision vary among the surveys, very useful general trends and parameters are apparent. Stars are variable throughout the H-R diagram but not with the same observed frequency. For example, red giants are nearly 100% variable while the A main sequence stars only show about a 5% rate. For all periodic variables, classification work often begins with period and amplitude, the two common photometrically measured parameters, with star color being of additional importance. The majority of periodic variables are normal pulsators and cover a large range in period and amplitude. [Figure 8.17](#) gives a schematic view of the known pulsator types shown in period-amplitude space. Each point represents a single well-studied member of the variable star class, and we can see the general trend for pulsators in that the larger the pulsation amplitude the longer the pulsation period. The smallest amplitude limit is about 0.01 mag and

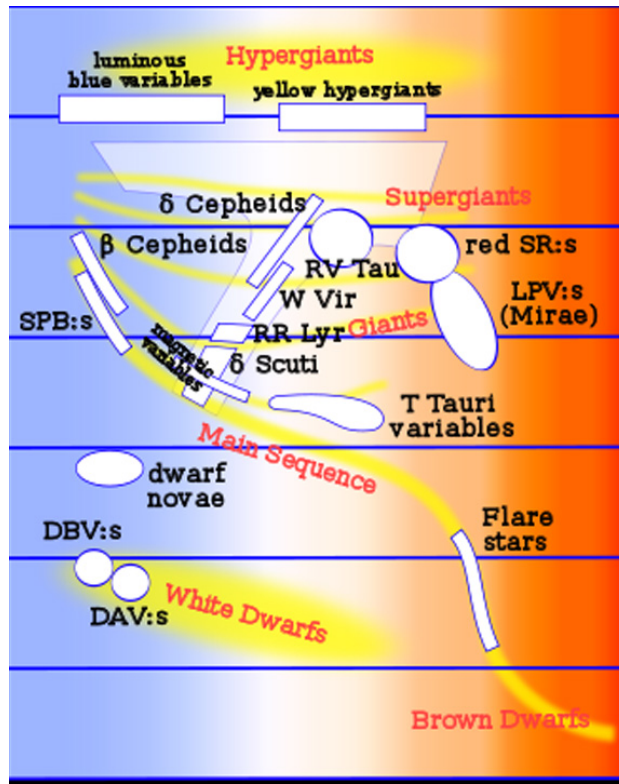


Figure 8.16: H-R Diagram showing the locations of currently known classes of variable stars, mostly comprised of pulsating variables: slowly pulsating B stars (SPBs), red semi-regular variables (red SRs), pulsating white dwarfs (DAV and DAB), and long period variables (LPVs). Also shown are cool flare stars and T Tauri stars. Note that while the absolute luminosity scale covers many orders of magnitude, the present day set of pulsators is limited to those variables that are bright. The exception to this is the pulsating white dwarfs due to their special status and targeted study. LSST will provide large uniform samples of pulsating variables and will allow the remainder of the H-R Diagram to be explored for additional variable types.

the period limits are  $\sim 0.1$  day to 1,000 days, values that will be greatly improved upon by the LSST, thereby likely increasing the discovery space even for normal pulsators.

Pietrukowicz et al. (2009) recently carried out a deep variability survey in a field in the Galactic plane using VLT/VIMOS, allowing an experimental quantification of the numbers and types of variable stars that the LSST survey may ultimately detect. This work is well suited for comparison with the LSST due to the large telescope aperture, similar exposure times, similar limiting magnitudes, and light curve quality. The survey lasted only four nights, but due to its depth and improved precision, the total number of variable stars found in this survey was higher than previous shallower surveys (like MACHO, OGLE, ASAS, etc.). Over this short time baseline, 0.69% of the observed stars had detectable variability.

Extrapolating from their results suggest that LSST will discover of order 135 million variable stars. Of these, 57 million will be eclipsing/ellipsoidal variables, 59 million will be pulsating variables, 2.7 million will be flaring stars, and 0.78 million will exhibit variability due to extrasolar planetary transits.

From a sample of four photometric surveys designed to discover variability, Howell (2008) discusses

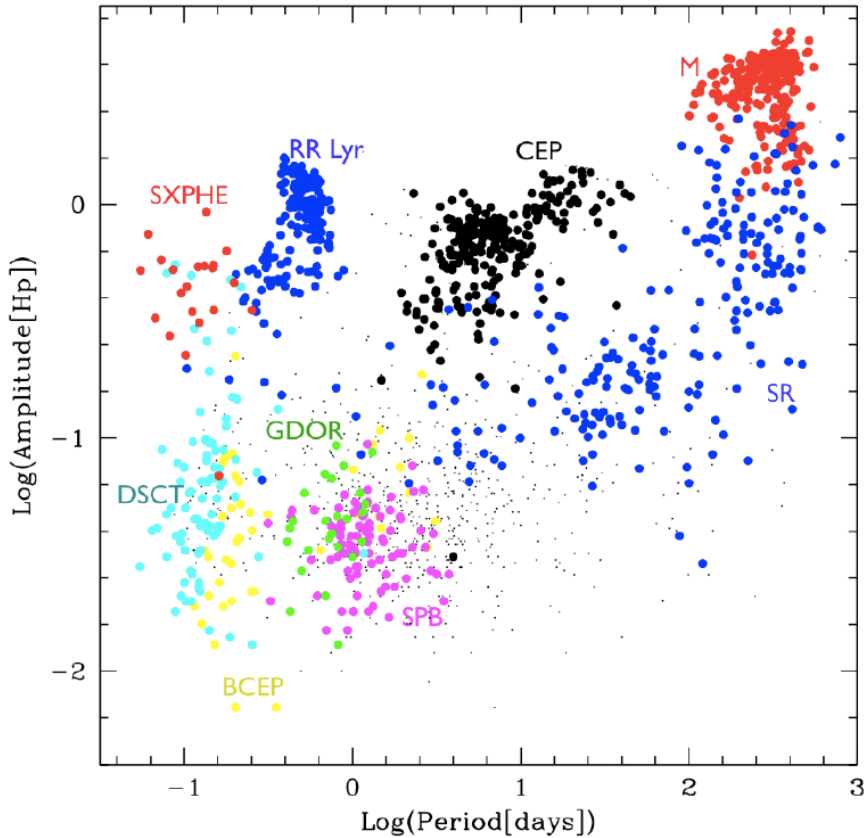


Figure 8.17: The Period-Amplitude diagram for different classes of pulsating variables as known today:  $\delta$  Scutis (DSCT), SX PHe (SXPHE),  $\gamma$  Dor (GDOR),  $\beta$  Cepheid (BCEP), Cepheids (CEP), RR Lyraes (RRL), semi-regular variables (SR), slowly pulsating B stars (SPB), and M dwarfs (M). Light curve measurements of pulsating variables provide two fundamental parameters; the pulsation period and the light curve amplitude. These measured parameters have a scaling relationship as they are proxies to energy transport within a stellar atmosphere. The larger the amplitude of a pulsation, the longer it takes for energy to be displaced and thus the period of this action is longer as well. The LSST will extend this diagram in the regions of longer periods and smaller amplitudes as well as identify completely new members to add to the plot. (Adapted from Eyer & Mowlavi 2008).

the relationship between variable fraction and the photometric precision of the survey. The general finding, shown schematically in Figure 8.18, illustrates the exponential increase in variable fraction of the observed sources as a function of improved photometric precision of the survey. This plot is averaged over a number of observational biases, survey lengths, and other parameters and should be viewed as an approximate guideline. However, its predictions for the number of variables a survey will find at a specific photometric precision are in fair agreement with the numerical results of the HIPPARCOS, ASAS, and OGLE surveys. For the LSST baseline relative photometric precision per 15 sec exposure at  $r$  magnitude of 17-19 ( $1\sigma \sim 0.005$  mag), it is probable that several tens of percent of the observed sources will be variable in some manner. For  $r$  magnitudes of 22 to 23, the precision will be of order 0.01 mag, suggesting that  $\sim 5\%$  of the sources in this magnitude range will be variable.

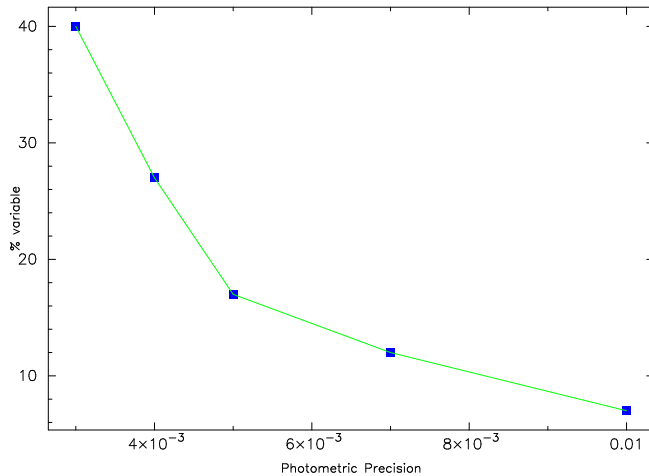


Figure 8.18: Schematic diagram relating the percentage of variable sources a given survey will detect compared with the best photometric precision of that survey. Combining the information gleaned from many surveys designed to search for variability, the figure shows the general trend observed. As the photometric precision of a survey improves, the number of sources observed to be variable goes up, steeping considerably below 0.005 mag.

### 8.6.1 Models of Variable Star Light Curves

*K. Simon Krughoff, R. Lynne Jones, Andrew C. Becker, Steve B. Howell*

In order to assess the output light curves that the LSST survey will produce for variable stars, we have produced model outputs based on the LSST light curve interpolation tool, which convolves template light-curves of objects with the expected cadence of observations (§ 3.1).

#### *The Light Curve Interpolation Tool*

In brief, the light curve interpolation tool is intended to facilitate the simulation of observations of time variable objects with LSST cadences. Developed in Python by K. Simon Krughoff at the University of Washington, the tool operates in three phases. Phase one is interpolation of the input time series with optional error estimates. One of two fitting methods may be chosen. A univariate splining method may be used for smoothly varying idealized curves. If the input time series contains noise or has sharp discontinuities (as is the case with transiting exoplanets, for example), the polyfit (<http://phoebe.fiz.uni-lj.si/?q=node/103>) method is optimal. In phase two, the user specifies the data necessary to turn the time series into an observed light curve. These parameters include period, position, and version of the Operations Simulator output. The tool turns this information into a MySQL query and sends it to the database. Exposure time in MJD and the  $5\sigma$  limiting magnitude for all pointings in the Operations Simulation (§ 3.1) that overlap the specified position (defined as the  $1.75^\circ$  radius circular aperture) are returned to the tool. Phase three is construction of the observed “light curve” for the input time series. The time series is sampled at the times specified by the operations simulation pointings that overlap the position.

The photometric errors are calculated based on the returned  $5\sigma$  limiting magnitude. Optionally, the interpolated points are randomly “jiggled” by an amount consistent with the computed error, assuming normal errors.

### ***Example Observations of Variable Stars***

For a preliminary evaluation of LSST’s ability to identify and characterize different types of variable stars, we have taken ten well known variable stars of various types, generated “template” light curves for each star, and produced “observations” of each star as would be seen by LSST using the light curve interpolation tool described above.

The template light curves were created from AAVSO V band data chosen to cover a representative two-year interval and assigned to the  $g$  band. We generated input light curves for the remaining five filters through a simple scaling of the  $g$  band light curve to brighter or fainter magnitudes based on the known colors of each type of variable star. While many variables actually change color as they vary, this is a second order effect to our goals in this preliminary effort. The set of six light curves ( $u, g, r, i, z, y$ ) were then scaled to represent LSST observed stars with  $g$  magnitudes of 18 to 27, in one magnitude steps, each with properly scaled uncertainties. The input light curves were smoothed a bit to reduce their sensitivity to day/night and seasonal variations and to light curve value uncertainty for a given night.

The results show that in some regions there is a good chance that a variable star could be reliably identified after some time period of data is collected. We have baselined this time period here to be two years to allow the reader to get a sense of the sampling efficiency and temporal nature. Using variability time scale, amplitude, and color information, gross categorization of variable sources from LSST observations can begin within the first few months of operations. Not surprisingly, the most complete variability information comes from the deep drilling fields (§ 2.1) with their rapid candence. Identification also depends on the average magnitude of the source itself; sometimes fields are observed when the star is below the limiting magnitude in the field, and thus no measurements were simulated with our tool (although the imaging pipeline will still report a meaningful upper limit for that position). Our preliminary study shows that matching each variable source light curve (time scale, amplitude, color) to well-observed templates can provide very good to good classification probabilities, especially as the database grows over the ten years of the survey, although further study must be done to expand the range of templates tested.

We show two examples of reasonably well observed variables in Figure 8.19. The input light curve templates for these variables are AAVSO observed light curves for the RV Tau star, Z UMa, and the cataclysmic variable, SS Cyg. These templates were assembled as described above. Z UMa changes its brightness due to pulsations where a fundamental and first overtone period tend to operate simultaneously. SS Cyg has small amplitude variability while the larger (2 magnitude) brightenings are due to semi-regular dwarf nova outbursts. These figures show the “observations” that LSST would make for each star; with a knowledge of the typical template light curve, the difference between these variable stars is measurable.

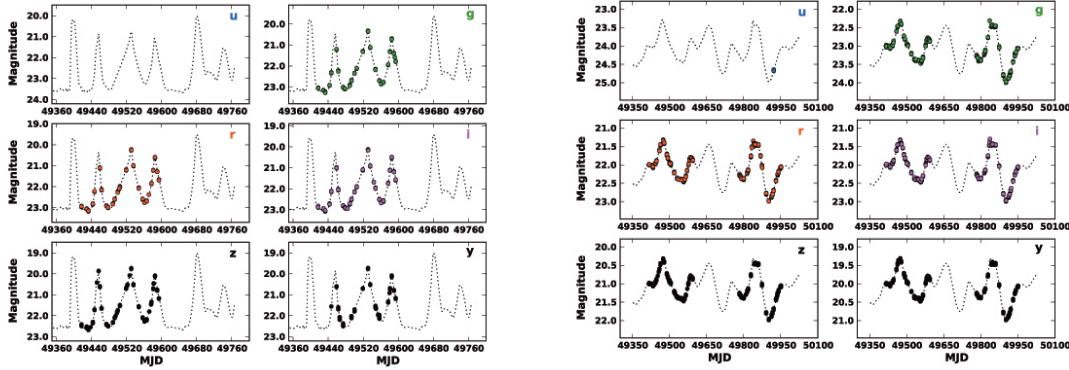


Figure 8.19: In these figures we have used the light curve sampling tool to generate “observations” of two very different variable stars, SS Cyg and Z UMa (left and right respectively), as they (or stars like them) would be sampled by LSST for approximately one and two years (respectively), if the average magnitude of each variable were  $\langle g \rangle = 22$  or  $\langle g \rangle = 23$  (respectively). The stars were assumed to be placed in the deep drilling fields. The dashed line indicates the input variability light-curve, while the filled circles illustrate the “observations” LSST would make in each filter,  $u$ ,  $g$ ,  $r$ ,  $i$ ,  $z$ , and  $y$ . Estimated errors on each datapoint are shown, but are smaller than the circles. These figures show that template light curve fitting for LSST should be able to distinguish between variable stars of different types, as long as those templates are known. These observations come from what is potentially the best case scenario for variable stars in LSST’s observing cadence – the deep drilling (or “supernova”) fields.

### 8.6.2 A Study of RR Lyrae Period Recovery

*Hakeem Oluseyi, Julius Allison, Andrew C. Becker, Christopher S. Culliton, Muhammad Furqan, Keri Hoadley*

Here we explore LSST’s light curve recovery capability for RR Lyrae stars as a function of stellar distance and LSST observing cadence.

Templates for input to the light curve tool (see § 8.6.1) were obtained from Marconi et al. (2006). The non-linear, non-local time-dependent convective RR Lyrae stellar models used for this study span a range of metallicity, helium content, stellar mass, and luminosity for both fundamental and first overtone pulsators.

The RR Lyrae light curves were tested against a set of many locations on the sky, distributed between universal cadence overlap regions (which receive roughly twice the number of observations as the bulk of the sky) and deep drilling fields.

The  $ugriz$  light-curves of the Marconi et al. (2006) RR Lyrae model were placed in each observation field and sampled with the LSST simulation tool, which returned realistic limiting magnitudes and photometric scatter based on historic seeing and weather data at the LSST site on Cerro Pachón, Chile. The LSST  $y$ -band data were simulated by using Marconi’s  $z$ -band data. The  $g$ -band stellar magnitudes  $\langle m_g \rangle$  ranged from 17<sup>th</sup> to 26<sup>th</sup> with  $\Delta \langle m_g \rangle = 0.5$  mag, for survey lengths of 1, 2, 5 and 10 years.

The period of the unequally spaced time-sampled and noised periodic data was fit using periodograms and least squares estimation methods (Reimann 1994). The simulated data was then phased and fit, via a  $\chi^2$  minimization, to a Fourier series of the form:

$$m_i(t) = \langle m_i \rangle + \sum_{k=1}^5 A_k \cos [2\pi k f(t - t_0) + \phi_k], \quad (8.10)$$

where  $\langle m_i \rangle$  represents the mean stellar magnitude in filter  $i$ ,  $A_k$  is the amplitude of the  $k$ -component of the Fourier series,  $f = 1/P$  is the frequency (where  $P$  is period of the magnitude variation), and  $\phi_k$  is the phase of the  $k$ -component at  $t - t_0$ . Only the first five Fourier terms were included in the series, consistent with typical fits described in the literature.

The calculated period and Fourier parameters were compared with the input values. A period was considered successfully determined if it was within 0.1% of the input value. [Figure 8.20](#) shows LSST's ability to successfully recover light curves as a function of stellar magnitude and survey length, using only  $g$  band data. The ability to successfully recover the pulsational periods and light curve shapes depended on magnitude, field, and filter. Two years of data were sufficient to recover <90% of the periods for RR Lyraes brighter than  $g = 24$  in the deep drilling fields, while closer to six years of data were required for the overlap fields covered by the universal cadence.

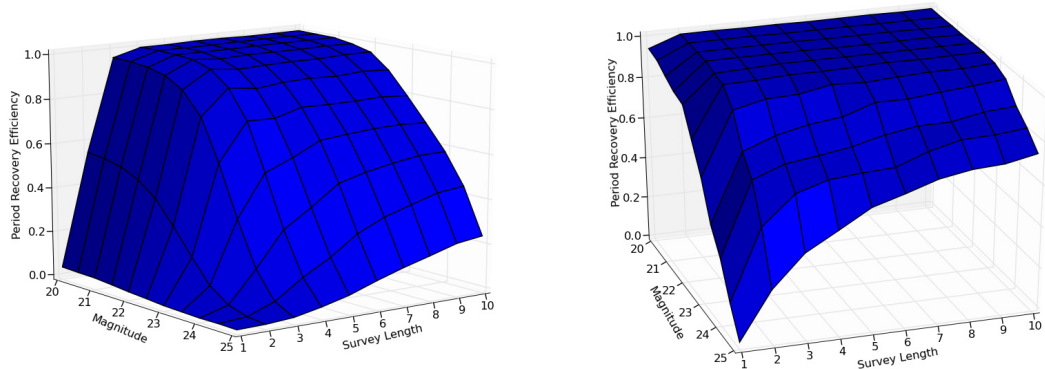


Figure 8.20: Percentage of the time that the  $g$ -band light curves of RR Lyrae stars placed in the overlap cadence overlap regions (left) or deep drilling fields (right) were successfully recovered, as a function of  $\langle m_g \rangle$  and survey length. A successful recovery was defined as determination of the light curve's period to within 0.1%.

## 8.7 Pulsating Variable Stars

Pulsating stars make up the vast majority of periodic variables on the H-R diagram. The period/luminosity (PL) relations of RR Lyrae, Cepheids and Miras make them useful for calibrating the cosmic distance ladder and tracing Galactic structure. The pulsations of these stars can also shed light on the fundamental physics of stellar atmospheres, e.g., by studying how metallicity variations affect the period/luminosity relationship. Because of their far-reaching utility as a population, these pulsators are discussed in a number of other sections in this book (see, for example, [§ 6.4.2](#)).

We focus this section on pulsators *not* extensively covered elsewhere: asymptotic giant branch stars (AGB stars, also discussed briefly in [Chapter 6](#)) and pulsating white dwarfs.

### 8.7.1 AGB Stars

*Stephen T. Ridgway, Kem H. Cook, Željko Ivezić*

The Asymptotic Giant Branch (AGB) phase of stellar evolution occurs when core helium is exhausted but the star is not massive enough to ignite its carbon/oxygen core, so there is helium and hydrogen shell burning. The helium shell burning is exquisitely temperature sensitive and thus unstable, resulting in shell “flashes,” which can dredge up carbon. This mixes CNO products to the surface and creates carbon stars. Stars on the AGB are bright, unstable, and produce prodigious mass loss, returning a large part (up to 50-70%) of their mass, including nucleosynthetic products, to the interstellar medium. While all low and intermediate mass stars are believed to pass through the AGB stage, they are rare owing to the brief AGB lifetime. Thanks to their ubiquity and their high luminosity, they are a guide to the evolution of stellar populations. Accounting for their numbers and colors is important to modeling color evolution of galaxies (Maraston et al. 2009). There are many targets for study. Fraser et al. (2005) catalog 22,000 AGB variable stars in the Large Magellanic Cloud. Jackson et al. (2002) estimate an AGB population of 200,000 for the Milky Way. LSST will obtain good photometric time series for AGB stars throughout the Galaxy and the Local Group. Near-infrared photometry for these stars already exists in the 2MASS survey. AGB stars will be easy to identify from a combination of O/IR colors and variability patterns. The LSST colors will show an extremely red star, reddened by a circumstellar shell, with long period variability. The infrared colors will show emission from the photosphere and from the shell. The LSST sampling cadence is well matched to these slowly varying stars.

The Mira stars are AGB stars in the fundamental mode of pulsation. For the Miras, distances can be obtained to about 10% from a PL relation. With this information for a large, unbiased set of objects, it is possible to investigate questions of Galactic structure in the Milky Way (Feast & Whitelock 2000, see Chapter 7) and in other galaxies (Girardi & Marigo 2007). For example, Mira periods select for main sequence mass, and hence age, and thus periods greater or less than  $\sim 300$  days can be used to distinguish membership in the thick or thin disk (Jura 1994). By qualifying this technique in the Local Group, a powerful tool will be available for population studies far beyond the Local Group when future larger apertures with higher spatial resolution are available.

A deep catalog will show throughout the Galaxy where AGB stars are actively returning nucleosynthesis products to the interstellar medium. From AGB distributions, one can infer past rates of star formation and the current production rates of planetary nebulae and stellar remnants. Complementary mid-infrared measurements, such as from WISE (Mainzer et al. 2005), will stringently constrain the actual mass loss rates.

Mira stars in the solar neighborhood and the Magellanic Clouds are consistent with a universal PL relationship (Whitelock et al. 2008), and have been used to extend Mira-calibrated distances beyond the local group to Cen A, with  $\pm 0.11$  uncertainty in distance modulus (Rejkuba 2004). Parallaxes from the coming Gaia mission, augmented with LSST astrometry for the most extinguished objects (Saha & Monet 2005), can be used to strengthen the PL relation, offering the opportunity to further refine the usefulness of Miras as a distance indicator. For a single visit  $5\sigma$  magnitude of  $y = 22$ , LSST will detect Mira stars at minimum brightness to a distance of 2.5 Mpc. With typical periods of several hundred days, and a  $y$  band amplitude  $\sim 2$  magnitudes (Alvarez et al. 1997),

Mira stars are easily recognized from their light curves, and with 100-200 measurements over a 10-year program, mean periods will be measured to  $\sim 1\%$ .

AGB stars occasionally show period, amplitude, or mode shifts. Some of these simply show the complexity of pulsation with multiple resonances and mixed modes, but some must be associated with changes in the internal structure involving mixing, shell flashes, or relaxation. A very large data set will reveal or strongly bound the frequency and character of such events (Templeton et al. 2005). Mira light curve shapes may in some cases reveal the action of nucleosynthesis at the base of the convective envelope (Feast 2008).

### 8.7.2 Pulsating White Dwarfs

*Anjum S. Mukadam*

Non-interacting white dwarf pulsators are found in distinct instability strips along the cooling track. Hydrogen atmosphere white dwarf pulsators (DAVs or ZZ Ceti stars) are observed to pulsate between 11,000 K and 12,000 K. Helium atmosphere white dwarf variables (DBVs) pulsate around 25,000 K, while hot white dwarf pulsators are observed in the broad range of 70,000 K to 140,000 K. All pulsating white dwarfs exhibit nonradial gravity-mode pulsations. Pulsations probe up to the inner 99% of the mass of white dwarf models; pulsating white dwarfs provide us with a unique opportunity to probe the stellar interior through seismology. Each pulsation frequency is an independent constraint on the structure of the star. A unique model fit to the observed periods of the variable white dwarf can reveal information about the stellar mass, core composition, age, rotation rate, magnetic field strength, and distance.

The observed pulsation periods of the DAVs and DBVs lie in the range of about 50-1,400 s with amplitudes in the range of 0.1% to 10% (0.001 to 0.1 mag). Hot white dwarf pulsators show pulsation periods in the range of a few hundred to a few thousand seconds. High amplitude white dwarf pulsators will exhibit a higher photometric scatter in LSST photometry than non-pulsating white dwarfs. Detection probability increases with the number of measurements irrespective of cadence. White dwarf pulsators of all amplitudes can be discovered by selecting suitable candidates from a  $u - g$  vs.  $g - r$  diagram ( $0.3 \leq u - g \leq 0.6$ ;  $-0.26 \leq g - r \leq -0.16$ ; see Figure 6.22) for follow-up photometry with an expected success rate of  $\sim 25\%$  (Mukadam et al. 2004). Sixty white dwarf pulsators were known in 2002; discoveries from the SDSS have increased to more than 150. Follow-up photometry of suitable candidates from LSST should increase the known population of white dwarf pulsators brighter than 20th mag to well over a thousand.

#### **What Can We Learn from White Dwarf Pulsators?**

The core composition of a white dwarf is effectively determined by nuclear reaction rates in the red giant stage. Therefore, pulsating white dwarfs allow us the opportunity to study nuclear reaction rates  $^{12}C(\alpha, \gamma)^{16}O$  in red giant cores (Metcalfe et al. 2001). White dwarf models with  $T_{\text{eff}} \geq 25,000$  K show plasmon neutrinos as a dominant form of energy loss. Measuring the cooling rates of these stars can serve as a strong test of electroweak theory (Winget et al. 2004). Montgomery (2005) fit the observed non-sinusoidal light curves of large amplitude pulsating white dwarfs to study convection, a fundamental pursuit widely applicable in several domains of physics and astronomy.

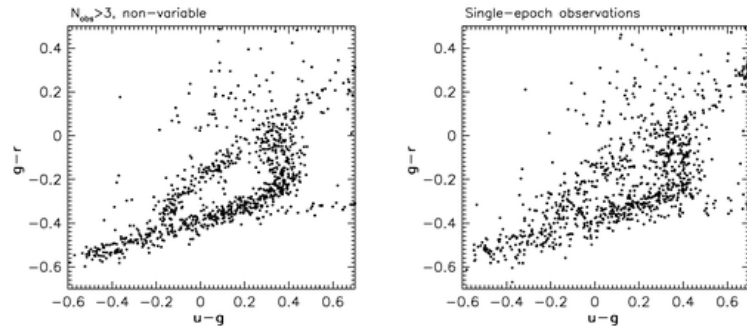


Figure 8.21: SDSS color–color diagram for objects near the white dwarf cooling sequence. The *right* panel shows the colors for all sources seen to be non–variable over many epochs, but only shows their photometric measurements from one epoch. The *left* panel shows the mean colors for these objects over all epochs, and resolves cooling sequences much less apparent in the single epoch photometry. Adapted from Figure 24 of Ivezic et al. (2007). A simulated color–color diagram of these two white dwarf sequences as observed in LSST is shown in Figure 6.22.

Pulsating low mass ( $\log g \leq 7.6$ ) white dwarfs are expected to be helium core white dwarfs. Their pulsations should allow us to probe their currently unknown equation of state with tremendous implications for fundamental physics. Metcalfe et al. (2004) present strong seismological evidence that the massive ( $\log g \geq 8.5$ ) cool white dwarf pulsator BPM 37093 is 90% crystallized; this directly tests the theory of crystallization in stellar plasma (Winget et al. 1997). Such a study also has implications for models of neutron stars and pulsars, which are thought to have crystalline crusts.

Measuring the cooling rates of pulsators helps in calibrating the white dwarf cooling curves, which reduces the uncertainty in using cool white dwarfs at  $T_{\text{eff}} \leq 4,500$  K as Galactic chronometers. We can also use the cooling rates of ZZ Ceti pulsators to study exotic particles such as axions (Isern et al. 1992; Bischoff-Kim et al. 2008). Should stable white dwarf pulsators have an orbiting planet around them, their reflex motion around the center of mass of the system would provide a means of detecting the planet. Winget et al. (2003) describe the sensitivity of this technique and Mullally et al. (2008) find that GD 66 may harbor a  $2 M_J$  planet in a 4.5-yr orbit. We can use these flickering candles to measure distances that are typically more accurate than what we determine from measured parallax (e.g., Bradley 2001).

An illustrative experiment was carried out by Ivezic et al. (2007), using data from SDSS repeat observations. Figure 8.21 shows the colors of non–variable ( $\sigma_g < 0.05$ ;  $\sigma_r < 0.05$ ) objects near the white dwarf cooling sequences. The rightmost panel shows single–epoch colors taken from SDSS DR5. The left panel shows the averaged colors of the objects over  $\sim 10$  epochs. With the higher S/N photometry, multiple sequences are apparent, two of which correspond to the cooling curves of H and He white dwarfs (Bergeron et al. 1995). These are fundamental tests of degenerate matter that cannot be replicated in the lab. While LSST can identify the variability, followup observations in a blue filter will be needed to pin down the pulsation periods, and spectra will be needed to determine accurate temperatures.

## 8.8 Interacting Binaries

*Paula Szkody, Scott F. Anderson, Julie Lutz*

As the majority of stars are binaries, it is astrophysically important to understand the implications of binaries for stellar evolution. Binaries that form close enough that they will interact at sometime in their evolutionary lifetime are particularly interesting for LSST, as the interaction alters the evolution process in many ways that can result in spectacular transient and variable phenomena. In addition, the mass transfer and angular momentum losses during the interaction time have dramatic consequences on the evolution of the individual stars. For common low-mass stars, this evolution involves starting as two normal non-interacting main sequence stars, followed by the giant stage of the more massive star, which causes a common envelope resulting in angular momentum loss which brings the stars much closer together (Nelemans & Tout 2005). This stage is followed by the subsequent evolution of a normal star with a remnant white dwarf until continued angular momentum losses bring the stars close enough so the companion fills its Roche lobe and starts mass transfer (Verbunt & Zwaan 1981). Variations on this type of scenario can result in X-ray binaries and symbiotic stars (for more massive stars), cataclysmic variables (including novae, dwarf novae and novalikes) and ultimately, the AM CVn systems (Tutukov & Yungelson 1996).

The variability that is known so far for these types of systems is summarized in [Table 8.5](#) below. The challenge for LSST lies in detecting the variability and determining that the object is one of these types. As discussed in [§ 8.6.1](#), templates of various light curves have been run through the simulators to determine detectability. Determining the type of object requires both color and variability information. Close binaries that have not yet begun mass transfer will be easy to pick out because the colors of WD+MS stars are well known from SDSS (Smolčić et al. 2004; Silvestri et al. 2006, 2007). Other objects such as novae and dwarf novae will be selected on the basis of their variability. Objects with disks have a wide range in color based on the characteristics of the disks but generally are blue in color because they contain hot sources. This means that the selection will improve as LSST completes the full color information of the survey area and as templates of light curves of various objects are available for match up. After two years of survey operations, we anticipate both of these will be in place. While individual science goals (discussed below) vary for each type of object, a common goal for all close binaries for LSST lies in determining the correct space density of objects. LSST will reach to much fainter magnitudes (hence greater distances from Earth), and be more complete in reaching binaries with lower mass companions and with lower mass transfer rates than previous surveys. The derivation of the correct numbers will be matched with population and evolution models to determine the correct scenario for close binary evolution. In all cases, followup of candidates from the ground will enhance the science output. This includes determinations of orbital period, mass, and distance from spectroscopy and time-resolved photometry. Much of this work will involve the amateur community of observers in conjunction with professional astronomers.

### 8.8.1 Cataclysmic Variables

By definition, cataclysmic variables (CVs) are close binaries with mass transfer from a late type main sequence star to a primary white dwarf. Depending on the magnetic field strength of the white dwarf, the mass transfer will result in an accretion disk around the white dwarf (fields under

a MG), an accretion ring with inner area funneled to the magnetic poles for fields of 1-10 MG (intermediate polars), or direct transfer to the magnetic poles for fields over 10 MG (polars). The orbital periods range from 67 min to 2 days, with the majority of systems having periods under 2 hrs. A comprehensive review of all CVs can be found in [Warner \(1995\)](#).

For systems with disks, the mass transfer can lead to a thermonuclear runaway on the white dwarf (nova). When the H-rich accreted matter reaches about  $10^{-5} M_{\odot}$  and 1 km depth, the pressure becomes large enough to start nuclear fusion, which becomes a runaway due to the electron degeneracy. The rapid nuclear energy release causes the large rise in luminosity (7-15 mags) and the ejection of the envelope. These novae outbursts repeat on timescales of 10 yrs (recurrent novae) to  $10^4$  yrs. Between nova outbursts, the systems exist as dwarf novae or novalikes. The dwarf nova outbursts are due to a disk instability and can recur on timescales of days to decades, with a particular timescale and amplitude associated with the mass transfer rate. At high rates, the disk is stable with no outbursts and the systems are termed novalikes. At the lowest rates, the buildup to an outburst takes decades and the resulting outburst is very large (8 mags). For unknown reasons, the mass transfer can also stop completely for months to years, causing a drop in brightness by 4-5 mags (these times are termed low states). Since polars have no disks, they do not outburst and only show high and low states of accretion.

Table 8.5: Summary of Close Binary Timescales and Amplitudes

Variability	Typical Timescale	Amplitude (mag)
Flickering	sec – min	tenths
WD pulsation	4–10 min	0.01–0.1
AM CVn orbital period	10–65 min	0.1–1
WD spin (intermediate polars)	20–60 min	0.02–0.4
CV orbital period	10 min–10hrs	0.1–4
Accretion Disks	2–12 hrs	0.4
AM CVn Outbursts	1–5 days	2–5
Dwarf novae Outbursts	4 days–30 yrs	2–8
Symbiotic Outbursts	weeks–months	1–3
Symbiotic orbital period	months–yrs	0.1–2
Novalike High-Low states	days–years	2–5
Recurrent Novae	10–20 yrs	6–11
Novae	1000–10,000 yrs	7–15

The colors of CVs are clues to their accretion rates and their types. High mass transfer rate CVs are very blue ( $u - g < 0.0$ ) because their light is dominated by the accretion disk or column. Polars can be very red ( $i - z \sim 1$ ), when their emission is primarily from cyclotron harmonics. Very low mass transfer systems are both blue and red, because the accretion disk or column becomes a minor contributor to the optical light and the underlying star can be seen. Because the color range is so large, the optimum search for CVs must involve both variability and color.

In some cases, both stars have evolved to white dwarfs and the binary periods can be even shorter

(10 min) while the outbursts will be hotter due to the presence of a helium rather than a hydrogen accretion disk (AM CVns, see § 8.8.2). The orbital period can be revealed from photometry when the inclination is high enough to cause an eclipse, when there is a prominent hot spot on the disk where the mass transfer stream intersects the disk, or when the accretion area in a polar passes by the line of sight. In the latter case, the strong magnetic field locks the spin of the white dwarf to the orbit so all variation is at the orbital period. For intermediate polars, the spin of the white dwarf is seen as a periodic 10–20 min variation in the blue. If the white dwarf is in a specific temperature range (11,000–16,000K), it may have non-radial pulsations on the order of minutes.

If the mass transfer continues onto a white dwarf near the Chandrasekhar limit, a Type I SN may result (Ruiz-Lapuente et al. 2004); see the discussion in § 8.2.1.

Below we summarize two major science drivers for CVs in LSST:

### ***Determining the Space Density of CVs***

Identification of cataclysmic variables with LSST is important primarily for understanding the long term evolution and ages of close binary systems. Population models predict almost all close binaries should have evolved to the period minimum in the lifetime of the Galaxy (see Figure 8.22 below from Howell et al. 2001). Past surveys have been skewed by selection effects, which find the brightest and most active systems with outbursts. The true numbers of systems at various orbital periods are needed to sort out the evolution for different categories of systems, which is dependent on the angular momentum losses. The CVs found in SDSS have shown (Gänsicke et al. 2009) that the evolution model predictions of Howell et al. (2001) are correct in terms of predicting percentages of systems at various orbital periods down to 21st mag and in predicting an orbital period spike near 81 min (critical for confirming the angular momentum prescription and the white dwarf history). This model predicts the majority of CVs (70%) should be past the period minimum and have magnitudes of 22–24 (Politano 2004). LSST will be the first survey to test this endpoint of evolution. While LSST will identify the faintest CVs, followup observations (either continuous photometry to detect orbital variations due to hot spots in the disk or on the magnetic white dwarf or spectroscopy with large telescopes to obtain radial velocity curves) will be needed to find the correct periods.

While no disk CVs are known with periods between two and three hours, the period distribution of magnetic systems does not show this gap. This, and the unknown effects of a strong magnetic field on angular momentum losses, suggests that the evolution of the two types should be different, which might manifest itself as different number densities of the two populations. A related question is how much time systems spend in low states as they evolve. Also, the numbers of systems that contain pulsating white dwarfs is important in order to determine the instability zones of accreting pulsating white dwarf vs. non-interacting ones (Szkody et al. 2007).

SDSS was able to probe deeper than previous surveys and determine a space density of CVs of  $0.03 \text{ deg}^{-2}$  down to  $r \sim 21$  (Szkody et al. 2003) and  $M_v = 11.6 \pm 0.7$  at the period minimum (Gänsicke et al. 2009). However, SDSS observed primarily out of the Galactic plane, where the space density is lower. Estimates of the space density of these objects range from  $10^{-4}$  to  $10^{-6} \text{ pc}^{-3}$ , with a million objects expected in our Galaxy. LSST will go almost four mag deeper and closer to the

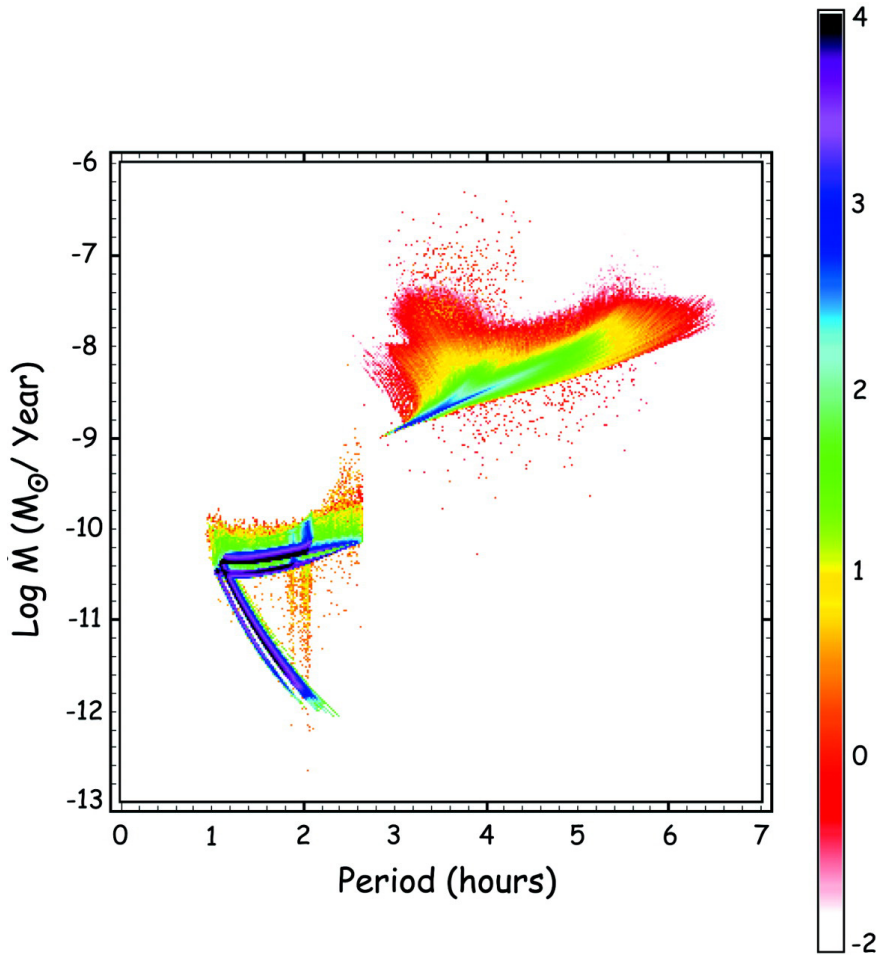


Figure 8.22: Predicted present-day population of cataclysmic variables in the Milky Way (from Howell et al. 2001). The models are presented in the mass transfer ( $\dot{M}$ ) - orbital period plane and shown as a density distribution. The scale on the right side gives the number of CVs per colored dot as a log scale and the majority of present-day systems are expected to lie at very short orbital period (less than two hours) and have very little mass transfer, and thus will be intrinsically very faint. The LSST survey will be the first survey to allow the majority of the systems modeled here to be discovered.

Galactic plane, the coverage will extend to larger distances and lower mass transfer rates (both of which contribute to fainter observed magnitudes).

### *Nova as Probes of Mass, Composition, and Distance*

Nova are the intrinsically brightest CVs during outburst ( $M_v = -6$  to  $-9$ ) and can thus serve as a probe of conditions in our own Galaxy as well as other galaxies. While novae generally have fast rise times of a few days, the decline time and shape give important information as to the mass, distance, and composition. Due to the mass-radius relation of white dwarfs, there is a tight correlation of a nova peak luminosity and time to decline by 2-3 magnitudes (Shara 1981). Slow novae are more common, have absolute magnitudes fainter than  $-7$ , show FeII lines in their

spectra, and are located in the bulge of our Galaxy (Della Valle & Livio 1998). Fast novae occur on more massive white dwarfs, are brighter, show He and N in their spectra, forbidden lines of O, Ne, and Mg in their ejecta (Gehrz et al. 1986; Starrfield et al. 1992), and are generally found in the disk.

Since the two types of novae are found in different locations and are important in the production of CNO isotopes, the correct rates are needed to understand Galactic chemical evolution and star formation history (the latter since the rate is dependent on binary star formation and evolution). LSST will be able to find the fainter novae to greater distance in our Galaxy and provide improved estimates of the nova rate and type in the Milky Way to compare to those found in other galaxies. Estimates of the nova rate in the Milky Way currently are on the order of  $35 \pm 10/\text{yr}$ , with rates in other galaxies scaling as the mass (Shafter 2002). While LSST will only observe a few novae from the Milky Way each year, some of these will be close enough to observe the precursor star within a few days of the actual outburst, thus providing new information on the outburst process. The numbers of recurrent novae are thought to be underestimated by a factor of 100 (Schaefer 2009) due to missed outbursts. This number is especially important to pin down because these could be Type Ia SN progenitors.

### 8.8.2 AM CVn Systems

AM CVn binaries are extremely rare relatives of cataclysmic variables with ultra-short orbital periods; the most extreme cases have orbital periods of tens of minutes, arguably encompassing the shortest orbital periods of any known class of binaries (see review by Nelemans 2005). AM CVn systems are so compact that both binary components must be degenerate (or least partially so), likely with mass-transfer driven by gravitational radiation from a helium-rich degenerate ( $\sim 0.02M_{\odot}$ ) onto a more standard white dwarf. Their optical spectra are distinct from typical CVs: membership in the AM CVn class requires a near absence of hydrogen, and helium lines are instead prominent. There are about 20 known at the present time.

The unusual nature of the prototype, AM CVn, was recognized some time ago (Smak 1967; Paczyński 1967), but the next four decades yielded less than a dozen additional discoveries. Though elusive, AM CVns have emerged as objects of renewed interest for several reasons: their evolutionary link to and possible insights about an earlier common envelope phase; as possible SN Ia progenitors (e.g., Liebert et al. 1997); and perhaps notably on the LSST timescale, as one of the most common objects likely detectable by upcoming gravitational wave experiments. For example, some formation and evolutionary models suggest that up to  $\sim 10^4$  AM CVns and related double-degenerates may be detected/resolved in gravity waves by LISA (Nelemans et al. 2004).

Eight new AM CVn systems have been discovered in the past few years especially from SDSS (Roelofs et al. 2005; Anderson et al. 2005), including the first eclipsing AM CVn. The bulk of known AM CVns occupy a relatively small region of multicolor space (see Figure 2 in Anderson et al. 2005), and so (similar) LSST-filter imaging should provide a basis for multicolor selection. However, there are still plenty of other objects in this region of color space, such as normal white dwarfs, quasars, and ordinary CVs, and only a small fraction of randomly selected objects with such colors in SDSS (to  $m \leq 20.5$ ) are subsequently verified as AM CVns. Multicolor selection alone is not efficient.

The additional time domain information available in LSST imaging will provide an important additional sieve to find these rare objects, as the variability of AM CVns will distinguish them from normal white dwarfs. Groups are currently engaged in variability-selection programs focused especially on AM CVns, and these results can guide LSST efforts. Optical variability for AM CVn's is typically  $\sim 0.1$  mag on orbital timescales of tens of minutes, but  $\sim 1$  mag for the one known eclipsing case (sharp 1-minute eclipses on a 28 min orbital period); and, often a few tenths of a mag on longer timescales (weeks, months, years). Strong variations of up to several magnitudes are seen in the substantial subset of AM CVn's that show outbursts.

The surface density of AM CVns is highly uncertain, due to survey completeness. SDSS discoveries suggest a surface density  $\geq 0.001\text{deg}^{-2}$  ([Anderson et al. 2005](#)). But some AM CVn population models ([Nelemans et al. 2004](#)) predict a population of thousands of AM CVn to a modest depth of  $m < 22$ , easily accessible to LSST.

The availability of accurate LSST colors, plus LSST light curve information, should yield an excellent list of AM CVn candidates with quantifiable selection. Followup confirmation via detailed light curves and/or spectroscopy will be required in many cases. Candidate lists from LSST should, of course, also be cross-correlated with available all-sky X-ray surveys (most AM CVn are X-ray sources), and ultimately (but more speculatively) future catalogs of sources of gravitational radiation. As example science, the AM CVn orbital period distribution (usually from the optical), coupled with mass-transfer rates (often from X-ray measures), are key ingredients in testing evolutionary models for AM CVn and related double degenerates in the presence of marked gravitational radiation (e.g., [Nelemans 2005](#)).

### 8.8.3 Symbiotic Stars

Symbiotic stars (SS) show variability on a variety of timescales and magnitude ranges. The classic symbiotic system has an M-type star (often a giant, which is called the primary in these systems) in a binary system with a white dwarf (secondary) that is close, but not so close that the system exhibits the sort of chaotic phenomena present in cataclysmic variables. Some of the primaries in SS are Mira variables with periods of hundreds of days and amplitudes of several magnitudes, while others are semi-regular variables with smaller amplitudes. Some don't appear to be variable at all. Not all the primaries are red stars. There is a group of SS known as the "yellow symbiotic stars" which have F, G, or K stars as the primary. In addition, a few systems have K stars instead of white dwarf secondaries. SS show two distinct groups in the near-infrared (S-type symbiotic stars have declining flux while D-type show the signature of warm dust accretion disks, presumably around the dimmer stars). Thus, the range of colors of SS is large.

Some SS have dramatic sudden non-periodic outbursts of several magnitudes. The brighter ones are sometimes called "slow novae" because they brighten by a few magnitudes and remain bright for months. Others outburst and decline in weeks. LSST will contribute greatly to SS research by determining the number, timescales, and shapes of the outbursts. LSST alerts will enable intensive followup observations as soon as an outburst is reported. Some SS also show flickering in the  $u$  filter (caused by the accretion disk or hot spot(s)) on timescales of minutes to hours. LSST will determine if there are long-term changes or periodicities in these systems. For many SS, not enough observations have been made to know for sure whether or not they are variable. They were

identified as SS in a spectroscopic survey (M-type star plus chromospheric emission lines). This is especially true in the southern hemisphere, where there are many in the plane of the Galaxy at declinations  $< -25^\circ$ . Thus, LSST can refine the definition of the SS class (e.g., how many SS are really variable and with what timescales and magnitudes in various wavelength bands?).

## 8.9 Magnetic Activity: Flares and Stellar Cycles

### 8.9.1 Flaring in Cool Stars

*Eric J. Hilton, Adam Kowalski, Suzanne L. Hawley, Lucianne M. Walkowicz, Andrew A. West*

Because low mass stars comprise nearly 70% of stars in the Galaxy, their flares represent a major source of transient variability in time domain surveys such as LSST (§ 8.2.2). These flares are manifestations of internal magnetic field production and the subsequent emergence of these fields at the stellar surface – processes which are poorly understood even in the Sun, but particularly elude physical description in late-type M dwarfs. As stars become fully convective below  $\sim 0.3 M_\odot$  (Chabrier & Baraffe 1997), the nature of the magnetic dynamo changes, which may alter the relationship between *quiescent* magnetic activity (persistent chromospheric and coronal emission in the optical, UV, and X-ray) and the large transient increases in the continuum and line emission caused by *flare* activity. The flare rate may also be influenced by the effective temperature of the star, with lower temperatures inhibiting field emergence in the quiescent state, but promoting field storage and eruption of huge flares (Mohanty et al. 2002). Stellar flares also have interesting implications for astrobiology because the cumulative effect of high energy irradiation by flares may impact the evolution and eventual habitability of planets (Lammer et al. 2007). Because low mass, largely convective M dwarfs are the most numerous of potential planetary hosts, it is essential to understand how frequently and powerfully these stars flare.

LSST will obtain an unprecedented data set of M dwarf flares over a range in activity level, mass, and age. Since individual flares will only be observed once or at most twice by LSST, these sparsely sampled light curves of M dwarfs require sophisticated interpretation. Using repeat photometric observations of SDSS Stripe 82 ( $\sim 250 \text{ deg}^2$ ) in combination with a new model of the Galaxy, we are currently developing the analysis tools needed for interpreting the LSST flare data. Our new Galactic model includes the most current mass and luminosity functions of low mass stars (Covey et al. 2008; Bochanski et al. 2007a, 2008; West et al. 2008). In this section, we present preliminary estimates of the flares that LSST will observe using this model Galaxy.

#### *Activity in Low Mass Stars*

Previous large scale surveys have been instrumental in understanding activity in low mass stars. Observations of over 38,000 M dwarfs in the SDSS revealed that the fraction of “active” stars (those which have H $\alpha$  emission with equivalent width  $> 1\text{\AA}$ ) increases dramatically from types M0 to M6, peaking near spectral type M7-M8. The observed active fraction depends on distance; stellar activity declines with age, and stars that are further out of the plane are likely to be older than nearby stars (West et al. 2008). Although cool stars are designated as active or inactive by whether they have H $\alpha$  in emission or absorption, most so-called “inactive” stars actually possess

low to moderate levels of magnetic activity. Therefore, while most flare stars will belong to the “active” population, low to moderate activity stars may also flare.

Flares have been observed throughout the M spectral class, as well as on the less massive L dwarfs (e.g., Liebert et al. 1999; Schmidt et al. 2007). It has been suggested that activity in ultra-cool dwarfs is confined primarily to large flares, with little or no “quiescent” emission (Rutledge et al. 2000; Linsky et al. 1995; Fleming et al. 2000). In contrast, UV spectra of active M7-M9 dwarfs have shown that quiescent transition region (C IV) emission is present at levels comparable to those seen in earlier active M dwarfs (Hawley & Johns-Krull 2003). Activity (in the form of persistent H $\alpha$  emission) has been detected on a number of nearby T dwarfs, but to date no T dwarf flares have been observed (Burgasser et al. 2002).

Flare light curves (see Hawley & Pettersen 1991; Eason et al. 1992; Hawley et al. 2003; Martín & Ardila 2001, for examples and discussion) generally consist of a sudden increase in brightness that is most extreme in the near UV and blue optical, followed by a long tail as the star gradually returns to its quiescent state. The largest flares cause brightness enhancements of  $\sim 5$  magnitudes in  $u$  and persist for over an hour, although small flares of fractions of a magnitude and a few minutes’ duration are much more common. The magnitude changes associated with flares are dependent on both the spectral type of the object and the observation filter. In early M dwarfs, the quiescent flux in the optical is much higher than in the ultra-cool M and L dwarfs—therefore the optical contrast between the quiescent star and the flare emission is higher in later type stars. While the flare contrast is greatest in  $u$ , most flares will be visible (although with a smaller increase in brightness) in  $g$ ,  $r$ , and to a lesser extent in  $i$ .

### ***Preparing for LSST: Results from SDSS Repeat Photometry***

The repeat photometry of SDSS Stripe 82 (Ivezić et al. 2007) provides a useful test set of observations for developing analysis tools for LSST. Although the sky area ( $250 \text{ deg}^2$ ) is much smaller, the data less deep and the cadence less frequent, the Stripe 82 data are qualitatively similar to those that LSST will produce. We here summarize the results of the flare analysis of Kowalski et al. (2009).

Considering stars of spectral types M0–M6 with  $u_{\text{quiet}} < 22$  on Stripe 82, SDSS detected 270 flares with a  $u$ -band magnitude change of at least 0.7. Flares as large as  $\Delta u \sim 5$  magnitudes were observed in both early and late type M stars, but flares of  $\Delta u < 2$  magnitude dominate the sample. Later type stars show a higher flaring rate. Ninety-two percent of the stars that have spectra and also show flares in the SDSS photometry have H $\alpha$  emission during quiescence. One of 10,000 total SDSS observations of M dwarfs show flares, but the flare fraction rises to  $\sim 30$  out of 10,000 observations of *active* M dwarfs (i.e., those with emission lines) show flares. Clearly the stars that have quiescent magnetic activity are more likely to flare.

The observed flare rate is very strongly dependent on the line of sight through the Galaxy, since this changes both the number of stars per  $\text{deg}^2$ , and the age and activity of the stars observed. Given the high flare rate for active stars, it is not surprising that the flaring fraction decreases sharply with Galactic  $Z$  for all spectral types:  $\sim 95\%$  of the flaring observations occur on stars that are within 300 pc of the plane, and the flare rate ranges from 0 to 8 flares,  $\text{hr}^{-1} \text{deg}^{-2}$  depending on Galactic latitude.

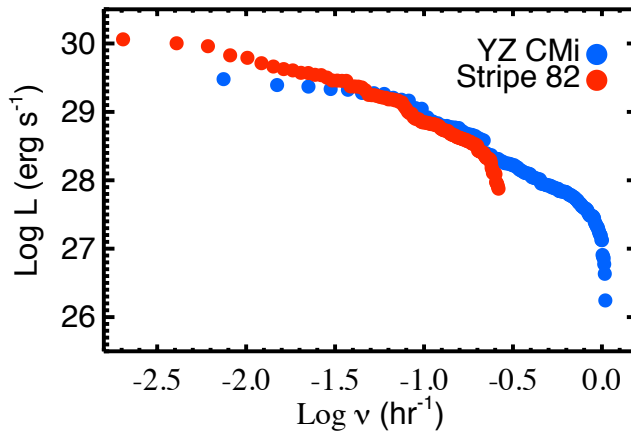


Figure 8.23: The flare luminosity distribution of  $\sim 40$  M4-5 stars in SDSS Stripe 82 compared to extensive flare observations of the M4.5 flare star YZ CMi (from [Lacy et al. 1976](#)). We will similarly be able to compare sparsely sampled photometric observations of millions of M dwarfs in LSST to a handful of closely monitored, well-known flare stars in the solar neighborhood.

Analyzing flares at the Stripe 82 cadence (or even that of LSST) is difficult because any individual flare is only observed once. Without time resolution, it is impossible to determine when during the flare the observation occurred, and therefore know the total energy, peak luminosity, or flare duration. However, we can use the instantaneous luminosity of the flare to infer its properties. [Figure 8.23](#) compares the distribution of flare luminosities of  $\sim 40$  M4-5 dwarfs in Stripe 82 to results from the optical flare rate survey of [Lacy et al. \(1976\)](#) for the M4.5 dwarf YZ CMi. In the case of the YZ CMi observations, where the light curve captures the entire flare, we calculate the average flare luminosity. The close agreement between the flare luminosity distributions found from the Stripe 82 sparsely sampled light curves and the very well-sampled light curves of YZ CMi shows that we are able both to confidently identify flares in the data and to determine their average luminosity.

### Flares in LSST

In addition to being astrophysically interesting, stellar flares also represent a source of confusion for “true” transient events, as stars that are below the detection limit in quiescence may be visible during flare events ([§ 8.2.2](#)). The flare energy cut-off, spectral types, stellar ages, and activity status, along with the line of sight, all contribute to the flaring rate determined for an observed sample of M dwarfs.

In order to understand the rate and energy distribution of flares LSST will observe, we are developing a new model of M dwarf flares in the Galaxy. Existing observations will be combined with a new flare monitoring effort (E. Hilton, PhD thesis, in preparation) to empirically determine the rate and energy distribution of M dwarf flares. We can then use this flare frequency distribution to construct light curves for each M dwarf in our model Galaxy. Every star in the model has a

position, distance, and quiescent magnitude in each SDSS/LSST filter, and a light curve populated with flares, allowing us to “observe” stars using simulated LSST cadences.

In [Figure 8.24](#), we demonstrate how our model may be used to interpret flare observations in LSST. The top panel shows our theoretical prediction for how often a star is observed at a given increase in brightness ( $\Delta u$ ). Since stars are in quiescence much of the time, this distribution peaks at  $\Delta u = 0$ , and because large flares are much less frequent than smaller flares, the distribution has a long tail towards larger  $\Delta u$ . The red and blue lines represent two flare frequency distributions, given by  $\log \nu = \alpha + \beta \log E_u$ , where  $\nu$  is the number of flares per hour,  $E_u$  is the total flare energy in ergs/sec,  $\beta = -1$ , and  $\alpha$  varies from 21.5 to 22.0.

The bottom panel shows the result of sampling this theoretical distribution using the LSST operations simulation cadences ([§ 3.1](#)) for 300 identical  $u = 20$  M dwarfs at eight different telescope pointings. Photon sky noise gives the broad peak around  $\Delta u = 0$  magnitudes. For flares with  $\Delta u \gtrsim 0.07$  magnitudes, the two distributions are quite distinct.

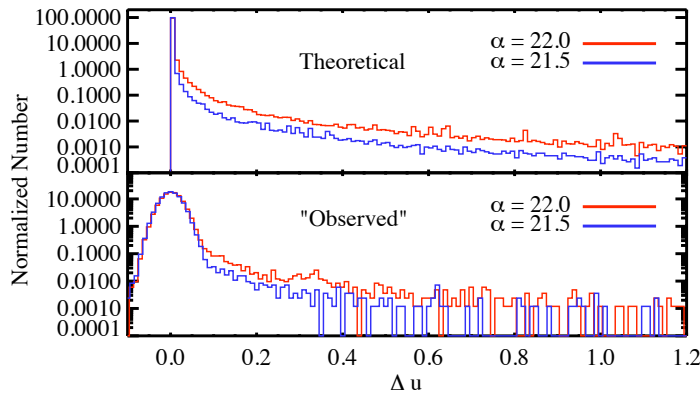


[Figure 8.24:](#) *Top panel:* Model flare frequency distributions. *Bottom panel:* These distributions “observed” for 300 identical stars at  $u = 20$  using the operations simulation and simulated seeing effects.

The model can also be used to calculate the amount of time a flare will appear to be a truly transient event, i.e., how often a star not detected in quiescence will brighten above the detection limit. In [Figure 8.25](#), we show the number of stars along a particular line of sight in our model, along with the number of stars that are invisible as a function of survey limiting magnitude. The superior depth of LSST, particularly in the deep drilling fields, means that for certain lines of sight we will likely observe *all* M dwarfs.

Using our model, we can thus predict the number and brightness of flares that LSST will see before data collection begins. These predictions will be useful to separate flares from other variable objects of interest. Once LSST is gathering data, we will compare our model predictions to the empirical data to refine the model and produce a better description of M dwarf flare frequency distributions as a function of spectral type.

The unique power of LSST to open the time domain will allow us to statistically determine the flare frequency distribution as a function of stellar type, age, and activity level with unprecedented

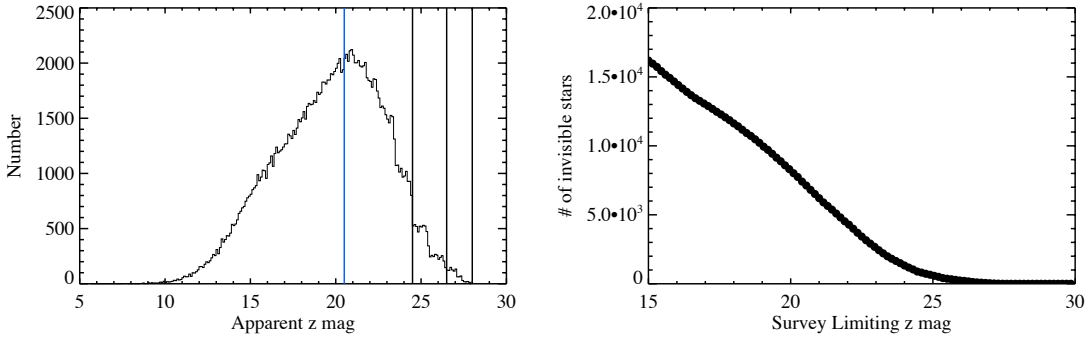


Figure 8.25: The apparent  $z$  magnitude distribution of M dwarfs along a line of sight in a model representation of the Milky Way. The model includes the most current mass and luminosity functions of low mass stars (Covey et al. 2008; Bochanski et al. 2007a, 2008; West et al. 2008). The blue line is the SDSS  $z$ -band limiting magnitude. The black lines are LSST single visit, co-add, and deep drilling limits. Notice that for this sight line, SDSS is unable to detect a large fraction of the M dwarfs in the Galaxy, while LSST will detect the vast majority. Shown on the right is the number of objects not seen in quiescence as a function of survey limiting depth. As expected, it decreases monotonically. Note that it becomes completely negligible around  $z = 27$ . Flares on objects not seen in quiescence will appear as true optical transients, whereas flares on known objects will be easier to categorize.

accuracy. The flare rates will be interpreted from the data with the aid of models and tools for finding flares with sparsely sampled light curves that are already in development. At the excellent photometric accuracy of LSST, it will be possible to resolve even relatively small flares, and therefore constrain chromospheric and coronal heating mechanisms in the outer atmospheres of these stars.

### 8.9.2 Resolving the Stellar Dynamo: Activity Cycles Across the Main Sequence

*Stylani (Stella) Kafka*

The Mount Wilson Observatory HK survey (Wilson 1982) produced the first comprehensive sample of long-term stellar light curves of stars with spectral types F5 to M2. These light curves indicated that while most stars have activity cycles, which are not necessarily similar to the solar cycle in amplitude and duration. Since then, studies of stellar activity have revealed fundamental properties of magnetic field generation and evolution in stars of all spectral types, but these revelations have produced a rather confusing picture. Oláh et al. (2007) report variations of the length of stellar and solar activity cycles and a connection with stellar rotation in that stars with long rotation periods have longer cycle periods (Oláh et al. 2000). The Baliunas et al. (1995) study of 111 dwarfs with spectral types between G0 and K7 from the Mount Wilson HK sample, indicate that only 1.5% of the stars display cycles similar to the Sun's. According to that study, F dwarfs seem to either have non-detectable cycles or very long ones, while K dwarfs seem to have very pronounced cycles, and Maunder-minima-like activity levels are detected only in solar-like stars. Activity cycles in fast rotating, young solar-type stars seem to range from 2.1 to  $\sim 10$  years (Messina & Guinan 2003). At the same time, the existing theory of magnetic field generation and stellar activity dictates that an  $\alpha\Omega$  type dynamo acting in the interface between the convection zone and radiative core of stars

(the tachocline) is responsible for the large-scale, solar-like dipole field. Such a dynamo is in action for *all* stars with a tachocline, and it provides the means for magnetic braking which is the main angular momentum loss mechanism in stars. However, the diversity in the cycle behavior – even within the same stellar spectral types – suggests that our understanding of the stellar magnetic field generation and evolution is still not clear.

Current studies of stellar activity use snapshot observations of a large number of field stars to assess the properties of activity for stars of various spectral types. However, we still have not been able to reach a coherent picture of the properties (amplitude, duration, variability, and so on) of activity cycles for stars across the main sequence, especially when it comes to the lower mass objects (late K and M dwarfs). Although the simple model of solar-like magnetic field generation should not apply in these low mass, fully convective stars, the level and character of their activity seems to be indistinguishable from that of earlier spectral type stars. A plethora of new models have attempted to explain this phenomenon by focusing on the effects of fast rotation alone on magnetic field generation (e.g., Chabrier & Küker 2006; Baliunas et al. 2006) with no satisfactory results. The lack of evidence that activity changes character when stars become fully convective and the numerous alternative proposed mechanisms (none of which can be securely confirmed or dismissed) demonstrate the need of a large, unbiased statistical sample to study properties of activity cycles in main sequence stars.

An ideal sample would consist of a number of open star cluster members for which ages and metallicities are easily extracted. Existing data are restricted to the brighter cluster members, leaving late K and M stars out of the equation. Long-term monitoring of order thousands of K/M dwarfs would provide solid and secure results freed from small number statistic biases and serendipitous discoveries. Spot coverage during activity cycles is a ubiquitous fingerprint of the underlying dynamo action over long periods of time; therefore, long-term monitoring is desired in order to reveal the mechanism in action for stars of different spectral types and in different environments. Thus far the few existing studies of stellar cycles resulted from visual observations of bright nearby stars by amateur astronomers and/or observations with 1-m class automatic photometric telescopes (APTs) focused on specific objects and/or limited parts of the sky. Especially for late K/M dwarfs, the length and intensity of relevant activity cycles has not been systematically investigated. One of the few examples is Proxima Centauri (M5.5V), which is found to have a  $\sim 6$  year activity cycle (Jason et al. 2007)<sup>5</sup>. Prior to LSST, CoRoT and Kepler will define properties of short-term (minutes to months) secular stellar brightness variations due to starspot evolution on field stars (over a small portion of their activity cycle). However, even those observations are time and frequency limited, and address an inhomogeneous stellar population (field stars). Long-term, multi-epoch observations, covering the time and frequency domain for a large number of objects sharing common properties, are essential to reveal the characteristics of activity cycles of stars of all spectral types.

For the first time, LSST will provide the large (and faint!) sample population required to reveal properties of activity cycles in stars of different spectral types and ages. Using LSST data we will build the first long-term, multi-frequency light curves of stars past the mass limit of full convection. This will suffice to reach the end of the main sequence in a large number of open star clusters, observing stars of all ages and metallicities – parameters that are hard to obtain for field stars. With a limiting magnitude of  $r = 24.7$  per visit, LSST will provide  $\sim 1,000$  points for each star

<sup>5</sup>Although this star is fully convective, its activity characteristics appear to be solar-like.

(in each filter) during the first 5 years of its operation. Although activity cycles can be longer (5 years is  $\sim 50\%$  of the cycle for a solar twin), a five-year coverage will allow us to detect long-term modulations in the light curves of thousands of stars. In turn, these long baseline light curves will allow us to probe the character and evolution of stellar activity cycles in an unbiased way, deriving correlations between cycle duration, stellar ages, and spectral type (or depth of the convective zone) for cluster members.

The length of activity cycles will provide constraints for existing dynamo models and identify trends in various stellar cluster populations. We will be able to determine average timescales and the amplitude of variations in stellar cycles, answering fundamental questions: How does the stellar dynamo evolve over a cycle for different stellar masses? Is there a dependence of the amplitude and duration of cycles on stellar age and/or metallicity for stars of specific spectral types? Can we identify changes of the dynamo properties (in terms of activity cycle characteristics) in M stars at the mass regime where their interior becomes fully convective? Do fully convective stars have activity cycles? Do all stars have Maunder minimum-like characteristics? Furthermore, LSST will resolve how cycle-related stellar flux variations affect a star's habitable zone, providing essential information on how common the Earth's environment is in the Universe.

## 8.10 Non-Degenerate Eruptive Variables

### 8.10.1 The Death Rattle of High Mass Stars: Luminous Blue Variables and Cool Supergiants

*Nathan Smith, Lucianne M. Walkowicz*

The scarcity of high mass stars poses a serious challenge to our understanding of stellar evolution atop the H-R diagram. As O-type stars evolve off the main sequence, they may become Luminous Blue Variables (LBVs), red supergiants, yellow hypergiants, blue supergiants, or they may evolve through several of these phases sequentially, depending on their initial mass, metallicity, and rotation (e.g., Chiosi & Maeder 1986; Meynet et al. 1994; Langer 2004). These death throes can sometimes be characterized by extreme mass loss and explosive outbursts that in some cases are short-lived and possibly intermittent (Smith & Owocki 2006; Humphreys & Davidson 1994). There are only a handful of nearby massive stars that are caught in this phase at any given time (as in the case of  $\eta$  Carinae), and as a result, they appear unique or exceptional when considered in context with other stars. They may nevertheless represent a very important phase that most massive stars pass through, but it is difficult to judge how representative they are or how best to account for their influence in models of stellar evolution. The lack of extensive data for these stars makes it very difficult to connect distant explosions (supernovae and GRBs) to their underlying stellar populations.

Although LBV outbursts can be seen up to 80 Mpc away, the best-studied LBVs are in the plane of our own Galaxy (predominantly in the southern hemisphere). Unfortunately, the Galactic LBVs are few, and so these and cooler outbursting stars have eluded meaningful statistical study to date. A small number of them have been studied in very nearby galaxies (e.g., Hubble & Sandage 1953; Tammann & Sandage 1968; Humphreys & Davidson 1994; Drissen et al. 1997; Massey et al. 2007). However, the improved breadth and sensitivity of LSST are ideally suited to the study of

these intrinsically rare objects. LSST will make these extremely luminous stars accessible in many galaxies, offering a new opportunity to improve the sample of known evolved massive stars.

Time resolved observations of variability in the new sample provided by LSST will quantify the statistical distribution of time dependent mass loss rate, luminosity, radiated energy, total ejected mass, duration of outbursts, time between outbursts, and connections to the pre-outburst stars. Outbursts last anywhere from  $\sim 100$  days to a year, so the universal cadence of LSST will revisit their evolving light curves several times in multiple passbands as the outburst progresses. In the case of red supergiants, variability provides a key discriminating factor between foreground red dwarfs and extragalactic massive stars. Time domain observations may also resolve the evolution in the amplitude and timescale of variability as these stars expand and cast off their outer layers.

New observations will inform models of massive star evolution, providing prescriptions for the time-dependent properties mentioned above so that they can be included in stellar evolution codes in a meaningful way. Stellar evolution codes that predict the fates of massive stars over a range of mass and metallicity (e.g., Heger et al. 2003) do not currently include the effects of LBV-like outbursts because an empirical assessment of their properties as functions of initial mass and metallicity does not yet exist. LBV eruptions are currently ignored in stellar evolution codes, even though they may dominate the total mass lost by a massive star in its lifetime and may, therefore, be key to the formation of Wolf-Rayet stars and GRB progenitors over a range of metallicity (Smith & Owocki 2006). Many model grids do not extend to sufficiently cool temperatures at high masses, leaving the formation of the most luminous red supergiants largely unexplained by detailed theory. Most evolution codes also do not include the effects of pulsations that drive large temperature variations in red supergiants, in some cases pushing them far cooler than the Hayashi limit for periods of time (although see Heger et al. 1997).

By providing a new sample of these stars in other galaxies, LSST will also enable studies of high mass stellar evolution as a function of metallicity. Absorption by lines of highly ionized metals plays a major role in accelerating winds in these objects (e.g., Castor et al. 1975), thereby driving mass loss and affecting the duration of late stages of evolution (Chiosi & Maeder 1986). Current theory holds that metallicity affects the relative number of blue versus red supergiants by changing the duration of these end stages (Meynet et al. 1994), but these models do not include the effects of pulsation-driven or outburst-driven mass loss. In a complementary fashion, further study of these stars will also improve our understanding of their contribution to galactic feedback and enrichment of the interstellar medium.

LSST will also bring insight to another open question: the true nature of core collapse supernova (CCSN) progenitors (e.g., Smartt et al. 2009). A large sample of evolved massive stars will propel our understanding of the diversity of CCSN progenitors. Among the large sample of luminous stars monitored in nearby galaxies, some will explode *while they are being monitored*. This will provide not only an estimate of the star's pre-explosion luminosity and temperature, but also its variability and potential instability in the final years of its life. For example, red supergiants that explode as Type II-P SNe may exhibit strong photometric variability, and this must be accounted for when using pre-explosion data to infer the star's initial mass and radius. Additionally, there is growing evidence that a subset of massive stars suffer violent precursor outbursts, ejecting large amounts of mass in the decades leading up to core collapse (Smith et al. 2007). The resulting SNe are called Type IIn because of the narrow H lines that arise in the dense shocked circumstellar gas (Filippenko 1997). These Type IIn SNe come in a wide range of luminosity and spectral properties and may

trace a diverse group of progenitors that suffer precursor outbursts. These pre-SN outbursts are neither predicted by nor explained by current stellar evolution theory. With an observed record of pre-SN variability, we can connect properties of these precursor outbursts and the resulting SN to determine which outbursts are pre-SN and which are not. Furthermore, the enormous outbursts of LBVs themselves may masquerade as low luminosity Type IIn SNe (e.g., [Van Dyk et al. 2000](#)). Time resolved observations of relatively large samples of potential CCSN progenitors will provide new insight into the nature of this intriguing population. With high enough imaging resolution, stellar population studies of the surrounding field stars can constrain the local star formation history, and thus constrain the delay time between star formation and core collapse.

### 8.10.2 Eruptive Variability in Pre-Main Sequence Stars

*Peregrine M. McGehee*

Variability is one of the distinguishing features of pre-main sequence stars and can result from a diverse collection of physical phenomena including rotational modulation of large starspots due to kiloGauss magnetic fields, hot spots formed by the impact of accretion streams onto the stellar photosphere, variations in the mass accretion rate, thermal emission from the circumstellar disk, and changes in the line of sight extinction. These physical processes generate irregular variability across the entire LSST wavelength range (320–1040 nm) with amplitudes of tenths to several magnitudes on timescales ranging from minutes to years and will be detectable by LSST.

Due to its sensitivity and anticipated ten-year operations lifetime, LSST will also address the issue of the eruptive variability found in a rare class of young stellar objects - the FUor and EXor stars. FUor and EXor variables are named after the prototypes FU Orionis ([Hartmann & Kenyon 1996](#)) and EX Lupi ([Herbig et al. 2001](#)) respectively. These stars exhibit outburst behavior characterized by an up to 6 magnitude increase in optical brightness, with high states persisting from several years to many decades. Both classes of objects are interpreted as pre-main sequence stars undergoing significantly increased mass accretion rate possibly due to instabilities in the circumstellar accretion disk. The mass accretion rates during eruption have been observed to increase by 3 to 4 orders of magnitude over the  $\sim 10^{-9}$  to  $10^{-7} M_{\odot}$  per year typical of Classical T Tauri stars. Whether FUor/EXor eruptions are indeed the signature of an evolutionary phase in all young stars and whether these outbursts share common mechanisms and differ only in scale is still an open issue.

To date only about 10 FUors, whose eruptions last for decades, having been observed to transition into outburst ([Aspin et al. 2009](#)) with the last major outburst being that of V1057 Cyg ([Herbig 1977](#)). Repeat outbursts of several EXors have been studied, including those of EX Lupi ([Herbig et al. 2001](#)) and V1647 Ori ([Aspin et al. 2009](#)), the latter erupting in 1966, 2003, and 2008. The outbursts of EXors only persist for several months to roughly a year in contrast those of FUors, which may last for decades: for example, the prototype FU Ori has been in a high state for over 70 years. These eruptions can occur very early in the evolution of a protostar as shown by the detection of EXor outbursts from a deeply embedded Class I protostar in the Serpens star formation region ([Hodapp et al. 1996](#)). The observed rarity of the FUor/EXor phenomenon may be due to the combination of both the relatively brief (less than 1 Myr) duration of the pre-T Tauri stage and the high line of sight extinction to these embedded objects hampering observation at optical and near-IR wavelengths.

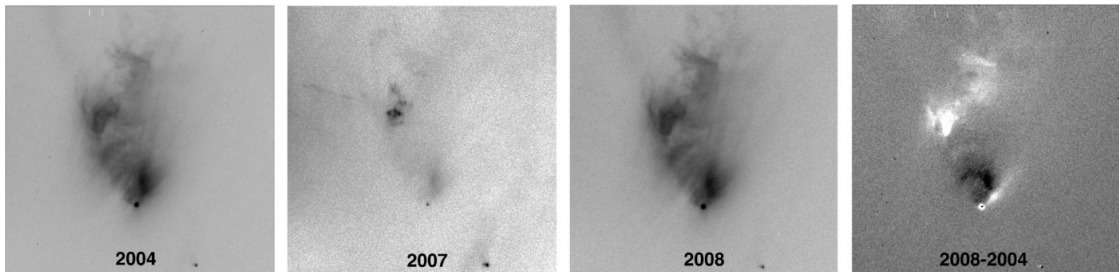


Figure 8.26: This series of images from Aspin et al. (2009) shows the region containing McNeil’s Nebula and the EXor V1647 Orionis (seen at the apex of the nebula). The observations span (*left*) 2004 to (*middle right*) 2008 and include two outbursts and an intervening quiescent period. On the right is the difference image between the 2004 and 2008 outbursts.

V1647 Ori is a well-studied EXor found in the Orion star formation region ( $m - M = 8$ ) and thus is a suitable case study for discussion of LSST observations. Figure 8.26 shows  $r'$  and  $R$  imaging of V1647 Ori (Aspin et al. 2009) demonstrating the appearance of the protostar and surrounding nebulosity during the two most recent eruptions and the intervening low state. The inferred extinction is  $A_r \sim 11$  magnitudes which coupled with the observed  $r$  range of 23 to nearly 17 during outburst (McGehee et al. 2004) suggest that  $M_r$  varies from 4 to  $-2$  magnitudes.

The LSST single visit  $5\sigma$  depth for point sources is  $r \sim 24.7$ , thus analogs of V1647 Ori will be detectable in the  $r$  band during quiescence to  $(m - M) + A_r = 20.5$  and at maximum light to  $(m - M) + A_r = 26.5$ . The corresponding distance limits are 800 pc to 12 kpc assuming  $A_r = 11$ . For objects at the distance of Orion the extinction limits for LSST  $r$ -band detections of a V1647 Ori analog are  $A_r = 12.5$  and  $A_r = 17.5$ . These are conservative limits as V1647 Ori was several magnitudes brighter at longer wavelengths ( $iz$  bands) during both outburst and quiescence indicating that the LSST observations in  $izy$  will be even more sensitive to embedded FUor/EXor stars.

LSST will increase the sample size for detailed follow-up observations due its ability to survey star formations at large heliocentric distances and to detect variability in embedded and highly extincted young objects that would otherwise be missed in shallower surveys. During its operations LSST will also provide statistics on the durations of high states, at least for the shorter duration EXor variables.

## 8.11 Identifying Transiting Planets with LSST

*Mark W. Claire, John J. Bochanski, Joshua Pepper*

Large planets in close orbits (a.k.a “hot Jupiters”) spend 1–5% of their orbital period transiting their host stars, if viewed edge-on. Thus, given optimal geometry, 10–50 of the  $\sim 1,000$  LSST observations of a given star with a transiting hot Jupiter will occur in eclipse. Preliminary results from the Operations Simulator (§ 3.1) indicate that LSST will dramatically increase the number of known hot Jupiter systems, expanding their census to greater Galactic depths.

### 8.11.1 What Will We Learn about Transiting Planets from LSST?

The primary scientific gains will lie in three areas:

*Studying the hot Jupiter frequency distribution at large distances.* By the conclusion of LSST's ten-year science run, the frequency of nearby hot Jupiters should be relatively well-known as a function of spectral type and metallicity due to dedicated radial velocity (eg., MARVELS, HARPS) and transit (eg., COROT, Kepler) surveys. LSST may detect thousands to tens of thousands of planetary transit candidates – numbers which should remain significant in the mid 2020s. LSST will thus enable investigation of how hot Jupiter frequencies derived for the solar neighborhood extrapolate to thick disk and halo stars. Within the thin disk, LSST will constrain radial gradients in planetary frequency, and if these are correlated, with metallicity.

*Providing statistical constraints on planetary migration theory.* Hot Jupiters are not thought to form *in situ*, and hence require migration through protoplanetary discs. Planetary migration theory is still in its infancy and cannot yet predict distributions of feasible planetary radii and distances. LSST will enable statistically significant constraints of various formation theories by revealing how planetary system architecture varies with stellar/planetary masses and metallicity.

*Examining the effects of intense stellar irradiation on planetary atmospheres.* The atmospheres of hot Jupiters can be heated enough to drive hydrodynamic escape. By identifying the shortest period planets, LSST will help constrain the energy absorption limit beyond which a hot Jupiter cannot maintain its atmosphere for the life of the stellar system (Koskinen et al. 2007).

Any transiting planet candidates found will require follow-up for full confirmation. Even in 2025, radial velocity studies with sufficient precision will likely be difficult at the distances of most LSST stars. Given that active follow-up on potentially tens of thousands of targets may be infeasible, results drawn from LSST may be statistical in nature (Sahu et al. 2006), and care must be taken to identify the best candidates for follow-up.

### 8.11.2 How Many Planets will LSST Detect?

#### *Q1) What is LSST's Chance of Detecting a Transiting Planet Around a Given Star?*

A simulation pipeline is initiated by specifying values of stellar radius ( $R_s$ ), planetary radius ( $R_p$ ), period ( $P$ ), ra ( $\alpha$ ), dec ( $\delta$ ), distance ( $d$ ), and inclination ( $i$ ). A normalized planetary transit light curve (Seager & Mallén-Ornelas 2003) is assigned a random initial phase ( $\phi$ ). Stellar  $ugriz$  colors are interpolated from Covey et al. (2007), and  $y$  colors are estimated by the integration of Kurucz model fluxes through LSST filter curves for warm stars and with template spectra (Cushing et al. 2005; Bochanski et al. 2007b) for cool stars. The specified distance is used to create apparent magnitude light curves in each filter, which are then realized through the Operations Simulation via the light curve simulation tool (§ 8.6.1), assuming dithering of field locations.

Points with excellent photometry from a six-filter normalized light curve are scanned for box type periodicity from 0.5 to 40 days in one second intervals. Nearly all pipelines runs return either an exact period/alias or a complete non-detection of a period, with very few (<0.1%) “false positives” in which a periodic signal is detected that was not present in the initial light curve. Of these false

positives,  $\sim 60\%$  are periods of  $\simeq 1$  day, which can be easily screened. False positives are reported as negative results in these estimates, but potentially  $\sim 1$  of every 1,000 planets “detected” by this method might be spurious due to inability to cull false positives. Further complicating factors such as correlated red noise and binary contamination may also increase false positives, and require future attention.

Assuming that detection probabilities ( $\Phi$ ) from changing distance, inclination, and position on the sky are independent of the parameters of the planetary systems enables computation of  $\Phi = \Phi_{detect}(Rs, Rp, P, \phi) \times \Phi_{detect}(\alpha, \delta) \times \Phi_{detect}(d) \times \Phi_{detect}(i)$ . The effects of initial phase and instrument properties are averaged over as described below.

Stars of different spectral types have distance-dependent changes in their magnitude errors, given differing bright and faint limits in each filter. In addition, the transit depth signal varies as  $(Rp/Rs)^2$ . As  $Rs$  is not independent of the other parameters under consideration,  $Rs$  is fixed and a suite of results for differing spectral types is constructed. A “best-case scenario” distance is chosen so that a star of that spectral type will be observable at 1% photometry in a maximum number of LSST filters. With  $Rs$  and  $d$  fixed (and with  $i = 90^\circ$ ), the remaining independent variables  $(Rp, P, \phi)$  are explored.  $\Phi_{detect}(Rs, Rp, P, \phi)$  is reported as the number of positive detections in 50 pipeline runs of varying initial phase.

[Figure 8.27](#) is a contour plot of  $\Phi_{detect}(Rs, Rp, P, \phi)$  for hot Jupiters around a  $0.7 R_\odot$  star at 1 kpc, calculated for a star at  $(248^\circ, -30^\circ)$ . To test the effect of changing sky position, deviations from a case where  $\Phi_{detect}(Rs, Rp, P, \phi) = 100\%$  were computed. The simulation results (not shown) show  $\sim 10\%$  deviations in  $\Phi_{detect}(\alpha, \delta)$ , and generally follow the pattern seen in the number of visits per field ([Figure 2.1](#)).

[Figure 8.28](#) examines  $\Phi_{detect}(d)$  as a  $0.7 R_\odot$  star with a 1.35 Jupiter radii planet in a 2.725 day period observed at  $(248^\circ, -30^\circ)$  is placed at various distances from the Sun.

## *Q2) How Many Transiting Hot Jupiters will LSST Detect?*

To predict the number of hot Jupiters that LSST might detect requires an estimate of the number of observable stars as a function of spectral type, position, and distance on the sky, making allowances for the fractions of stars that are non-variable and non-binary, and those that might have planets in edge-on configurations. A Monte Carlo simulation over relevant planetary system parameters applied to computed detection probabilities will allow quantification of the number of detectable planets in that volume using methodology similar to [Pepper & Gaudi \(2005\)](#).

A simple analytic calculation predicts that LSST could observe  $\sim 20,000$  transiting hot Jupiters ([Gaudi 2007](#)), but cites the need for the more detailed treatment that is underway. The calculations are too preliminary to provide an answer to Question 2 at this moment, but the project outlined above will provide predictions that are more closely tied to the actual observation conditions. LSST’s planet finding capabilities will be immense, given that most of the stars in the sky have radii smaller than  $0.7 R_\odot$ , and thus will have an expanded phase space in which  $\Phi_{detect} = 100\%$ .

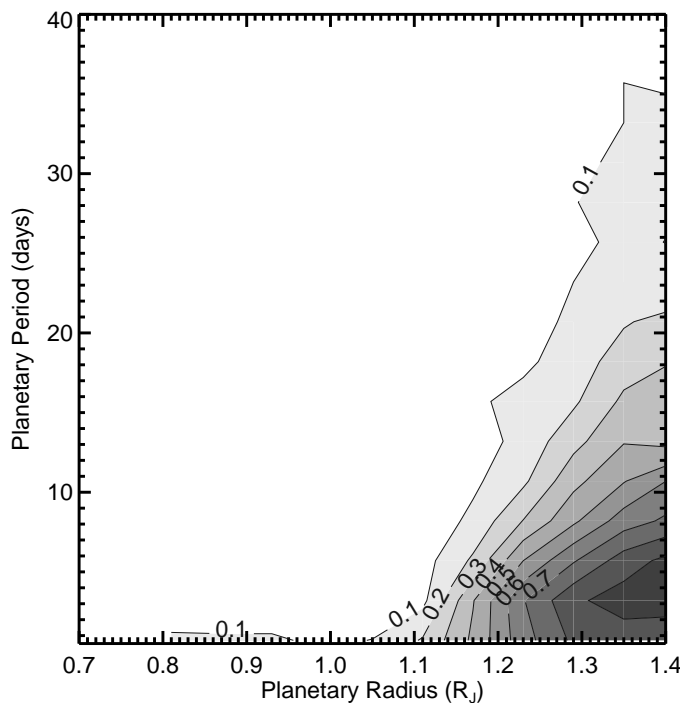


Figure 8.27: Planetary transit detection probabilities for a  $0.7 R_{\odot}$  star at 1 kpc, calculated at each grid point as the period recovery percentage for 50 runs at random initial phases. Planetary radii are in units of Jupiter radii.

## 8.12 EPO Opportunities

*Paula Szkody, Steve B. Howell, Robert R. Gibson*

After the first year or two of operations, LSST will have a large collection of well sampled, multi-color light curves. These can be used by the project to assign a confidence level to a new “event” such as a transient or for assignment of a sparsely sampled light curve to a specific variable type (§ 8.4). A useful tool for the presentation of the template observations and the additional LSST light curves would be to develop a “VO Broker” that allows a database search ability and can produce a light curve, a phased light curve, and other variable star tools. This tool would be highly useful to the project, other scientists, and the interested public.

Citizen scientists can play a role in classifying light curves in this initial archive of several hundred thousand variable stars from the early science proposal. By comparing the shape of light curves in the LSST sample against templates of known sources, initial classifications can be assigned for further weighting and analysis by researchers. This idea could be developed as part of the Light Curve Zoo Citizen Science Project described in [Chapter 4](#).

Light curves, the graphical representation of changes in brightness with time, have educational value in several settings. Learning to read, construct, and interpret line graphs are critical skills at all levels of the National Council of Teachers of Mathematics’ Standards as is the ability to use representations to model and interpret physical, social, and mathematical phenomena ([National](#)

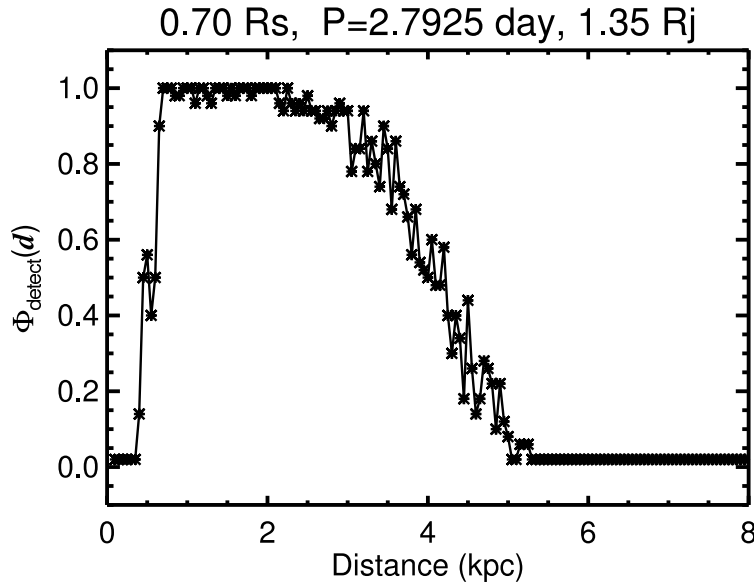


Figure 8.28: Planetary transit detection probability as a function of distance of the star. Saturation of the LSST detectors (§ 3.2) was taken into account.

Council of Teachers of Mathematics 2000). Light curves also can be converted to audio and represented by sound, letting people “listen to the light curve” and hear differences between light curves of different types of variable objects. A supernova light curve would sound different from an AGN light curve, which is different from a Cepheid light curve, and so on. This learning technique would be useful to multiple learning styles including the visually impaired, and could be explored in a web-based tutorial on variability and integrated into a training module on light curve identification.

Amateur astronomers can provide a valuable service in following up the brighter sources with their telescopes, enabling identifications in addition to those completed by professional astronomers. Tens of thousands of variable object alerts are predicted nightly, a rate beyond the capability of professional telescopes to monitor. Effective partnerships between professionals and amateurs can be developed that capitalize on the opportunities offered by LSST alerts and increasingly sophisticated capabilities of the amateur community. AAVSO (American Association of Variable Star Observers), VSNET (Variable Star Network in Japan) and CBA (Center for Backyard Astrophysics) are prime organizations with a record of CCD observations of variables and high interest in their communities.

## References

- Alcock, C. et al., 2000, *ApJ*, 541, 270
- Alvarez, R., Mennessier, M.-O., Barthes, D., Luri, X., & Mattei, J. A., 1997, *A&A*, 327, 656
- Anderson, S. F. et al., 2005, *AJ*, 130, 2230
- Arnett, D., 1996, Supernovae and Nucleosynthesis: An Investigation of the History of Matter from the Big Bang to the Present. Princeton: Princeton University Press
- Aspin, C. et al., 2009, *ApJL*, 692, L67

- Baade, W., & Zwicky, F., 1934a, Proceedings of the National Academy of Science, 20, 259  
 —, 1934b, Proceedings of the National Academy of Science, 20, 254
- Baliunas, S., Frick, P., Moss, D., Popova, E., Sokoloff, D., & Soon, W., 2006, *MNRAS*, 365, 181
- Baliunas, S. L. et al., 1995, *ApJ*, 438, 269
- Barbary, K. et al., 2009, *ApJ*, 690, 1358
- Bergeron, P., Saumon, D., & Wesemael, F., 1995, *ApJ*, 443, 764
- Bildsten, L., Shen, K. J., Weinberg, N. N., & Nelemans, G., 2007, *ApJL*, 662, L95
- Bischoff-Kim, A., Montgomery, M. H., & Winget, D. E., 2008, *ApJ*, 675, 1512
- Bloom, J. S. et al., 2006, *ApJ*, 638, 354
- Bochanski, J. J., Hawley, S. L., Reid, I. N., Covey, K. R., West, A. A., Golimowski, D. A., & Ivezić, Ž., 2008, ArXiv e-prints, 0810.2343
- Bochanski, J. J., Munn, J. A., Hawley, S. L., West, A. A., Covey, K. R., & Schneider, D. P., 2007a, *AJ*, 134, 2418
- Bochanski, J. J., West, A. A., Hawley, S. L., & Covey, K. R., 2007b, *AJ*, 133, 531
- Bond, H. E., Bonanos, A. Z., Humphreys, R. M., Berto Monard, L. A. G., Prieto, J. L., & Walter, F. M., 2009, ArXiv e-prints, 0901.0198
- Borne, K., Becla, J., Davidson, I., Szalay, A., & Tyson, J. A., 2008, in American Institute of Physics Conference Series, Vol. 1082, American Institute of Physics Conference Series, C. A. L. Bailer-Jones, ed., pp. 347–351
- Borne, K. D., 2008, *Astronomische Nachrichten*, 329, 255
- Bradley, P. A., 2001, *ApJ*, 552, 326
- Burgasser, A. J., Liebert, J., Kirkpatrick, J. D., & Gizis, J. E., 2002, *AJ*, 123, 2744
- Castor, J. I., Abbott, D. C., & Klein, R. I., 1975, *ApJ*, 195, 157
- Chabrier, G., & Baraffe, I., 1997, *A&A*, 327, 1039
- Chabrier, G., & Küker, M., 2006, *A&A*, 446, 1027
- Chiosi, C., & Maeder, A., 1986, *ARA&A*, 24, 329
- Covey, K. R. et al., 2008, *AJ*, 136, 1778  
 —, 2007, *AJ*, 134, 2398
- Cushing, M. C., Rayner, J. T., & Vacca, W. D., 2005, *ApJ*, 623, 1115
- Della Valle, M. et al., 2006, *Nature*, 444, 1050
- Della Valle, M., & Livio, M., 1995, *ApJ*, 452, 704  
 —, 1998, *ApJ*, 506, 818
- Di Stefano, R., 2007, Bulletin of the American Astronomical Society, Vol. 38, Microlensing, Mesolensing, and Wide Field Monitoring, p. 166  
 —, 2008a, *ApJ*, 684, 59  
 —, 2008b, *ApJ*, 684, 46
- Di Stefano, R., & Night, C., 2008, ArXiv e-prints, 0801.1510
- Di Stefano, R., & Perna, R., 1997, *ApJ*, 488, 55
- Di Stefano, R., & Scalzo, R. A., 1999a, *ApJ*, 512, 564  
 —, 1999b, *ApJ*, 512, 579
- Dominik, M., & Sahu, K. C., 2000, *ApJ*, 534, 213
- Downes, R. A., & Duerbeck, H. W., 2000, *AJ*, 120, 2007
- Drissen, L., Roy, J.-R., & Robert, C., 1997, *ApJL*, 474, L35
- Eason, E. L. E., Giampapa, M. S., Radick, R. R., Worden, S. P., & Hege, E. K., 1992, *AJ*, 104, 1161
- Einstein, A., 1936, *Science*, 84, 506
- Eyer, L., & Mowlavi, N., 2008, Journal of Physics Conference Series, 118, 012010
- Feast, M. W., 2008, ArXiv e-prints, 0806.3019
- Feast, M. W., & Whitelock, P. A., 2000, *MNRAS*, 317, 460
- Filippenko, A. V., 1997, *ARA&A*, 35, 309
- Fleming, T. A., Giampapa, M. S., & Schmitt, J. H. M. M., 2000, *ApJ*, 533, 372
- Fox, D. B. et al., 2005, *Nature*, 437, 845
- Fraser, O. J., Hawley, S. L., Cook, K. H., & Keller, S. C., 2005, *AJ*, 129, 768
- Fryer, C. L., Hungerford, A. L., & Young, P. A., 2007, *ApJL*, 662, L55
- Fukui, A. et al., 2007, *ApJ*, 670, 423
- Fynbo, J. P. U. et al., 2006, *Nature*, 444, 1047
- Gaensicke, B. T., Levan, A. J., Marsh, T. R., & Wheatley, P. J., 2008, ArXiv e-prints, 0809.2562
- Gal-Yam, A. et al., 2006, *Nature*, 444, 1053
- Gänsicke, B. T. et al., 2009, *MNRAS*, submitted

- Gaudi, B. S. et al., 2008, *ApJ*, 677, 1268
- Gaudi, S., 2007, in Astronomical Society of the Pacific Conference Series, Vol. 366, Transiting Extrapolar Planets Workshop, C. Afonso, D. Weldrake, & T. Henning, eds., p. 273
- Gehrz, R. D., Grasdalen, G. L., & Hackwell, J. A., 1986, *ApJL*, 306, L49
- Girardi, L., & Marigo, P., 2007, in Astronomical Society of the Pacific Conference Series, Vol. 378, Why Galaxies Care About AGB Stars: Their Importance as Actors and Probes, F. Kerschbaum, C. Charbonnel, & R. F. Wing, eds., p. 20
- Gould, A., & Loeb, A., 1992, *ApJ*, 396, 104
- Hartmann, L., & Kenyon, S. J., 1996, *ARA&A*, 34, 207
- Hawley, S. L. et al., 2003, *ApJ*, 597, 535
- Hawley, S. L., & Johns-Krull, C. M., 2003, *ApJL*, 588, L109
- Hawley, S. L., & Pettersen, B. R., 1991, *ApJ*, 378, 725
- Heger, A., Fryer, C. L., Woosley, S. E., Langer, N., & Hartmann, D. H., 2003, *ApJ*, 591, 288
- Heger, A., Jeannin, L., Langer, N., & Baraffe, I., 1997, *A&A*, 327, 224
- Herbig, G. H., 1977, *ApJ*, 217, 693
- Herbig, G. H., Aspin, C., Gilmore, A. C., Imhoff, C. L., & Jones, A. F., 2001, *PASP*, 113, 1547
- Hidas, M. G., Hawkins, E., Walker, Z., Brown, T. M., & Rosing, W. E., 2008, *Astronomische Nachrichten*, 329, 269
- Hodapp, K.-W., Hora, J. L., Rayner, J. T., Pickles, A. J., & Ladd, E. F., 1996, *ApJ*, 468, 861
- Howell, S. B., 2008, *AN*, 329, 259
- Howell, S. B., Nelson, L. A., & Rappaport, S., 2001, *ApJ*, 550, 897
- Hubble, E., & Sandage, A., 1953, *ApJ*, 118, 353
- Hubble, E. P., 1929, *ApJ*, 69, 103
- Humphreys, R. M., & Davidson, K., 1994, *PASP*, 106, 1025
- Isern, J., Hernanz, M., & Garcia-Berro, E., 1992, *ApJL*, 392, L23
- Ivezić, Ž. et al., 2007, *AJ*, 134, 973
- Ivezić, Ž. et al., 2008, ArXiv e-prints, 0805.2366
- Jackson, T., Ivezić, Ž., & Knapp, G. R., 2002, *MNRAS*, 337, 749
- Jason, M., Guinan, E., Engle, S., & Pojmanski, G., 2007, Bulletin of the American Astronomical Society, Vol. 38, Living With A Red Dwarf: Rotation, Starspots, Activity Cycles, Coronal X-ray Activity And X-uv Irradiances Of Proxima Centauri. p. 921
- Jura, M., 1994, *Ap&SS*, 217, 101
- Kasen, D., Heger, A., & Woosley, S., 2008, in American Institute of Physics Conference Series, Vol. 990, First Stars III, B. W. O'Shea & A. Heger, eds., pp. 263–267
- Kitaura, F. S., Janka, H.-T., & Hillebrandt, W., 2006, *A&A*, 450, 345
- Kochanek, C. S., Beacom, J. F., Kistler, M. D., Prieto, J. L., Stanek, K. Z., Thompson, T. A., & Yüksel, H., 2008, *ApJ*, 684, 1336
- Koskinen, T. T., Aylward, A. D., & Miller, S., 2007, *Nature*, 450, 845
- Kowalski, A., Hawley, S. L., Hilton, E. J., Becker, A. C., West, A. A., Bochanski, J. J., & Sesar, B., 2009, ArXiv eprint, 0906.3637
- Kulkarni, S. R., 2005, ArXiv Astrophysics e-prints, arXiv:astro-ph/0510256
- Kulkarni, S. R. et al., 2007, *Nature*, 447, 458
- Lacy, C. H., Moffett, T. J., & Evans, D. S., 1976, *ApJS*, 30, 85
- Lammer, H. et al., 2007, *Astrobiology*, 7, 185
- Langer, N., 2004, Rotation in core collapse progenitors: single and binary stars, P. Höflich, P. Kumar, & J. C. Wheeler, eds., p. 191
- Law, N. M. et al., 2009, ArXiv e-prints, 0906.5350
- Leavitt, H. S., & Pickering, E. C., 1912, Harvard College Observatory Circular, 173, 1
- Lépine, S., 2008, *AJ*, 135, 2177
- Li, L.-X., & Paczyński, B., 1998, *ApJL*, 507, L59
- Liebert, J., Arnett, D., & Benz, W., 1997, in Advances in Stellar Evolution, R. T. Rood & A. Renzini, eds., p. 253
- Liebert, J., Kirkpatrick, J. D., Reid, I. N., & Fisher, M. D., 1999, *ApJ*, 519, 345
- Linsky, J. L., Wood, B. E., Brown, A., Giampapa, M. S., & Ambruster, C., 1995, *ApJ*, 455, 670
- Loredo, T. J., & Chernoff, D. F., 2003, Bayesian adaptive exploration, E. D. Feigelson & G. J. Babu, eds., Springer, pp. 57–70
- Mahabal, A. et al., 2008a, *Astronomische Nachrichten*, 329, 288
- , 2008b, American Institute of Physics Conference Series, Vol. 1082, Towards Real-time Classification of Astro-

- nomical Transients. pp. 287–293
- Mainzer, A. K., Eisenhardt, P., Wright, E. L., Liu, F.-C., Irace, W., Heinrichsen, I., Cutri, R., & Duval, V., 2005, Society of Photo-Optical Instrumentation Engineers (SPIE) Conference Series, Vol. 5899, Preliminary design of the Wide-Field Infrared Survey Explorer (WISE), H. A. MacEwen, ed. pp. 262–273
- Mao, S., & Paczynski, B., 1991, *ApJL*, 374, L37
- Maraston, C., Strömbäck, G., Thomas, D., Wake, D. A., & Nichol, R. C., 2009, *MNRAS*, 394, L107
- Marconi, M., Cignoni, M., Di Criscienzo, M., Ripepi, V., Castelli, F., Musella, I., & Ruoppo, A., 2006, *MNRAS*, 371, 1503
- Martín, E. L., & Ardila, D. R., 2001, *AJ*, 121, 2758
- Massey, P., McNeill, R. T., Olsen, K. A. G., Hodge, P. W., Blaha, C., Jacoby, G. H., Smith, R. C., & Strong, S. B., 2007, *AJ*, 134, 2474
- McGehee, P. M., Smith, J. A., Henden, A. A., Richmond, M. W., Knapp, G. R., Finkbeiner, D. P., Ivezić, Ž., & Brinkmann, J., 2004, *ApJ*, 616, 1058
- Messina, S., & Guinan, E. F., 2003, in The Future of Cool-Star Astrophysics: 12th Cambridge Workshop on Cool Stars, Stellar Systems, and the Sun, A. Brown, G. M. Harper, & T. R. Ayres, eds., Vol. 12, pp. 941–945
- Metcalfe, T. S., Montgomery, M. H., & Kanaan, A., 2004, *ApJL*, 605, L133
- Metcalfe, T. S., Winget, D. E., & Charbonneau, P., 2001, *ApJ*, 557, 1021
- Metzger, B. D., Piro, A. L., & Quataert, E., 2008, ArXiv e-prints, 0812.3656
- Meynet, G., Maeder, A., Schaller, G., Schaerer, D., & Charbonnel, C., 1994, *A&AS*, 103, 97
- Mohanty, S., Basri, G., Shu, F., Allard, F., & Chabrier, G., 2002, *ApJ*, 571, 469
- Montgomery, M. H., 2005, *ApJ*, 633, 1142
- Mukadam, A. S., Winget, D. E., von Hippel, T., Montgomery, M. H., Kepler, S. O., & Costa, A. F. M., 2004, *ApJ*, 612, 1052
- Mullally, F., Winget, D. E., Degennaro, S., Jeffery, E., Thompson, S. E., Chandler, D., & Kepler, S. O., 2008, *ApJ*, 676, 573
- Nakar, E., & Piran, T., 2003, *New Astronomy*, 8, 141
- National Council of Teachers of Mathematics, 2000, Principles and Standards for School Mathematics. National Council of Teachers of Mathematics, p. 402
- Nelemans, G., 2005, in Astronomical Society of the Pacific Conference Series, Vol. 330, The Astrophysics of Cataclysmic Variables and Related Objects, J.-M. Hameury & J.-P. Lasota, eds., p. 27
- Nelemans, G., & Tout, C. A., 2005, *MNRAS*, 356, 753
- Nelemans, G., Yungelson, L. R., & Portegies Zwart, S. F., 2004, *MNRAS*, 349, 181
- Night, C., Di Stefano, R., & Schwamb, M., 2008, *ApJ*, 686, 785
- Ofek, E. O. et al., 2007a, *ApJ*, 659, L13
- , 2007b, *ApJ*, 662, 1129
- Oláh, K., Kolláth, Z., & Strassmeier, K. G., 2000, *A&A*, 356, 643
- Oláh, K., Strassmeier, K. G., Granzer, T., Soon, W., & Baliunas, S. L., 2007, *Astronomische Nachrichten*, 328, 1072
- Paczynski, B., 1967, *Acta Astronomica*, 17, 287
- Paczynski, B., 1986, *ApJ*, 304, 1
- Padmanabhan, P., 2000, Theoretical astrophysics. Vol.1: Astrophysical processes. Cambridge, MA: Cambridge University Press
- Pepper, J., & Gaudi, B. S., 2005, *ApJ*, 631, 581
- Perets, H. B. et al., 2009, ArXiv e-prints, 0906.2003
- Perlmutter, S. et al., 1999, *ApJ*, 517, 565
- Phillips, M. M., 1993, *ApJL*, 413, L105
- Pietrukowicz, P. et al., 2009, ArXiv e-prints, 0905.4275
- Politano, M., 2004, *ApJ*, 604, 817
- Quimby, R. M., Aldering, G., Wheeler, J. C., Höflich, P., Akerlof, C. W., & Rykoff, E. S., 2007, *ApJ*, 668, L99
- Racusin, J. L. et al., 2008, *Nature*, 455, 183
- Rau, A., 2008, *PASP*, submitted
- Rau, A. et al., 2009a, ArXiv eprint, 0906.5350
- , 2009b, ArXiv e-prints, 0906.5355
- Rau, A., Ofek, E. O., Kulkarni, S. R., Madore, B. F., Pevunova, O., & Ajello, M., 2008, *ApJ*, 682, 1205
- Reimann, J. D., 1994, PhD thesis, University of California, Berkeley
- Rejkuba, M., 2004, *A&A*, 413, 903
- Rhoads, J. E., 1997, *ApJL*, 487, L1

- , 1999, *ApJ*, 525, 737  
 —, 2003, *ApJ*, 591, 1097  
 Riess, A. G. et al., 1998, *AJ*, 116, 1009  
 Roelofs, G. H. A., Groot, P. J., Marsh, T. R., Steeghs, D., Barros, S. C. C., & Nelemans, G., 2005, *MNRAS*, 361, 487  
 Ruiz-Lapuente, P. et al., 2004, *Nature*, 431, 1069  
 Rutledge, R. E., Basri, G., Martín, E. L., & Bildsten, L., 2000, *ApJL*, 538, L141  
 Saha, A., & Monet, D., 2005, Bulletin of the American Astronomical Society, Vol. 37, LSST Astrometric Science. p. 1203  
 Sahu, K. C. et al., 2006, *Nature*, 443, 534  
 Sari, R., Piran, T., & Halpern, J. P., 1999, *ApJL*, 519, L17  
 Scannapieco, E., Madau, P., Woosley, S., Heger, A., & Ferrara, A., 2005, *ApJ*, 633, 1031  
 Schaefer, B. E., 2009, American Astronomical Society Meeting Abstracts, Vol. 213, Comprehensive Photometric Histories of All Known Galactic Recurrent Novae. p. #491.04  
 Schmidt, S. J., Cruz, K. L., Bongiorno, B. J., Liebert, J., & Reid, I. N., 2007, *AJ*, 133, 2258  
 Seager, S., & Mallén-Ornelas, G., 2003, *ApJ*, 585, 1038  
 Shafter, A. W., 2002, in American Institute of Physics Conference Series, Vol. 637, Classical Nova Explosions, M. Hernanz & J. José, eds., pp. 462–471  
 Shara, M. M., 1981, *ApJ*, 243, 926  
 Silvestri, N. M., Hawley, S. L., Dang, L. C., Krogsrud, D. A., Smoke, K., Wolfe, M. A., & Mannikko, L., 2006, Bulletin of the American Astronomical Society, Vol. 38, New Close Binary Systems from the SDSS-I (Data Release Five) and the Orbital Periods for a Subset of Close White Dwarf + M Dwarf Systems. p. 1128  
 Silvestri, N. M. et al., 2007, *AJ*, 134, 741  
 Smak, J., 1967, *Acta Astronomica*, 17, 255  
 Smartt, S. J., Eldridge, J. J., Crockett, R. M., & Maund, J. R., 2009, *MNRAS*, 395, 1409  
 Smith, N., Ganeshalingam, M., Li, W., Chornock, R., Steele, T. N., Silverman, J. M., Filippenko, A. V., & Mobberley, M. P., 2008, ArXiv e-prints, 0811.3929  
 Smith, N. et al., 2007, *ApJ*, 666, 1116  
 Smith, N., & McCray, R., 2007, *ApJL*, 671, L17  
 Smith, N., & Owocki, S. P., 2006, *ApJL*, 645, L45  
 Smolčić, V. et al., 2004, *ApJL*, 615, L141  
 Soker, N., Frankowski, A., & Kashi, A., 2008, ArXiv e-prints, 0812.1402  
 Starrfield, S., Shore, S. N., Sparks, W. M., Sonneborn, G., Truran, J. W., & Politano, M., 1992, *ApJL*, 391, L71  
 Szkody, P. et al., 2003, *AJ*, 126, 1499  
 —, 2007, *ApJ*, 658, 1188  
 Tammann, G. A., & Sandage, A., 1968, *ApJ*, 151, 825  
 Templeton, M. R., Mattei, J. A., & Willson, L. A., 2005, *AJ*, 130, 776  
 The Pierre Auger Collaboration, 2007, *Science*, 318, 938  
 Thompson, T. A., Prieto, J. L., Stanek, K. Z., Kistler, M. D., Beacom, J. F., & Kochanek, C. S., 2008, ArXiv e-prints, 0809.0510  
 Totani, T., & Panaiteescu, A., 2002, *ApJ*, 576, 120  
 Tsapras, Y. et al., 2009, *Astronomische Nachrichten*, 330, 4  
 Tutukov, A., & Yungelson, L., 1996, *MNRAS*, 280, 1035  
 Tyson, J. A., 2006, *Nature*, 442, 364  
 Udalski, A., 2003, *Acta Astronomica*, 53, 291  
 Valenti, S. et al., 2009, ArXiv e-prints, 0901.2074  
 van den Heuvel, E. P. J., 2008, *Nature*, 451, 775  
 Van Dyk, S. D., Peng, C. Y., King, J. Y., Filippenko, A. V., Treffers, R. R., Li, W., & Richmond, M. W., 2000, *PASP*, 112, 1532  
 Verbunt, F., & Zwaan, C., 1981, *A&A*, 100, L7  
 Warner, B., 1995, *Cambridge Astrophysics Series*  
 West, A. A., Hawley, S. L., Bochanski, J. J., Covey, K. R., Reid, I. N., Dhital, S., Hilton, E. J., & Masuda, M., 2008, *AJ*, 135, 785  
 Whitelock, P. A., Feast, M. W., & van Leeuwen, F., 2008, *MNRAS*, 386, 313  
 Williams, R. D., Djorgovski, S. G., Drake, A. J., Graham, M. J., & Mahabal, A., 2009, ArXiv e-prints, 0906.2186  
 Wilson, O. C., 1982, *ApJ*, 257, 179

## *Chapter 8: References*

---

- Winget, D. E. et al., 2003, in Astronomical Society of the Pacific Conference Series, Vol. 294, Scientific Frontiers in Research on Extrasolar Planets, D. Deming & S. Seager, eds., pp. 59–64
- Winget, D. E., Kepler, S. O., Kanaan, A., Montgomery, M. H., & Giovannini, O., 1997, *ApJL*, 487, L191
- Winget, D. E., Sullivan, D. J., Metcalf, T. S., Kawaler, S. D., & Montgomery, M. H., 2004, *ApJL*, 602, L109
- Woosley, S. E., 1993, *ApJ*, 405, 273
- Woosley, S. E., & Bloom, J. S., 2006, *ARA&A*, 44, 507